EXPERIMENTAL AND MODELING STUDY OF SO_2 BEHAVIOR DURING OXY COMBUSTION IN FLUIDIZED BEDS

by

Liyong Wang

A dissertation submitted to the faculty of
The University of Utah
in partial fulfillment of the requirements for the degree of

Doctor of Philosophy

Department of Chemical Engineering

The University of Utah

December 2012

Copyright © Liyong Wang 2012

All Rights Reserved

The University of Utah Graduate School

STATEMENT OF DISSERTATION APPROVAL

The dissertation of **Liyong Wang**

has been approved by the following supervisory committee members:

Eric G. Eddings	, Chair	**08/16/2012** Date Approved
Jost O.L. Wendt	, Member	**08/16//2012** Date Approved
JoAnn Lighty	, Member	**08/16//2012** Date Approved
Geoffrey Silcox	, Member	**08/16//2012** Date Approved
Lawrence E. Bool III	, Member	**08/16/2012** Date Approved

and by **JoAnn Lighty** , Chair of the Department of **Chemical Engineering**

and by Charles A. Wight, Dean of The Graduate School.

ABSTRACT

SO_2 emissions from coal combustion have several harmful effects on the environment, including their contribution to acid rain. A variety of approaches have been developed to control SO_2 pollution. Direct dry sorbent (limestone) injection is a relatively simple and low-cost process. Fluidized beds have been one of the most popular furnaces for the application of direct sorbent injection. In addition, oxy fuel combustion is a promising, practical method to reduce greenhouse gas emissions. Thus, studies on the mechanisms related to the production of SO_2 emissions under oxy fuel conditions are important.

The sulfation mechanisms (direct or indirect) of limestone depend on whether the limestone is calcined. Direct sulfation takes place in an uncalcined state while an indirect sulfation happens with calcined limestone. Usually, in fluidized bed combustion conditions, direct sulfation occurs in oxy fuel combustion due to CO_2 inhibition, and indirect sulfation occurs in air combustion. A bench-scale bubbling fluidized bed (BFB) and a 330 KW pilot-scale circulating fluidized bed (CFB) were used to investigate SO_2 behavior in air and oxy coal combustion. SO_2 release with and without limestone sorbent were investigated in N_2/O_2 and CO_2/O_2 environments for the following conditions: temperature range (765— 902℃), O_2 concentration range (10—30%), and a wide range of Ca/S ratios. The bench-scale experiments without recycled flue gas (RFG)

and the equilibrium calculations of NASA Chemical Equilibrium with Applications (CEA) show no effect of combustion diluent (N_2, CO_2) on SO_2 emissions. Limestone addition shows greater SO_2 capture efficiency in air firing than that in oxy firing.

In addition, sulfation behavior of limestone in $N_2/O_2/SO_2$ and $CO_2/O_2/SO_2$ atmospheres was studied, exploring the mechanisms of indirect and direct sulfation in a wide range of temperatures (765– 874℃). A significant temperature effect on sulfation behavior of limestone was seen during direct sulfation reactions. However, limited effect was seen for an indirect sulfation reaction. A scanning electron microscope (SEM) and energy dispersive x-ray spectrometer (EDS) were used to exam the microstructure of sulfated limestone and their sulfur distribution.

A mathematical and computational framework for a single particle model was developed to understand the differences between indirect and direct sulfation and single coal particle combustion processes. The model framework presented here, however, provides a broader flexibility that could be used to address a range of particle sizes. The shrinking core particle model and fine single particle model are two specific applications of my general single particle model.

CONTENTS

LIST OF TABLES

ACKNOWLEDGEMENTS

As with any accomplishment, this work is truly the result of the efforts of many people. The author wishes to thank the many people who have lent their time and talents. First and foremost, I would like to extend my sincere appreciation to my advisor, Dr. Eric G. Eddings, for his continuous support, kindness, endless patience, invaluable guidance, and inspiration. I wish to express my appreciation to my committee members for serving on my committee and for their insightful comments and critiques of my work.

Thanks to Dana Overacker and Ryan Okerlund for all their advice, guidance, and help. I am very grateful to Dr. Hongzhi Zhang, Dr. Daniel Sweeney, Dr. Charles Reid, Dr. Randy Pummill, Dr. Astrid Sánchez, and Keith Gneshin for all their help.

And finally, great appreciation to my wife, Dr. Xiaoxia Jin, for her deep love, great patience, full understanding, and steadfast support through all these years. You are the most important person in my life.

This work was supported by the US Department of Energy (DE-NT0005015) and Praxair.

CHAPTER 1

INTRODUCTION

The increasing temperature of Earth's atmosphere, land, and oceans (global warming) leads to serious consequences: for example, changes in precipitation patterns. It also results in a rising sea level, the expansion of subtropical deserts, and the retreat of glaciers, etc. Global warming also brings extreme-weather occurrences, i.e., droughts, heavy rainfall, heat waves, species extinctions, and reduction of crop yields. Since the early 20^{th} century, the average global surface temperature has been raised by 0.8 °C, two thirds of which have been gained since 1980. Many believe that global warming is the result of human activities, i.e., the increasing greenhouse gas emissions, especially CO_2, which was released from burning fossil fuel, compounded by deforestation around the world. According to the US Environmental Protection Agency (EPA), the concentrations of CO_2 and CH_4 have been raised by 36% and 148% since 1750 [1], respectively.

.

1.1. Carbon capture and storage (CCS)

In order to reduce the effect of human activities on global warming, scientists have proposed various approaches to control greenhouse gases emissions, especially CO_2, into the atmosphere from fossil fuel utilization in power plants. Carbon capture and

storage (CCS) is one of the most effective approaches to prevent greenhouse gas emissions from entering the carbon cycle. A CCS approach usually includes two consecutive cycles:

i. CO_2 capture: Separation of CO_2 from the flue gas stream

ii. CO_2 storage: It is often called carbon sequestration

A few approaches have been proposed to capture CO_2 emissions from fossil fuel power plants, including postcombustion capture (PCC), oxy fuel combustion (OFC), integrated gasification combined cycle (IGCC), and chemical looping combustion (CLP). The costs of CO_2 separation, capture, and compression before injection into a sink account for about 75% of an entire geologic sequestration process [2].

Following the capture and scrubbing, CO_2 is injected into a geological formation for long-term storage. The CO_2 storage locations are usually either in deep geological formations (deep ocean) or in the form of mineral carbonates. There are two types of CO_2 disposal [3] based on the length of time period. Sequestration means permanent disposal, while storage is defined as a significant time period. Possible sinks include gas reservoirs, depleted oil fields, coal beds, deep ocean, and deep saline aquifers [3, 4].

Table 1 shows storage capacity and retention time of various disposal sites [5]. Deep ocean disposal seems to be less attractive due to the limitation in retention times, acidification of oceans, and the great risk of CO_2 escape from the site. Deep aquifers are considered to be the most promising sequestration locations. However, the risk of CO_2 leak from the mineral carbonate to the atmosphere is still a challenging area in the research and development.

1.2. Precombustion CO_2 capture and postcombustion CO_2 capture

Currently, there are several broad approaches to capture CO_2 emissions, including precombustion capture, postcombustion capture, oxy fuel combustion (OFC), and chemical looping combustion (CLC) [6].

i. Postcombustion capture (PCC): CO_2 is captured from coal firing power plants by scrubbing of the flue gas.

ii. Precombustion capture: for example, the integrated gasification combined cycle (IGCC) converts coal into synthesis gas and enhances H_2 content using the water-gas shift reaction. CO_2 is captured after syngas production.

iii. Oxy fuel combustion (OFC): This approach uses pure O_2 rather than air during the combustion. Often, O_2 is diluted by recycled flue gas (RFG) to avoid overheating. Relatively pure CO_2 stream is captured with no gas separation.

iv. Chemical looping combustion (CLC): metal oxide is employed as an oxygen carrier material to separate O_2 from air using a dual fluidized beds system.

Table 2 compares main characteristics of the CCS technologies [6]. PPC and OFC are feasible to retrofit current coal firing power plants. IGCC and PCC have been applied to partial capturing of CO_2 from flue gas emissions.

1.2.1. Gas scrubbing

Figure 1 illustrates a precombustion capture. Retrofit to existing coal firing power plants using PCC requires no significant modifications to the original plant [7, 8] .

As long as there is space available, the CO_2 capture unit can be added downstream of the boiler. Prior to the CO_2 capture unit, particulate matter, NO_x, and SO_x in the flue gas are required to be removed using electron spin resonance (ESP), selective catalytic reduction (SCR), and flue gas desulfurization (FGD), respectively. A CO_2 capture unit usually includes an absorber and a regenerator. In the absorber, CO_2 is captured by a chemically active agent, such as an amine-based compound (e.g., monoethanolamine (MEA), or methyldiethanolamine (MDEA)). At the same time, the captured CO_2 is released from the chemically active agent in the regenerator, where the chemically reactive agent is regenerated. Although using amine-based chemically reactive agents is a proven technology [9, 10], its cost is not cheap. Recently, limestone was proposed to be a chemically active agent due to its relative lower cost and lower energy penalty. It is introduced as carbonate looping, which has a great potential. However, carbonate looping demands a higher standard of impurity clean up (i.e., particulate matter, mercury, SO_x, NO_x) prior to the CO_2 capture, since impurities will significantly deactivate chemically active agents.

1.2.2. Integrated gasification combined cycle

Figure 2 shows how IGCC works. In an IGCC plant, synthesis gas (CO, CO_2, and H_2) is generated from gasification of coal. CO is converted into CO_2 by the water-gas shift conversion reaction. CO_2 thus can be removed prior to combustion, while H_2 is injected into a combustor. At the same time, impurities are removed from the synthesis gas prior to combustion. Alternatively, H_2 can be separated from synthesis gas, followed by

burning CO in a CO_2/O_2 atmosphere [11]. IGCC leads to lower pollution emissions (SO_x emissions, particulate matter, and mercury) [12]. Excess heat is then passed to a steam cycle, similar to a combined cycle gas turbine. Based on some researchers' technical and economic calculations [9, 13-15], IGCC has a high efficiency and is financially feasible [12]. However, IGCC requires high upfront capital expenses. In addition, IGCC-CCS is not a viable option for retrofit of existing coal firing power plants. Since the first plant was established in 1984, only a few IGCCs have been built for electricity generation, none of which has applied CCS. In the US, the Department of Energy (DOE) clean coal demonstration project helped to set up three IGCC power plants: Wabash River Power Station in West Terre Haute (IN), Polk Power Station in Tampa (FL), and Pinon Pine in Reno (NV). Also, Poland's Kędzierzyn will soon build a zero-emission power and chemical plant that combines gasification technology with CCS [16]. Industrial applications have been accumulating rapidly, although IGCC is still in the early stages of commercialization.

1.2.3. Oxy fuel combustion

Many researchers have studied oxygen fuel combustion (OFC) [17-35], which is described in Figure 3. In OFC, a fuel is burned with pure O_2, instead of air as the primary oxidant. The temperature will be excessively hot using pure O_2. In order to avoid overheating, the mixture of recycled flue gas (RFG) and pure O_2 is used to control flame temperature. The flame temperature is reduced to that in the conventional combustion.

Typically, 60-80% of the flue gas is recycled [5, 6, 21, 24]. The CO_2 concentration in the flue gas can reach 95%, and can be captured directly [5, 6, 24, 31].

During oxy fuel combustion, CO_2 and H_2O in RFG replace N_2 in the air. CO_2 and H_2O are termolecular gases, which present significant differences in heat transfer. Termolecular gases absorb and emit radiation much more than dimolecular nonpolar molecules, and lead to higher heat capacities, resulting in a lower temperature in the convective section of the boiler. Buhre et al. [24] described the difference between OFC with RFG and conventional air combustion:

i. To attain a similar adiabatic flame temperature, the O_2 concentration of the injection gases is typically 26-30%, higher than that (21%) in air combustion.

ii. The volume of gases passing through the boiler is reduced by about 80%.

iii. Concentrations of gaseous species (i.e., SO_x, water vapor) are higher, compared to air firing conditions.

iv. Oxy fuel combustion combined with CO_2 sequestration must provide power to several new units, such as flue gas compression. These compressors will result in an energy penalty. In addition, pure O_2 separation from N_2 requires excessive energy.

Buhre et al. [24] and Toftegaard et al. [5] in a more recent paper reviewed the effect of oxy fuel combustion on gaseous pollutant formation and emissions. Buhre et al. concluded that the SO_x emissions per ton of coal combusted is significantly unchanged [24]. Toftegaard et al. [5] pointed out a lot of contradictory observations on SO_x during air combustion and oxy fuel combustion .

Both reviews agreed that NO_x emissions per unit of energy are reduced during OFC. There are three main NO_x formation paths, as shown in Figure 4: thermal, prompt, and fuel [36-38].

i. Thermal: N_2 can react with O_2 at above 1873 K to form NO; the three principal reactions are well known as the extended Zeldovich.

ii. Prompt: Prompt NO tends to be formed in the fuel-rich zone. In addition, prompt NO mechanism can happen at lower temperatures.

iii. Fuel: The fuel NO mainly comes from either volatile-N or char-N. The first principal path is the oxidation of volatile-N species during the initial combustion. N released from the volatile will be decomposed into cyanide and amine species, which can form N_2 or NO, depending on reaction conditions. Volatile-N is oxidized into NO with oxidants. In comparison, volatile-N tends to form N_2 under a reducing atmosphere. The second path involves char-N, whose reaction is much slower than that of volatile-N. Only around 20% of the char-N eventually leads to NO, since 80% of the NO_x produced is reduced to N_2 by the char.

In conventional air combustion, about 20% of NO_x comes from thermal NO_x, and 80-100% of NO_x from fuel-N. NO_x from the prompt mechanism is negligible. It has been proved that OFC reduces NO_x emissions [28, 30, 31, 39-41]. The reduction of NO_x emissions has been a key motivation to develop OFC-CCS technology. Buhre et al. summarized possible reasons for the reduced NO_x emission from OFC [24], and pointed out the major reduction coming from reburning; the interactions among recycled NO_x, fuel-N, and hydrocarbons released from coal may further decrease NO_x formation.

1.2.4. CCS in postcombustion: carbonate looping

Carbonate looping is a PCC technology. Although substantial research and development for carbonate looping are still needed prior to a full-scale realization in coal firing power plants, the technology has its advantages. Firstly, carbonate looping has a relatively lower energy penalty. Secondly, limestone contributes to its overall low cost. Furthermore, it is noted that limestone reserves are enormous worldwide and usually very easy to be acquired. In general, PCC is one of the most straightforward ways to add CCS capability to coal firing power plants without extensive alteration of existing processes. Despite these advantages, carbonate looping processes are still not well understood, including their kinetic reactions, micromechanisms of carbonate and calcination, and a novel heat transfer design between two solid flows to reduce thermal energy dissipation.

The potential of carbonate looping was first proposed by Shimizu [42]. A carbonate looping system uses two interconnected fluidized beds (carbonator and calciner), as shown in Figure 5. CO_2 in a flue gas stream is removed in a carbonator at operating temperatures between 873 and 1023 K. The solids leaving the carbonator are injected into a calciner, in which free lime (CaO) is regenerated. The regenerated free lime is then fed back into the carbonator, to form a complete loop.

In contrast, thermal energy is needed in a calciner (1173-1273 K) to support an endothermic reaction. When CO_2 reacts to form free lime, substantial heat is released and removed to maintain the carbonator at 923-1023 K.

Pressure has a significant effect on the carbonation reaction rate. Yu et al. [43] studied carbonation kinetics of CaO derived from three different calcium-based sorbents using a magnetic suspension balance (MSB) analyzer at different pressures (1000-15000 torr) and with a wide range of CO_2 concentrations (10-30%). With a 20% concentration of CO_2, the reaction rate increases with pressure until it reaches 4000 torr; however, the reaction rate decreases with pressure beyond 4000 torr.

Deactivation of natural limestone poses another challenge of carbonate looping. Deactivation can be delayed by modifying natural limestone or synthesizing CaO-based sorbent. Florin et al. [44, 45] developed a synthetic CaO-based sorbent with 85 wt. % CaO, which showed a CO_2 uptake that was three times higher than that of a natural limestone after 30 cycles. In order to increase the reactivity of calcium-based sorbents, Blamey et al. [46] investigated the carbonation mechanism of a $Ca(OH)_2$-CaO system. They found a "superheated dehydration" effect in $Ca(OH)_2$ pellets and hydrated calcined limestone, but not in $Ca(OH)_2$ powder or hydrated calcined dolomite. Abonades et al. [47] presented their experimental results from a small test facility (30 KW) using dual circulating fluidized beds (CFB). CO_2 absorption efficiencies in their carbonator have achieved between 70 and 97%.

In addition to experiments, some models have been developed to investigate the carbonate process [48-50]. Lasheras et al. [48] implemented a 1D fluidized bed model using data from a 1052 MW coal firing power plant. CO_2 absorption efficiency achieved about 80% in the carbonator, leading to 88% CO_2 removal. A sensitivity analysis shows that the CO_2 absorption rate increases significantly with bed inventory and circulating

solid flow. The effect of the reactor height, the particle size, and make-up flow on the rate is negligible. Hawthorne et al. [50] modeled carbonate looping using Aspen plus, showing a total CO_2 absorption efficiency of 88%.

1.3. Fluidized bed technology

Fluidized bed combustion (FBC) was introduced in the 1970s to provide cleaner energy [51], and has become more and more popular throughout the world. It also provides fuel flexibility and reduces emissions (SO_x, NO_x). Countries with abundant quantities of low-grade coal, such as the USA, UK, China, and Germany, have been the main drivers in research and development. Countries with abundant biomass resources (peat, wood waste, sludge, and bark), especially in Northern Europe, are also very interested in FBC. FBC provides an improved heat and mass transfer by fluidization of a solid particulate substance.

Fluidization is a process in which granular materials (e.g., bed materials, coal particle, biomass, and limestone) are converted from a static solid-like state (10^3 kg/m^3) to a dynamic liquid-like state (0.1 kg/m^3) [52] subject to an upward high-velocity gas flow stream. A reduction of solid particle concentration will greatly improve heat and mass transfer. In the combustion zone of a fluidized bed, the heat transfer coefficient ranges from 250 to 750 W/m^{2}K, in comparison to less than 100 W/m^{2}K in the freeboard [52]. Therefore, fluidized bed combustors are often used to burn low-quality fuels with low calorific value, high moisture content, and high ash content. They also provide fuel flexibility, and reduced emissions (SO_x, NO_x).

As a mature technology, FBC was reviewed by many authors [53-62]. A primary upward air or O_2 stream passes through a distributor plate or bubble caps to achieve high velocities. A significant pressure drop also occurs as Bernoulli's principle describes. The velocity of the fluid increases with pressure or potential energy. Bed materials (usually sand) are fluidized by the high velocity gas stream, and a secondary gas stream is often injected from the side of the bed to ensure a complete combustion. Simultaneously, fuels (e.g., coal particle, biomass) or optional sorbents (e.g., limestone, dolomite) are injected into the fluidized bed from the feeders.

However, there are also some disadvantages of fluidized beds:

i. Increasing the combustor height: FBC usually has thin and tall shapes that require more initial capital expenses.

ii. Pressure drop: more pump power is demanded to achieve a higher gas velocity.

iii. Particle entrainment and agglomeration: collision between particles, particles and bed walls, especially at a high velocity, generates fine particles. It is very difficult to separate and collect them. Moreover, agglomeration happens under high operating temperatures, which leads to serious accidents (defluidization) [56].

iv. Erosion: particle collision into combustor walls also leads to severe erosion that requires expensive maintenance and repairs.

v. Limited theoretical understanding: most of current FBC designs are based on empirical experiences; it is still a very challenging task to simulate a fluidized bed.

The general development trend of a novel technology follows a standard pattern (S shape) [63]. This curve can be divided into three stages: innovation, commercialization and maturation. The innovation stage has no physical application to market, and takes from 10 to 60 years [63]. The development slope in this stage is not steep. During the commercialization stage, spending in research and development (R&D) leads to dramatic improvements in quality and cost. The rate of R&D slows down when potential improvements start to exhaust, the technology is widely used, and markets become saturated. Finally, the technology achieves the matured phase.

i. Innovation

In 1922, the research of FBC began with the Winkler patent [51]. In the 1960s, R&D accelerated the development of FBC. In 1965, the first experimental bubbling fluidized bed (BFB) combustor was constructed. The test proved the concept and showed potential for reducing SO_x emissions. In the same year, an atmospheric FBC programs was initiated in the US. The Environmental Protection Agency (EPA) considered FBC technology as a low pollution combustion technology. The first R&D on circulating fluidized beds (CFB) started in Germany in the mid-1970s [64]. In 1979, the first industrial-scale CFB was developed by Foster Wheeler.

ii. Commercialization

Northern European countries were interested in the FBC technology since they would like to burn low quality biomass (e.g. peat, wood waste, and sludge). The wide use of FBC in Finland and Sweden started in the 1980s and 1990s, respectively.

iii. Maturation

Today, FBC is a mature technology. Potential future R&D directions include fuel flexibility, boiler reliability, and pollution control. Compared to CFB, future development of BFB is likely to be limited, with no major industrial interest. Currently, Alstom and Foster Wheeler are the two largest CFB manufacturers in the world. Both of them are active worldwide and in North America with Foster Wheeler dominating 5 of the 7 defined markets. Kvaerner is the market leader of BFB technology, followed by Foster Wheeler; both of them have their market in Scandinavia. Kvaerner is the market leader in Europe, and Foster Wheeler dominates the market in Asia and North America.

There are two approaches to scale up FBC. The first approach is to use multiboilers, with identical single boilers. The second way is to increase single boiler capacity. The motivation for scaling up is to achieve higher efficiency for CFB. The following considerations are important in CFB scaling up:

i. Fluidization in large cross-section areas

ii. Increasing efficiency of particle separation systems

iii. Optimization of fuel and air distribution

iv. Heat management (e.g., flue gas cooling, external heat exchanger)

Energy R&D often focuses on three “efficiencies”: combustion efficiency, boiler efficiency, and thermal efficiency. The combustion efficiency is defined as the ratio

between burned fuel and injected fuel. The boiler efficiency is the ratio between the amounts of heat absorbed by the working fluid (water/steam). The thermal efficiency is the percentage of the amount of electricity produced over electricity requirement in a total energy input. The combustion efficiency for CFB can reach up to 99%, higher than that for BFB, since CFB has a better mass and heat transfer efficiency compared to BFB. The range of boiler efficiency for FBC is from 75% to 92% (HHV) [65]. BFB and CFB share a similar principle, but their design parameters are quite different. The main design parameters are summarized by Koornneef et al. [51] in Table 3.

The design of an FBC depends mainly on the type of fuel, required gas steam velocity, pollution emission requirements, and manufacturing site. For example, the gas stream velocity in a CFB is much higher than that in a BFB. Moreover, particle size in a CFB is smaller than that in a BFB. As a result, the particle concentration is much lower in a CFB. The higher velocities and vigorous mixing in a CFB have a significant effect on heat transfer patterns. The heat and particle concentration distributions show a gradual decrease along with combustor height in a CFB, while there is a significant decrease in particle concentration with the height in BFBs. Thus, the temperature and mass profile in a CFB shows much more homogeneity. The combustion temperature in a BFB is lower due to poor fuel quality, greater particle size, and high moisture content.

Particle collection and recirculation is required in CFB. Due to a higher gas stream velocity, high particle concentrations are also found in the upper regions of CFB (e.g., freeboard section, convective pass). A cyclone has to be used to separate particles (e.g., bed materials, unburned solid fuel particles) from the flue gas stream for

recirculation. The recirculation greatly increases the residence time so as to achieve high combustion efficiency. Combustion temperatures were also adjusted by varying solid particle and flue gas circulating ratio. However, a cyclone cannot provide enough centrifugal force to capture super fine particles. The remaining gas stream with super fine particles is separated by ESP, bag house, or other particle collection facilities prior to discharge.

1.4. SO_2 emissions

According to the EPA [66], the majority of SO_2 emissions come from power plants (73%) and other industrial facilities (20%). SO_2 is harmful to the environment; e.g., the occurrence of acid rains. EPA started to regulate SO_2 emissions in 1971. Recently, mechanisms of SO_2 reduction were also studied under oxy fuel conditions due to the combined benefit of simultaneous reduction of greenhouse gases. The main sulfur source in coal can be categorized as organic or inorganic sulfur (pyritic, sulfide sulfate).

i. Organic sulfur

Organic sulfur is directly bonded with carbon atoms and accounts for about 30-70% in total sulfur content of US coals. Organic sulfur can only be removed by chemical separation approaches [67-69]. Some of these approaches are greatly effective, but are relatively expensive.

ii. Pyritic or sulfide sulfur

The majority of inorganic sulfur exists as pyritic (sulfide sulfur, FeS_2). Different from organic sulfur, pyritic sulfur can be partially removed by conventional gravity

flotation coal cleaning prior to combustion.

iii. Sulfate sulfur

Sulfate sulfur represents only a few percent of the total inorganic sulfur. Sulfate salts such as gypsum are present in small quantities (typically less than 0.01%), with the exception of iron sulfates, which are all formed by oxidation of pyrite during combustion.

Some of the most useful industrial approaches to control SO_x emissions are summarized here:

i. Pyritic sulfur is removed from coal using physical separation (flotation).

ii. SO_x during combustion is captured by injecting limestone directly.

iii. SO_x in the flue gas is removed using flue gas desulfurization after combustion.

iv. Coal gasification or liquefaction, followed by removal by absorption.

v. High sulfur coals are blended with low sulfur coals.

1.4.1. SO_2 formation mechanism during oxy and air firing combustion

Different operating conditions between oxy and air firing combustion can affect SO_2 emissions. In the past decades, theoretical and experimental studies have been performed to understand the mechanism of SO_2 emissions. Efforts have focused on simulation [20, 70, 71] , thermodynamics [71], flame characteristics [18, 21, 22, 32, 33, 72-74], and NO_x/SO_x formation [39, 75-81]. Contradictory observations were reported on SO_2 emissions under air and oxy firing conditions. Some researchers showed that SO_2 emissions were reduced during oxy firing [41, 76, 82]. In contrast, others found no difference in experimental studies or concluded so using equilibrium models [40, 71, 75,

79, 83, 84]. In particular, most studies [75, 76] have shown that oxy fuel combustion with recycled flue gas would result in a higher SO_2 concentration (in ppm) but a lower SO_2 emission per energy content (mg/MJ). Some researchers [24] suggested that the lower SO_2 emission be the result of a high conversion of SO_2 compared to other sulfur species, such as SO_3, in oxy fuel combustion. Sarofim [85] indicated that a high SO_2 concentration could result in a high sulfur removal by sulfation of ash under oxy fuel combustion. Furthermore, it was suggested that the difference in SO_2 emission between wet and dry recycled flue gases comes from SO_3 deposition onto cooling transport lines. A wet flue gas recycle would have a higher SO_2 concentration in the furnace, compared to a dry flue gas recycle, because returning SO_3 will inhibit SO_2 conversion to SO_3, especially through the high temperature reaction pathway.

Ahn et al. [86] investigated SO_x formation during oxy coal combustion using a 330 kW pilot-scale circulating fluidized bed (CFB) and a 1.5 MW pilot-scale pulverized coal combustor (L1500). Both combustors were equipped with RFG. Two different bituminous coals (a high sulfur Illinois coal and a low sulfur Utah coal) were studied. The concentration of SO_2 was found to be much higher during oxy fuel combustion, with the SO_3 concentration 4-6 times greater than that in air combustion when high sulfur coal (Illinois #6) was used. In contrast, the SO_3 concentration was similar for oxy vs. air firing using a low sulfur Utah bituminous coal. Kiga et al. [82] investigated ignition characteristics, flame propagation, and NO_x and SO_x emissions using a pulverized coal combustor with wet RFG. They fired three types of coals with O_2/CO_2 and air, and accounted for all sulfur content, including SO_2 and sulfur in ash. Their results showed

that the SO_2 emission in oxy fuel combustion is lower than that in air combustion. Croiset et al. [76] studied the implications of O_2/CO_2 recycle on NO_x and SO_x emissions. They used a 0.21 MW combustor with a recycled flue gas stream containing 5% excess O_2 (dry basis). The experiments were carried out for both wet and dry flue gases. When SO_2 emissions were based on mass, the SO_2 emission with RFG was 280 ng/J, which was lower than that (~320 ng/J) without RFG under O_2/CO_2 conditions. The SO_2 emission with wet RFG was found to be close to that with dry RFG, although a lower SO_2 emission was expected for the dry RFG case. When SO_2 emissions were based on concentration (ppm), the SO_2 concentration with RFG (~1750 PPM) was twice that without RFG (700-950 PPM) under O_2/CO_2 conditions. Croiset et al. [76] also reported that the SO_2 emission increased with O_2 concentration, although the effect was not significant. Zheng et al. [71] simulated combustors under air and oxy firing using the Facility for Analysis of Chemical Thermodynamics (FACT); no RFG was considered in these studies. They found no difference in SO_2 emission during oxy fuel combustion. The SO_2 emission depends on the O_2 concentration, not on the CO_2 concentration. Moreover, the SO_3 concentration increases with SO_2. Liu et al. [79] also compared oxy fuel combustion with air combustion using a 20 kW down-firing combustor in the absence of RFG. Conversion of coal-S to SO_2 ranged from 86-90%. The authors concluded that SO_2 emissions are independent of the nitrogen presence. The authors suggested that the slight difference in observed SO_2 emission was probably caused by the difference in the overall char burnout for different combustion diluent (N_2 or CO_2).

1.4.2. The mechanisms of SO_2 removal by limestone

The operating temperature of FBC can remove SO_2 directly with added limestone. Despite many earlier efforts, e.g., Borgwardt et al. [87-94], Dan-Johansen et al. [95-101], Silcox et al. [102-104], and Anthony et al. [105-109], the mechanisms for SO_2 removal by limestone is still not fully understood. Weisweiler et al. [110] listed the following parameters related to the SO_2 removal efficiency.

i. Chemical composition of limestone.

ii. Limestone calcination time and temperature.

iii. Physical properties of calcined limestone (free limes).

iv. Sulfation reaction temperature.

v. Sulfation mechanism (direct or indirect sulfation).

vi. Miscellaneous properties.

1.4.2.1. Direct sulfation and indirect sulfation

Figure 6 shows the current understanding of the overall mechanism of SO_2 capture by limestone. Generally, the sulfation mechanisms (direct or indirect) of limestone depend on whether the limestone is calcined. A direct sulfation takes place in an uncalcined state while an indirect sulfation happens with calcined limestone. Usually, in fluidized bed combustion conditions, a direct sulfation occurs in oxy fuel combustion due to CO_2 inhibition of the calcination step, and an indirect sulfation occurs in air combustion. During an indirect sulfation, $CaCO_3$ decomposes into CaO and CO_2, followed by the reaction of CaO and SO_2 to form $CaSO_4$. In direct sulfation, a high concentration of

CO_2 and/or a relatively low operating temperature inhibits the decomposition of $CaCO_3$. $CaCO_3$ directly reacts with SO_2 to form $CaSO_4$.

i. Indirect sulfation (CaO-SO_2)

- Step 1 Calcination of $CaCO_3$: $CaCO_3 \longrightarrow CaO + CO_2(g)\uparrow$
- Step 2 Formation of sulfite : $CaO + SO_2 \longrightarrow CaSO_3$
- Step 3 Oxidation of sulfite: $CaSO_3 + \frac{1}{2}O_2 \longrightarrow CaSO_4$

ii. Direct sulfation ($CaCO_3$-SO_2)

- Step 1 Formation of sulfite: $CaCO_3 + SO_2 \longrightarrow CaSO_3 + CO_2(g)\uparrow$
- Step 2 Oxidation of sulfite : $CaSO_3 + \frac{1}{2}O_2 \longrightarrow CaSO_4$

1.4.2.2. Calcination and carbonation

Direct or indirect sulfation is decided by the occurrence of calcination, which in turn is determined by operating temperature, CO_2 concentration, and pressure. A number of researchers have studied the equilibrium CO_2 pressure over limestone [111, 112] under thermal treatment.

A local high CO_2 concentration can inhibit calcination, such as in pores of a large particle or in interstices of a packed bed. Correspondingly, operating temperature can be increased to promote calcination. Similarly, at operating temperatures of FBC, the partial pressure of CO_2 plays an important role on calcination.

Properties of limestone and calcined limestone (free lime) have been studied extensively [113-120]. In natural limestone, $CaCO_3$ accounts for more than 90% of the weight, and void volume ranges from 3% to 35%. If particle shrinkage is negligible during calcination, the porosity of free lime is much greater than that of limestone. Sintering tends to occur at high operating temperatures, which clogs pores and decreases porosity and surface area. Also, kinetics of calcination was also studied [102-104, 118, 120]. The relevant parameters include:

i. CO_2 concentration, which promotes the reverse reaction, called recarbonation.
ii. Operating temperature.
iii. A total pressure, which increases CO_2 partial pressure and inhibits calcination.
iv. Particle size, which determines thermal and mass transfer limitations [121-123].
v. Catalysis and/or inhibition by impurities.

The operating temperature is determined by balancing calcination and sintering. The degree of calcination increased at high operating temperatures, which also promotes the occurrence of sintering. At certain temperatures, recarbonation is possible, which is the reverse reaction of calcination.

1.4.2.3. Sulfation mechanisms

A few mechanisms have been proposed [101, 102, 124-127]. The mechanism of direct sulfation is not well understood. Little else can be confirmed except for $CaSO_4$ as the final product [128]. Direct injection of limestone to the furnace is a very attractive option to control SO_x emissions using oxy firing. The efficiency of sulfation with a high

CO_2 concentration differs from air combustion. Tullin [129] observed in experiments the inhibition effect of a high CO_2 concentration during direct sulfation. Currently, the mechanism of direct sulfation is described by the same models used for indirect sulfation, i.e., shrinking core particle model, $CaSO_4$ production layer, and diffusion limited control.

Liu et al. [77, 78, 127] presented a drastic reduction of SO_2 emissions during oxy firing. They argued that limestone can maintain a high reactivity under a high CO_2 partial pressure. They made two assumptions: the high concentration of SO_2 inhibits $CaSO_4$ decomposition; secondly, the diffusion resistance through the $CaSO_4$ layer is minimized due to suppressed limestone calcination. The point was cited in several review papers [5, 130]. Their points are debatable. (1) The typical temperatures in CFBs (1073-1173 K) are relatively low for significant decomposition of $CaSO_4$. (2) Intrinsic sulfation kinetics of limestone with a high CO_2 concentration is much lower than that in N_2, according to Liu's paper [127]. Some of Liu's experimental results are reproduced in Figure 7. If Liu's second argument is correct, the crossover point of sulfation degree for his data takes place after 4500 seconds (1123 K), as shown in Figure 7. This is the time elapsed before SO_2 removal in oxy firing exceeds that in air firing due to the diffusion layer's effect. This effect should not be significant since SO_2 residence time in CFBs is only a few seconds. Moreover, the limestone injection is continuous in practical industrial applications.

A sulfation process can be both kinetically controlled and diffusion controlled, depending upon the temperature. The rate of SO_2 removal by limestone is determined by the intrinsic reaction rate and the $CaSO_4$ effective diffusivity, which are competing

factors. Which factor dominates depends on experimental conditions; e.g., properties of the limestone, operating temperature, environmental gas concentrations, particle size, the properties of the $CaSO_4$ product layer, and the change of porosity. The formation of a $CaSO_4$ layer inside the particle will block or shrink pores because $CaSO_4$ has a larger molar volume than CaO or $CaCO_3$. At the beginning, the system is dominated by the intrinsic rate. After a $CaSO_4$ layer is formed, diffusion control competes with kinetic control. The diffusion barrier becomes more important and finally dominates the process. Therefore, sulfation in smaller particles is likely to be dominated by intrinsic rate, while that in larger particles is dominated by diffusion. Sulfation is usually dominated by diffusion at high temperatures, because diffusivity of particle increases more slowly than reaction rate with temperature.

Snow et al. [126] investigated the direct sulfation mechanism using TGA with a high CO_2 concentration and Iceland spar limestone. They found that the diffusion resistance through the product layer at a high CO_2 concentration (direct sulfation) was significantly lower than that with CaO under a N_2 atmosphere (indirect sulfation). They explained that the difference was due to $CaSO_4$ product layer porosity variations between indirect and direct sulfation. CO_2 generated during direct sulfation can keep the pore open or at least delay the pore closure or shrinking. This explanation has been cited repeatedly by others to explain observed high porosity in the product layer in a direct sulfation. However, Hu et al. [128] doubted whether the CO_2 generated is responsible for the porosity during a direct sulfation. They argued that 1.5 moles of

gaseous reactants was consumed to generate 1 mole of CO_2. Thus, the direction of net flux was from surface to inner particle.

Wang et al. [131] investigated the effect of water vapor on the sulfation of limestone. Their experiments were carried out by TGA, with a wide range in particle size (75 to 425 μm) and a synthetic flue gas of CO_2 (15%), O_2 (3%), H_2O (0 or 10%), SO_2 (1750 PPM), and N_2 (balance gas). They observed that water vapor enhances the sulfation degree, which attained as much as 60%. They also found that water vapor has a more significant effect on diffusion controlled systems, compared to kinetically controlled ones, suggesting that a $Ca(OH)_2$ transition species (formed by CaO and H_2O) plays a role in enhanced sulfation. Partial work by Hu et al. [128] reviewed kinetics rates of direct sulfation, and their summarization was adopted in Table 4.

1.5. The application of a single particle model

Single particle models including reaction and diffusion have been used in many industrial and research applications, such as coal combustion, $SO_2/CaCO_3/CaO$ system, and chemical vapor deposition (CVD). A few models, e.g., homogenous particle model, shrinking core particle model, and multigrains models, were developed for various applications.

A gas-solid and diffusion-reaction single particle system includes the following steps:

i. External diffusion: Reactant gas species need to diffuse from the bulk gas to the particle surface through a gas film. During this step, the moving of reactant gas

species is limited by gas diffusivity inside the gas film in the absence of chemical reaction. Chemical reactions, sometimes, happen during diffusion. For example, for large coal particles, O_2 diffusing to the surface can react with CO released from the coal particle. Therefore, the single film coal particle model (for tiny particles) and double films (for large particles) were developed to model the reacting boundary layer.

ii. Internal diffusion: The reactant gases diffuse into a single particle through pores of the solid phase. This process is dominated by diffusion.

iii. Adsorption: Reactant gases are adsorbed on the surface of the solid phase by chemical bonding and/or physical bonding. Langmuir was the first person to develop the theoretical background of adsorption.

iv. Chemical reaction: Gas-solid heterogeneous reactions happen after gaseous species is adsorbed on solid surface.

v. Desorption: A gaseous product is released from a solid surface.

vi. Gaseous products diffuse out to the particle surface through pores.

vii. Gaseous products diffuse from the particle surface to bulk gas.

1.5.1. Shrinking core particle model and grains model

The shrinking core particle model and grains model are often used for large particles. Since there are temperature and concentration gradients inside a large particle, the particle has to be divided into several different zones, instead of a single zone. The shrinking core particle model includes two zones: a reacted zone (product

layer) and an unreacted zone. A shrinking core particle is assumed to be nonporous, which results in a sharp boundary layer during the particle evolution. This assumption makes the analysis of a nonporous solid system much easier compared to that of a porous solid system. In reality, a sharp boundary is not a good assumption since particles are usually porous with diffusion and chemical reactions co-existing in the diffusion zone. To get a more accurate description, the grains model is used to model porous single particles.

1.5.2. Single coal/char particle combustion model

Shaddix et al. [23, 132, 133] have done a lot of experimental and modeling work on single coal particles during the combustion. As suggested by Biggs et al. [134], the temperature of a char particle is determined by the heat and mass transfer coefficients between the char particle and bulk gas, the char combustion kinetics, and the particle-related CO/CO_2 product ratio. If the particle temperature is low and the particle size is relatively small, the mechanism is likely to be kinetics controlled. Accordingly, temperature and mass species profiles are assumed to be homogenous. Pulverized coal particle combustion is a good example. On the contrary, for high temperatures and large particles, it is likely to be diffusion controlled. A gradient of mass species and temperature is considered. The shrinking core particle model is useful to explain diffusion controlled mechanism, by dividing a coal particle into reacted and unreacted zones. Furthermore, particle size influences reaction rates at higher temperatures,

whereas at lower temperatures (<425 K for certain coals), the rate could be essentially independent of the particle size [135-137].

1.5.3. $SO_2/CaCO_3/CaO$ particle model

For $SO_2/CaCO_3/CaO$ single particles, three major groups of models were developed. The first group focuses on the change of voids in the particle (pore), the second group considers solid phases (grains) in a particle, and the last group focuses on the progress of reactions through a homogeneous particle. Sometimes, these models can be combined with a single particle model. For example, one can choose the grains model together with an evolution model of pore structure as reactions progress. The combined model will take the advantage of both submodels.

The diffusion of reactants or products through internal voids [116, 138-140] is an important component for a gas-solid and reaction-diffusion particle model. Three diffusivities are considered: molecular diffusion in large pores ($\approx 10^{-4} m^2 s^{-1}$ in magnitude), Knudsen diffusion in micropores ($\approx 10^{-6} m^2 s^{-1}$), and diffusion through a product layer ($CaSO_4$) ($10^{-11\text{--}13} m^2 s^{-1}$). The range of diffusivity coefficients accounts for mechanical defects in product layers, such as cracks [138].

An unreacted shrinking core model [141, 142] is the most frequently used model for the kinetics of a direct sulfation [124-126, 143-147]. This model is a simplified model for gas-solid reactions, and it assumes a sharp boundary between the unreacted core and the product layer. As discussed before, this assumption is only valid for nonporous particles [114, 148] .

Table 1 Estimated storage capacities and retention times for CO_2 in different types of sinks (adapted from reference [5])

Sink	Storage capacity (Gton C)	Retention time (years)
Enhanced Oil Recovery (EOR)	20-65	$10\text{-}10^6$
Deep aquifers with structural traps	30-650	$10^5\text{-}10^6$
Deep aquifers without structural traps	14,000	$10^5\text{-}10^6$
Coal beds	40-260	$10^5\text{-}10^6$
Depleted oil and gas wells	130-500	$10^5\text{-}10^6$
Ocean disposal	400-1200	500-1000

Table 2 Comparison of main characteristics of CCS √[6]

		IGCC	OFC
Suitable for retrofit of existing power plant	√		√
Application on slip-stream (i.e., partial CO_2 capture)	√	√	
Does not require O_2 supply	√		
Does not require CO_2 capture prior to compression			√
Generates H_2 as alternative fuel		√	

Table 3 Design parameters for BFB and CFB (adapted from reference [51])

Design parameter	BFB	CFB
Operating temperature (°C)	760-870	800-900
Fuel particle size (mm)	0-50	0-25
Fluidization velocity (m/s)	1-3	3-10
Solid circulation	No	Yes
Particle concentration	High in bottom, low in freeboard	Gradually decreasing along furnace height
Limestone particle size (mm)	0.3-0.5	0.1-0.2
Steam flow	36 (13-139)	60 (12-360)
Steam temperature	466 (150-543)	506 (180-580)
Steam pressure	72 (10-160)	103 (10-275)

Table 4 Rate expression and rate constant of direct sulfation reaction (adapted from reference [128])

Author	Experimental condition						Rate expression	Rate constant
	Temperature (K)	Pressure (Mpa)	size (mm)	SO_2 (%)	O_2 (%)	CO_2 (%)		
Snow[126]	773-1373	0.1	2-106	0.3	5	95	$k_s C_{SO_2}$	$0.72\exp^{(-64046/(8.314T))}$ m/s
Hajaligol [125]	773-1213	0.1	2-106	0.3	5	95	$k_s C_{SO_2}$	$1.5\exp^{(-68650/(8.314T))}$ m/s
Fuertes [149]	923-1173	0.1	2-106	0.25	3.6	96.4	$k_s p_{SO_2}$	$104\exp^{(-95700/(8.314T))}$ mol/(m^2s atm)
Krishnan[144]	1123	0.1	53-350	0.15-0.6	6	96.4	$k_s C_{SO_2}^{0.4}$	0.00031–0.0015 $mol^{0.6}/(m^{0.8}.s)$
Zhong [124]	1073	0.1	4-5.4	0.1-0.5	10	70	$k_s C_{SO_2}$	0.0049, m/s Ea=35.9 kJ/mol
Zevenhoven[147]	1123	1.5	250-300	0.3	4	20	$k_s C_{SO_2}$	0.0007–0.0014 m/s
Alvarez et[150]	1073-1198	1.2-2.5	100-595	0.5	3-7	12, 15	$k_s C_{SO_2}$	0.00011 m/s at 1073K 0.0003 m/s at 1198K Ea =87.2 kJ/mol
Liu[127]	883-1123	1.5	8.4-54	0-0.24	10	20-80	$k_s C_{SO_2}$	$19\exp^{(-90000/(8.314T))}$ m/s
Qiu[145]	1123	0.6	125-180	0.35	5	30	$k_s C_{so_2}^{0.58}$	0.00015 $kmol^{0.42}/(m^{0.26}$ s)

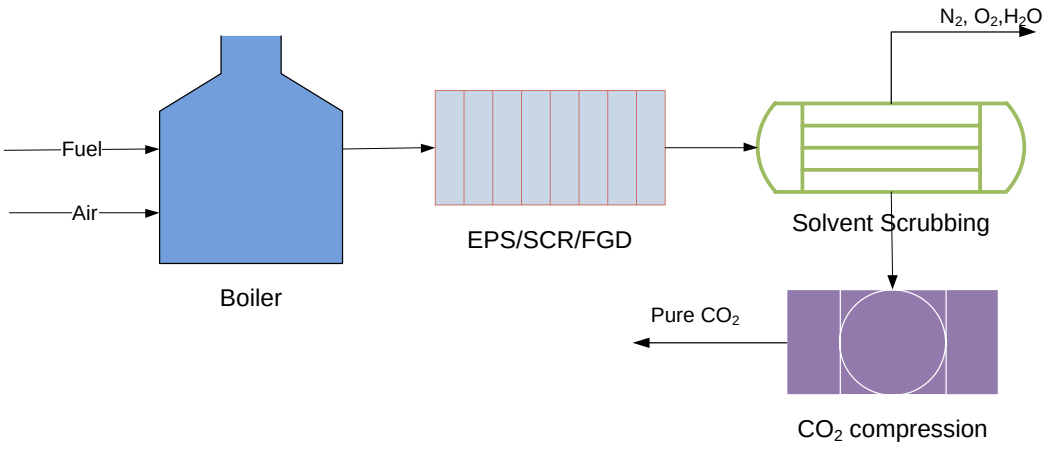

Figure 1 Schematic of postcombustion capture (PCC)

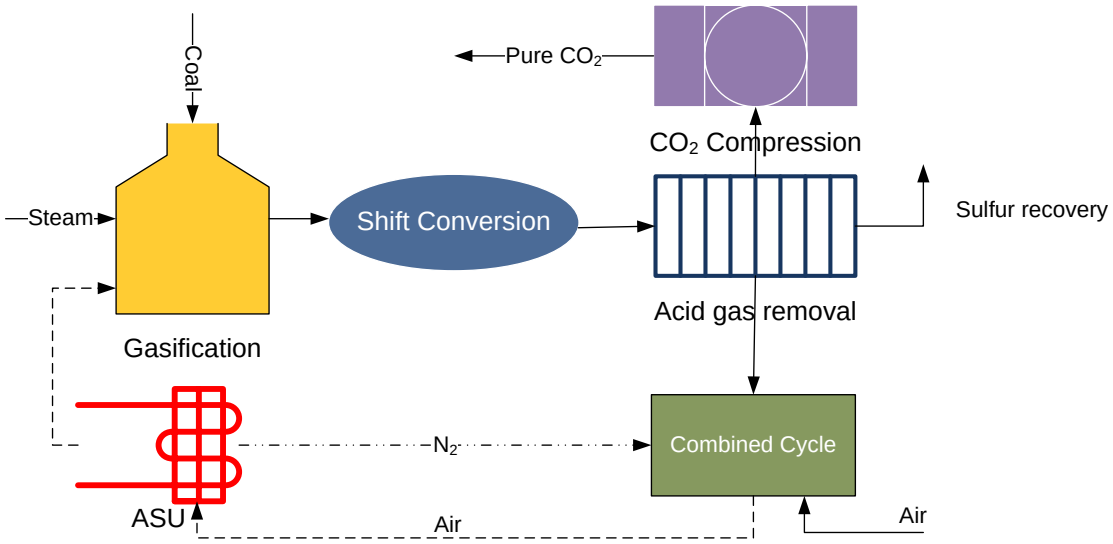

Figure 2 Schematic of precombustion capture (IGCC)

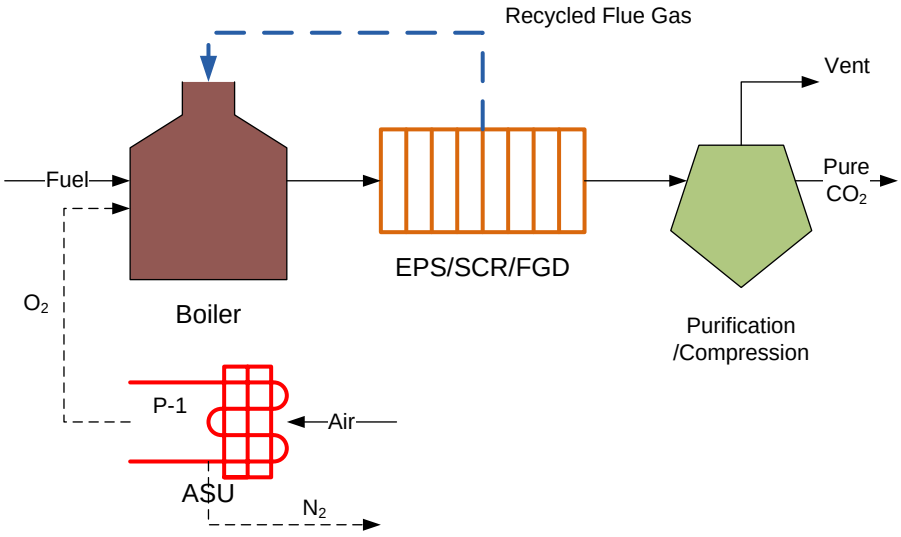

Figure 3 Schematic of oxy fuel combustion (OFC)

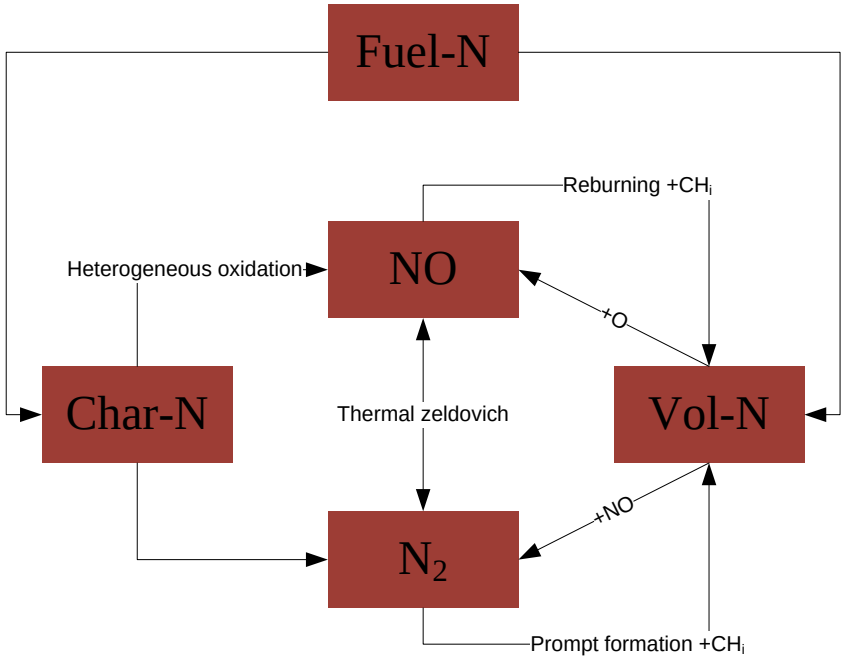

Figure 4 The Overall mechanism of NO formation and reduction [5]

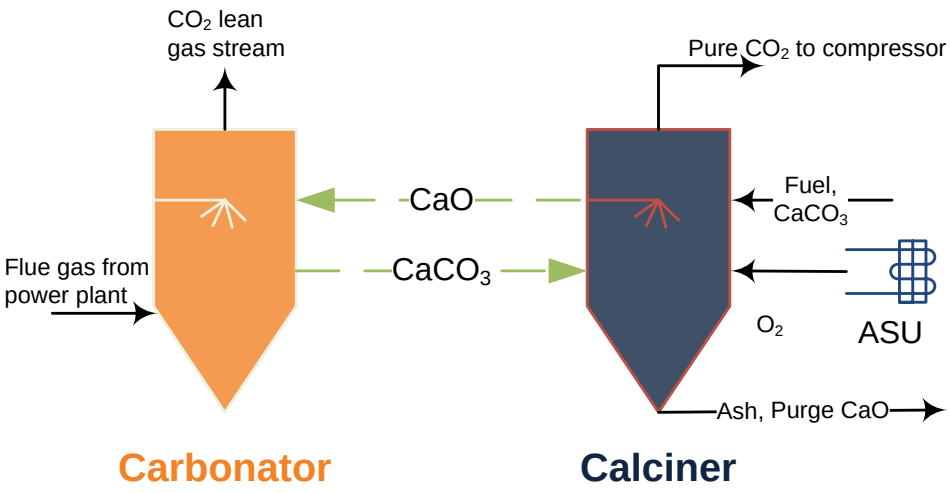

Figure 5 Schematic of the carbonate looping process

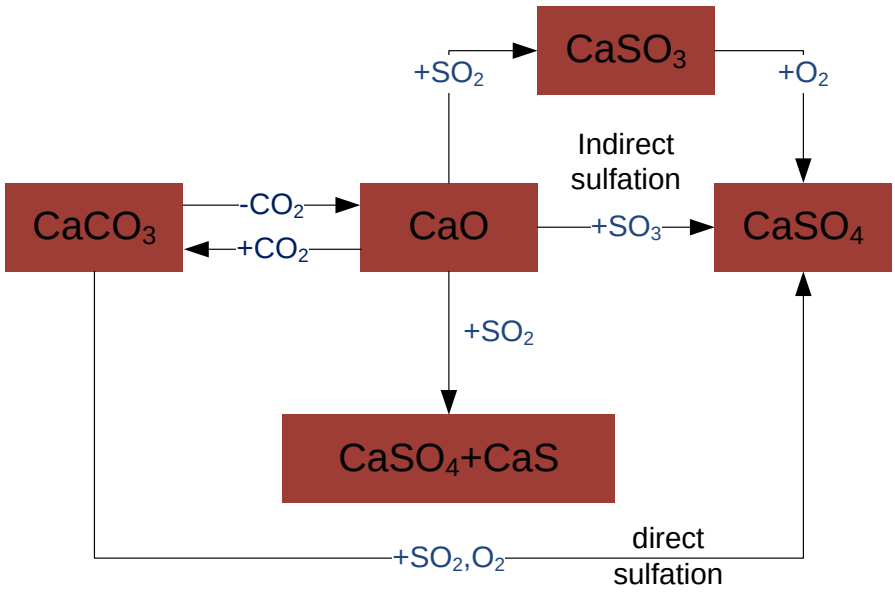

Figure 6 The overall mechanism of sulfation (indirect and direct sulfation)

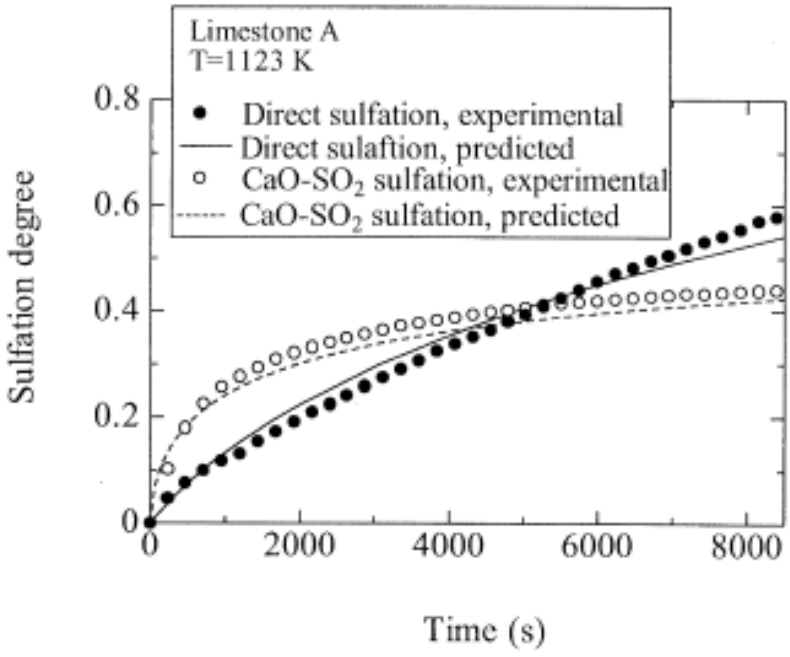

Figure 7 Sulfation degree in indirect sulfation and direct sulfation (adapted from reference [127])

CHAPTER 2

EXPERIMENTAL APPARATUS

2.1. Bench-scale bubbling fluidized bed (BFB)

In order to investigate transition SO_2 emissions from oxy or air firing combustors, a bench-scale single particle BFB was constructed. Compared with a pilot-scale FBC, a bench-scale BFB has its own advantages in cost and flexibility. The low operating cost enables us to repeat an experiment many times under the same conditions. Observational error is the difference between the true value and the measured value. It is always a huge challenge to reduce an observation error, which consists of random error and system error. Random error varies from observation to observation due to unpredictable fluctuations when reading an apparatus. The best way to reduce random error is to repeat the same measurement many times, averaging out the fluctuations. With enough repeated data points, a mean value can be derived that is very close to the true value. A bench-scale BFB reduces errors by facilitating repeat experiments. This is a strong advantage for fundamental studies, e.g., kinetics, thermodynamics, and fluid mechanics.

Flexibility of modification is another advantage of a bench-scale BFB. Ability to modify is essential during an experiment design to meet changing research goals. Modification of a pilot-scale FBC is complicated and expensive, and takes a long time to

realize. It is much easier and cheaper to modify a bench-scale BFB. The advantages in cost and flexibility make it possible to study transition emissions (NO_x or SO_x) during coal/char particle combustion.

Single particle coal combustion experiments were performed in a bench-scale BFB [39, 151]. The schematic of a bench-scale BFB is shown in Figure 8. It is a vertical, cylindrical, stainless-steel furnace with a combustion chamber of 771 mm and an inner diameter of 44 mm. The column has a 2 mm thick perforated plate distributor with 60 holes. Using a stainless lid with a clamp, it is easy to load coal particles into the bed. The gas flow rates were regulated by two digital mass flow controllers and were premixed before being introduced into the furnace. An electrical furnace provides the majority of thermal energy to the bed, supplemented by a heating tape. The furnace was heated to a desired temperature. The temperatures of bed materials, furnace wall, and gas phase are measured by K-type thermocouples connected to a digital temperature controller. The gas concentrations in the effluent are measured by a Magna-IR^{TM} Spectrometer 550 FTIR, after unburned fine particles and soot are removed by glass filter. The preheated furnace was purged by N_2/O_2 or CO_2/O_2 to maintain the same oxy or air firing conditions. A background spectrum of the purged gas was recorded after the change of combustion diluent.

2.1.1. Bed materials

Zirconium silicate ($ZrSiO_4$) ceramic beads' technical data are shown in Table 5. Their size and density are 250-425 μm and 3.86 g/cm^3, respectively, which are often

selected in FBCs. The majority of gas-solid reactions, FBC, and metallurgical phenomena are in this regime.

2.1.2. Electrical heating system

An FBC can be heated by either internal combustion or external heating supply. The pilot-scale CFB is heated mainly by coal combustion. An increased O_2 concentration (26-30%) in the primary gas stream (CO_2 + O_2) is required in oxy fuel combustion to match the temperature profile with air combustion. In contrast, the bench-scale BFB is heated mainly by an external electrical heating system, because the amount of coal is too small to provide enough heat.

A heating tape and an electrical heating furnace are used in the bench-scale BFB. A heating tape winding the bottom of the bed preheats the upward gas stream, and temperature is controlled by a K-type thermocouple connected with a temperature controller. Another thermocouple measures the temperature above the distributor plates with a controller to adjust the temperature of the reacting furnace. An external electrical heating furnace is used to heat up the fluidized bed evenly.

Since the temperature is controlled in the BFB, one can focus on the impact of combustion diluent (N_2 or CO_2) on SO_2 emission during oxy and air combustion. The heating system also affects the fluidization, because of the rapidly expanding gas volume leading to a higher gas velocity at the same mass flow. Before the design of a fluidized bed, the acceleration of the inlet gas stream due to external heating should be

examined carefully. In our experiment, the inlet gas is heated up gradually from ambient to about 1023—1173 K. The increased gas velocity led to a strong fluidization.

2.1.3. Gas mixture system: mass flow controller

Experiments were performed with various O_2 concentrations between 10 and 30%. The amount of various gases was controlled either by mass flow controllers or a tank of calibration gas. Calibration gas tanks will provide accurate gas concentration with, however, a high cost. Smart-trak series 100 mass flow controllers were used. In addition, a diameter of 6.4 cm and an effective area of 96 cm^3 filter holder is used to remove soot or fine particles before feeding gas into a FTIR.

2.2. Pilot-scale circulating fluidized bed (CFB)

The CFB at the University of Utah has been used to study fuel combustion and waste incineration. A flue gas recycle loop was added to accommodate direct oxy firing. The 330 KW CFB stands approximately 8.5m in height with an outer and inner shell diameter of 0.61m and 0.25m, respectively. As Figure 9 shows, the CFB consists of five main sections: plenum/distributor, lower bed (Sections 1 and 2), freeboard (Sections 3-6), transition/cyclone, and the loop seal/standpipe. O_2 can be injected from two oxidant lines into the furnace (primary, secondary).

Usually, the primary oxidant line was preheated up to 673 K using an electrical insertion heater, which is used to adjust the bed temperature. Air or flue gas (mainly CO_2) with enriched O_2 is introduced by the primary oxidant line passing through a distribution plate equipped with bubble caps. The bed materials were then fluidized

with limestone or coal particles. Meanwhile, coal was fed from a feed auger at the bottom of Section 3. Additional limestone was also injected using a second feed auger. An ash removal auger in Section 1 removed ash and excess bed material if the bed pressure was excessive. The cyclone efficiently separated effluent gas into a solid stream and a gas stream. The solids include limestone particles, unburned coal particles, and some bed materials, and were recirculated into the CFB. The system maintained enough pressure at the loop seals to push particulate matter into the CFB. The gas stream passed through a water-cooled heat exchanger, and divided into two steams in the bag house: an exhaust stream into the atmosphere, and recycled streams after mixing the pure O_2 stream, achieving the desired operating temperature. All oxidant lines can take in air or recycled flue gas, and were controlled by various valves and V-cones. In addition, CO_2 can be introduced to the loop seal lines.

Gaseous products were sampled at several locations (Sections 4-6 and the transition section). Temperatures at the sampling locations varied from 403 to 503 K to prevent SO_3 from condensing. The sample passed through a refrigerator to remove H_2O vapor before being introduced to gas analyzers. An online analyzer (CAI Model 601 NDIR) was used to determine the SO_2 content in the flue gas.

2.3. Gas measurement system

Multiple thermocouples and pressure meters measure temperatures and pressures at various locations. Gas flow rates are adjusted by electromagnetic valves, and gas samples are measured using on-line gas analyzers. Data are recorded by OPTO,

a manufacturing company specializing in hardware and software products for industrial automation, remote monitoring, and data acquisition. Before any gas sample is introduced into an analyzer, water vapor is removed by condensation to reduce the effect of water vapor. Gas samples pass through different analyzers, which are calibrated at regular intervals. California analytical model ZRH NDIR is used to measure CO_2 concentration. SO_2 concentration is measured by California analytical model 600 Nondispersive Infrared Analyzer (NDIR) and also by Western Research analyzer (UV). O_2 concentration is measured on-line by a Yokogawa Electric Corp. zirconia analyzer and a Rosemount paramagnetic oxygen analyzer.

2.3.1. Fourier Transform Infrared Spectroscopy (FTIR)

The structure of a chemical compound can be determined by their IR absorption. Gas species (e.g., CO_2, CO, SO_2) are detected simultaneously by a Nicolet 550 Magna Fourier Transform Infrared Spectroscope (FTIR). Contrary to Nondispersive Infrared Sensor (NDIR) which uses narrow wave numbers due to an optical filter, the wave number scan area of FTIR is much wider. Gas samples are analyzed through a gas cell with an IR light source and a modulator that “separates” the light into different frequencies. Consequently, it is possible for an FTIR to analyze different gases simultaneously. Compared to NDIR, FTIR is able to collect a larger amount of data at the same time, providing a reliable analysis given suitable calibration curves and correlation values.

FTIR does have some disadvantages. Firstly, FTIR is not sensitive enough to analyze a sub-ppm level gas content. Secondly, H_2O, CO_2, and CH_4 have super strong and wide absorbance peaks that can overlap other gases' absorbance area. In our experiments, the target gases (CO_2, CO, SO_2) are measured. It is necessary to clarify whether overlaps occur for those gases. Three calibration gases of CO_2 (2285-2390 cm^{-1}), CO (2065-2200 cm^{-1}), and SO_2 (1320-1400 cm^{-1}) balanced with N_2 were recorded by FTIR (Figure 10). The calibration curves of CO_2, CO, and SO_2 are performed in Appendix A. Omnic software is used to operate FTIR and analyze the data. A detector with mercury cadmium telluride (MCT, Hg-Cd-Te) is kept cooled to temperatures near 77K in order to reduce noise from thermally excited current carriers. There is a tradeoff among scan numbers, resolution, and collection time (Table 6). More scans lead to reliable averages, so that random error is reduced. Higher resolution means a narrower data space, indicating more data points are selected in a fixed range of wave numbers. A longer collection time is associated with higher resolution and scan numbers. Collection time is limited, however, during a transition combustion experiment to get evolution information from coal particles. Shorter collection time will reduce the resolution. In contrast, collection time is not relevant in the steady state, when data do not change over time. Thus, higher resolution and more scan numbers can be obtained. We used resolution (4) and scan number (8) in steady state experiments. It cost 9 seconds to record each spectrum. To obtain data in the BFB, a shorter collection time (4 seconds) was considered, with a corresponding scan number and resolution of 4 and 4, respectively.

2.4. Thermo gravimetric analyzer (TGA Q600)

A thermo gravimetric analyzer (TGA) is an instrument that records weight changes very accurately as a function of temperature. TGA Q600 was used to investigate limestone reactions (calcination and carbonation) with different CO_2 concentrations under a wide range of operating temperatures.

The Q600 provides measurements of weight change with a temperature ramp from room temperature to 1500 ˚C. TGA Q600 is a rugged, reliable, horizontal furnace with a perforated stainless steel cowling case. A sample cup and a reference cup were included in Q600. The horizontal purge gas system is regulated by a digital mass flow controller and integral gas switching, providing efficient removal of decomposition products from the sample area and preventing back diffusion. Exhaust gas ports can be readily connected to a MS for product identification. Platinum pans (40 and 110 µL) and ceramic cups (40 and 90 µL) are available for use with the Q600.

Ceramic cups (90 µL) were used in our experiments. In carbonate looping experiments, the calibration CO_2 gas tanks (20, 50, and 100%) balanced with N_2 provide the desired gas composition. In order to get more CO_2 concentrations, rotameters were used to mix CO_2 with a balanced N_2. The flow rate of the purge gas was set at 100 mL/min before a desired gas composition was supplied when the experiment begins.

2.5. Scanning electron microscope (SEM)

A FEI NovaNano FEG SEM 630 was employed to identify sulfated limestone microstructures. The Energy Dispersive X-Ray Spectrometer (EDS) provided the sulfur

distribution of the sulfated limestone. The sulfated limestone particle had to be cut in half for SEM, so the inside microstructures and sulfur distribution could be studied.

Table 5 Technical properties of zirconium silicate ($ZrSiO_4$) ceramic beads (BSLZ-3)

Property	Technical data
Specific weight	3.86 g/cm^3
Particle size	250 – 425 µm
Bulk weight:	>2.35 kg/ltr
Sphericity	≥96%
Melting point	≥2200 ^oC
Hardness	Mohs >7.2
Chemical composition	ZrO_2 (68.5%) SiO_2 (31.5%)

Table 6 Scan numbers, resolution, and collection time

Scan numbers	2	2	4	4	8	8
Resolution	2	4	2	4	2	4
Collection time (second)	4	2	8	4	17	9

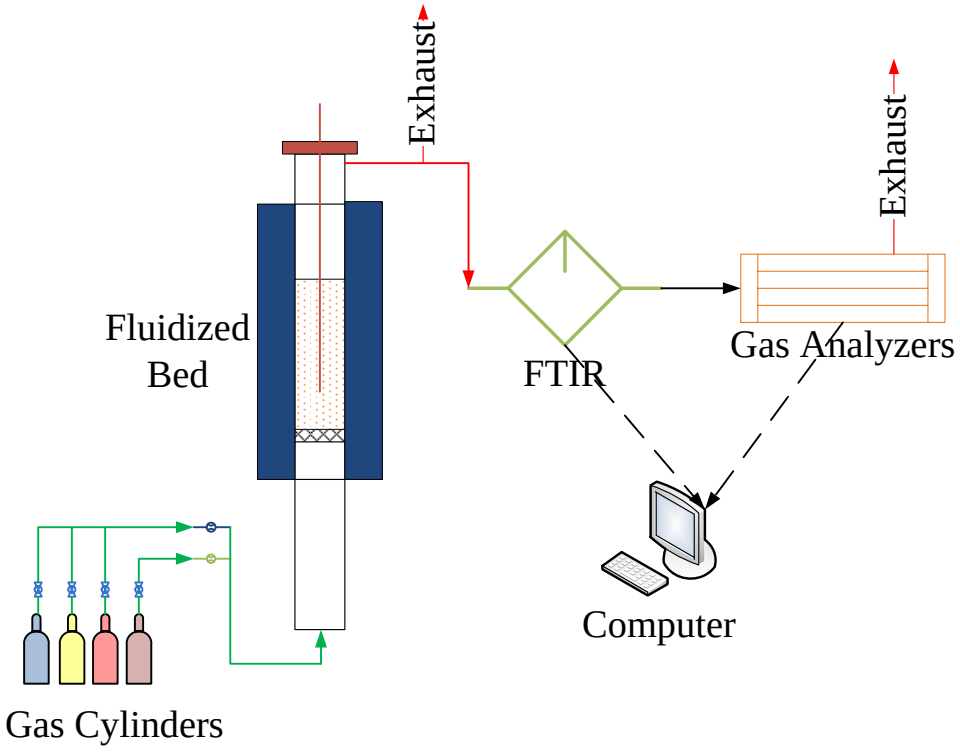

Figure 8. Schematic of the bench-scale bubbling fluidized bed (BFB)

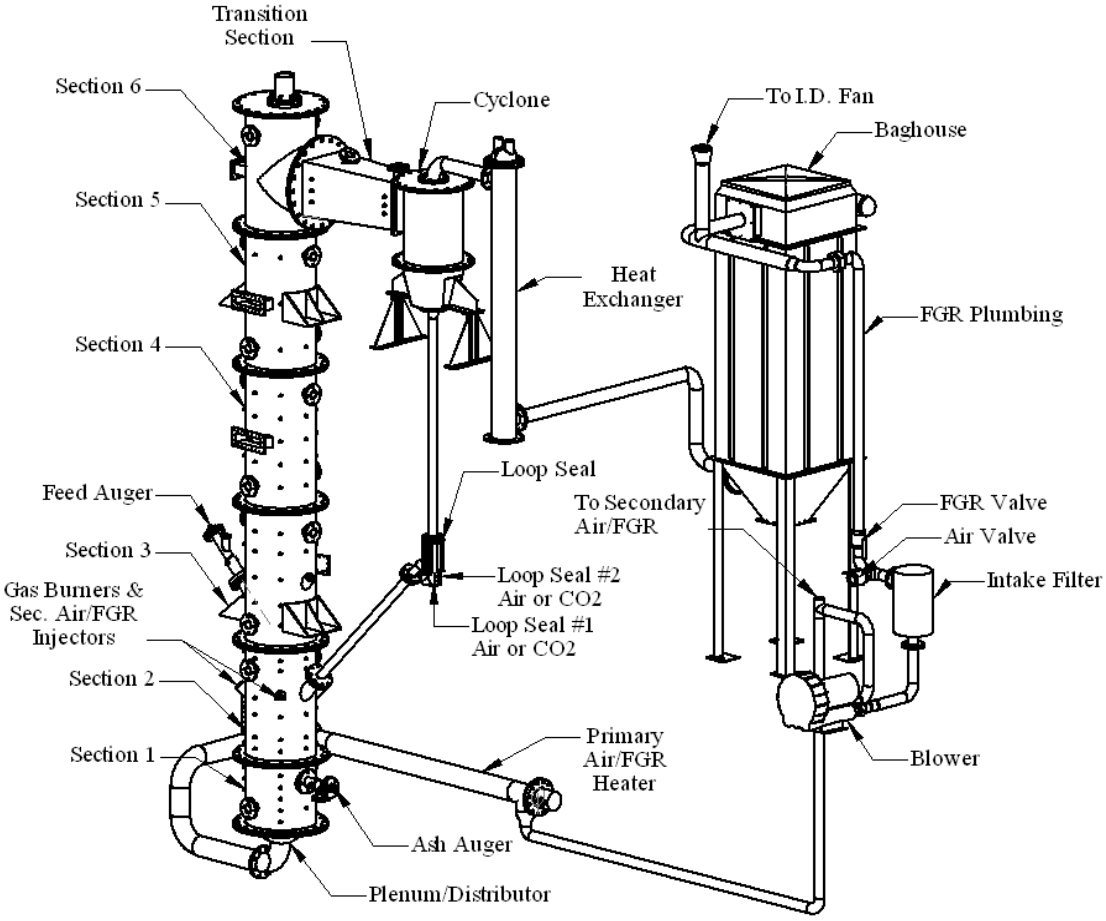

Figure 9 Schematic of pilot-scale circulation fluidized bed (CFB)

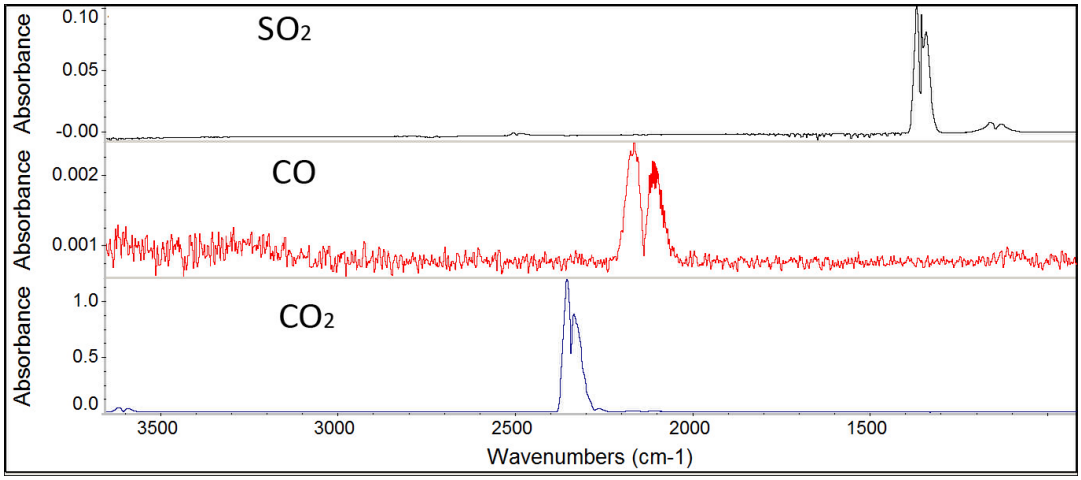

Figure 10 FTIR spectrum of SO_2 (upper), CO_2 (middle), and CO (bottom)

CHAPTER 3

SO_2 EMISSIONS IN OXY VS AIR COAL COMBUSTION

Coal combustion generated SO_2 is a regulated emission that is harmful to the environment. Hence, great efforts have been made in the last several decades to understand the mechanism of SO_2 emissions. Fluidized bed operation using oxy fuel or airfuel combustion has been well studied [152-165]. Contradictory observations regarding SO_2 emissions were reported. Some researchers [41, 76, 82] showed that SO_2 emissions are decreased in oxy firing combustion. By contrast, others [71, 79, 83] found no difference based on experimental observations and equilibrium models. In particular, most studies [75, 76] have shown that OFC with RFG leads to a higher SO_2 concentration (ppm) but a lower SO_2 emission on a mass (mg/MJ) basis, likely due to a higher conversion of SO_2 to other sulfur species, such as SO_3 [24]. Sarofim [85] indicated that a high concentration of SO_2 in OFC could result in a high sulfur removal by sulfation of ash.

3.1. Technical approach

Both research projects ("oxy coal single particle combustion: fluidized bed" and "pilot-scale oxy coal circulating fluidized bed combustion") were funded by the U.S. Department of Energy (DOE), with additional funding support from Praxair, Inc. Due to

the operational cost, only a few experiments were carried out in the pilot-scale circulating fluidized bed (CFB). We anticipate a clear comparison between air and oxy firing combustion in terms of SO_2 emissions.

It is important to understand the mechanism of SO_2 emission during oxy and air firing coal combustion in FBC. Otherwise, we will not be able to draw correct conclusions for SO_2 emissions when combustion conditions are changed, e.g., limestone addition or RFG. A bench-scale BFB and a pilot-scale CFB were used to investigate SO_2 emissions during oxy and air firing combustion. We highlight some major differences in these two experiments:

i. Most of the thermal energy comes from coal combustion in the pilot-scale CFB, while the electrical heating system is the main thermal source for the bench-scale BFB.

ii. RFG is adapted in the pilot-scale CFB, but not in the bench-scale BFB.

iii. The sources of combustion diluent (CO_2) for dilution were different. The pilot-scale CFB is equipped with a RFG. CO_2 from RFG dilutes the pure O_2 stream to prevent the equipment from being overheated. In the bench-scale BFB, CO_2 comes from the CO_2 gas tank, without a RFG feed.

iv. RFG brings impurities back to the CFB. The amount of impurities (e.g., SO_x, NO_x, fly ashes) in the pilot-scale CFB with a RFG is much higher than that in the bench-scale BFB without a RFG.

v. O_2 concentration in the pilot-scale CFB is higher than 21%, leading to the same temperature profile as in the air firing case.

In order to explore the effects of combustion diluents (CO_2 or N_2) and other factors, such as RFG, on SO_2 emissions, we have conducted the following studies:

i. The impact of O_2/CO_2 and O_2/N_2 environments on SO_2 emissions was investigated in a bench-scale BFB with a wide range of temperatures (1038 −1175 K) and O_2 concentrations (10-30%).

ii. We examined how temperature affected SO_2 emissions.

iii. The O_2 concentration in the oxidant stream (O_2/CO_2) was varied in order to attain the same temperature profile as in the air firing case.

iv. The level of SO_2 emissions during oxy and air firing combustion in terms of concentration (ppm) and mass (mg/MJ) were studied in the pilot-scale CFB.

v. SO_2 emissions from a bench-scale BFB and a pilot-scale CFB are investigated through comparison.

vi. An equilibrium model using NASA's Chemical Equilibrium with Applications (CEA) programs complement the study to simulate SO_2 emissions for both oxy and air firing cases.

3.2. Materials and methods

This section includes experimental installation, preparation of coal particles for the bench-scale BFB, design of the experimental matrix, and equilibrium model calculation.

3.2.1. Experimental installation

Single particle coal combustion experiments were carried out in a bench-scale fluidized bed [39, 151]. The details of the experimental apparatus are provided in

Chapter 2, which is summarized here. The bench-scale fluidized bed is a vertical, cylindrical, stainless-steel furnace. The effluent of CO_2, CO, and SO_2 was measured online by a Nicolet Magna-IR^{TM} Spectrometer 550 FTIR. A FTIR collects samples quickly enough that it can track the rapid evolution of sulfur and interdiluents. The spectrometer with a range of 650-4000 cm^{-1} is equipped with a mercury cadmium telluride detector cooled by liquid nitrogen. The software, Omnic version 5.2, is used to analyze the spectra. The experimental procedure is also summarized here:

i. The MCT detector in the FTIR was cooled by liquid N_2 to a low temperature.

ii. Scan number and resolution were set to be 4, 4, respectively, corresponding to a spectrum collection time of about 4 seconds.

iii. Two streams were mixed to obtain one stream (CO_2/N_2+O_2) with a desired O_2 concentration. A total flow rate was set to be 4 liters/min.

iv. The premix gas stream passed through the BFB and was scanned as a background spectrum prior to the combustion experiments.

v. The furnace is preheated, to achieve the desired operating temperature.

vi. About 0.12 grams of coal particles were put into the hot reactor, and then we closed its lid as quickly as possible.

vii. The effluent gas was scanned by FTIR.

viii. The spectrum data were analyzed by software Omnic version 5.2.

3.2.2. Preparation of single coal particles

Illinois #6 coal and Utah skyline coal were used in our experiments. The elemental and ultimate analyses of these two coals are shown in Table 7. To prepare single particles, a chunk of Illinois #6 coal was smashed by a hammer. Certain particles were selected by two stainless sieves. Their size range of 3.4-4.6 mm was selected, and sealed in a plastic bottle to prevent moisture from the air.

3.2.3. Design of experimental matrix

Although SO_2 emissions are the most fundamental issue of sulfur evolution during oxy fuel combustion, contradictory observations of SO_2 emissions have been reported [41, 75, 76, 82, 166, 167]. We carried out a series of 24 experiments using a BFB to study the sulfur evolution from Illinois #6 coal. Table 9 provides the experimental conditions. We used a wide range of temperatures between 765−902 ^{o}C and O_2 concentrations from 10 to 30%.

Because of the variation of sulfur content in coal particles, each experimental condition was repeated five times to obtain an average and an error bar. This was made possible using a BFB because of its low operating cost. Repetition reduces the random error. Premixed gases (N_2+O_2 or CO_2+O_2) were introduced into the bottom of the reactor, and passed upward through the distributor plate. About 0.12 g of coal particles was introduced into the reactor, which contained approximately 300 g of bed materials.

3.2.4. Equilibrium model: CEA programs

NASA's CEA program calculates product concentrations from any set of reactants and determines thermodynamic and transport properties for the product mixture [168]. Although the CEA program can provide the final product concentrations, it is still helpful in studying SO_2 formation.

A wide range of combustion temperatures and O_2 concentrations were considered in our Illinois #6 coal particles simulation (0.12 grams, Table 10). The flow rate is 4 liters/min and the total reaction time is 1 minute, which leads to a total gas volume of 4 liters. Two types of combustion are performed: air firing (N_2/O_2) and oxy firing (CO_2/O_2). The equilibrium calculation was expected to show the effects on SO_2 behavior of the following parameters:

i. Combustion diluent (CO_2 or N_2)

ii. Temperature

3.3. Results and discussion

We were interested in the effects of combustion diluent (CO_2, N_2) and temperature on SO_2 emission in a bench-scale BFB. As a comparison, some experiments using a pilot-scale CFB showed a difference in SO_2 emission in terms of concentration or mass. An equilibrium model was used to provide complementary information in identifying the most important parameters of SO_2 emission.

3.3.1. SO_2 emission in bench-scale BFB

3.3.1.1. Oxy versus air firing

Single particle coal combustion showed the transition nature of SO_2 evolution. A comparison of SO_2 emission during oxy and air firing processes is shown in Figure 11—Figure 22 with a combination of three O_2 concentrations (10, 20, 30%) and four temperatures (765, 835, 874, 902℃). SO_2 concentration (ppm) in the effluent is plotted as a function of residence time. The red curve with hollow circles represents the oxy firing process, and the blue curve with hollow diamonds for air firing. Coal combustion is a transition process, starting with drying and progressing through heating, devolatilization, and oxidation of volatiles and char. The moisture content is released right after coal particles are introduced. Devolatilization follows as volatile components from coal evolve, including organic sulfur. Gaseous organic sulfur reacts with O_2 to form SO_x, mainly SO_2. Particles get hotter, and the reaction rate increases exponentially with temperature. After devolatilization, the residual char continues to release a lot of heat by oxidation as the particle reaches a maximum temperature. Reaction heat disperses by radiation and convection. At that time, inorganic sulfur starts to react with O_2 assuming to form mainly SO_2.

Figure 11 shows that SO_2 is released mainly within the first minute, but the full burning out of char requires a few minutes, depending on experimental conditions. It is interesting to note that sulfur evolves more rapidly than carbon during single particle fluidized bed coal combustion. At the time of coal introduction, a low particle temperature results in a low sulfur emission. Coal particles are rapidly heated up first by

the surroundings, then by the reaction heat after ignition. The SO_2 emission reaches a maximum level between 6 to 12 seconds, and decreases when sulfur is depleted. In Figure 11—Figure 22, we compared SO_2 emissions between oxy fuel and air combustion. Little difference was found. Slight differences in some cases are likely experimental errors, resulting from coal particle sampling, experimental handling, or data reading. The overall pattern of SO_2 emission should be the same for both cases. Different combustion diluent (N_2, CO_2) leads to very similar SO_2 evolution profiles, for tests in the absence of recycle. However, some figures (Figure 15, Figure 17, Figure 19, Figure 20, and Figure 21) show a noticeable difference in their chronological order of highest peak. The cause is believed to result from experimental operation. Especially at higher temperatures, the rates of SO_2 emission should be relatively fast. A coal particle is put into the furnace, then the lid of the furnace is closed and a scan for emissions is started. It is very hard to ensure the consistency for the first measured point of the FTIR in all experiments, which results in the difference of the chronological order of the highest peak.

3.3.1.2. Temperature effects on SO_2 emission

The total SO_2 emission increases with temperature for both air and oxy firing combustion, as shown in Figure 23 and Figure 24, in the absence of recycle in a bubbling fluidized bed reactor. The lower emission at lower temperatures maybe results from a higher sulfur capture by ash. In addition, sulfur can remain in coal particles when particles are not completely burned out at low temperatures. Unfortunately, sulfur

content in the ash was not analyzed, and we cannot make a decisive conclusion on this issue.

3.3.2. SO_2 emission in a pilot-scale CFB

We compared SO_2 emission results from a pilot-scale CFB with that from a bench-scale BFB at a similar temperature profile as air firing. We operated those experiments at a similar temperature profile for air firing and oxy firing cases.

3.3.2.1. Measured SO_2 emissions

SO_2 concentrations (in ppm) were measured and compared for both cases in Figure 25. It is obvious that the oxy firing experiment (26% O_2) gave higher concentrations (600 - 1400 ppm) in comparison with 200-400 ppm for the air firing case. The SO_2 emission is 2—4 times higher during the oxy firing combustion. Since recycle flue gas (RFG) is equipped in the oxy firing case, instead of the air firing case, some SO_2 in the flue gas is recycled into the CFB, increasing SO_2 concentration (ppm). In addition, a comparison of the total SO_2 emission in terms of mass (lb/MMBtu) is shown in Figure 26. Generally, a mass unit is often used in industrial and environmental emission reports. SO_2 emission is lower in oxy firing combustion in terms of total SO_2 mass. The increased SO_2 concentration (ppm) in the oxy firing case could enhance the ability of SO_2 removal by fly ash.

3.3.3. Comparison of SO_2 emission between BFB and CFB with RFG

From experimental results presented earlier, different emission patterns exist between a bench-scale BFB and a pilot-scale CFB. No difference was found in SO_2 emission during oxy and air firing combustion using the bench-scale BFB. In contrast, for the CFB, the SO_2 emission is higher in the oxy firing in terms of concentration, but is lower in terms of total mass. Inconsistent results have been reported as well in many publications.

In our experiments, there are two major differences between the BFB and CFB: combustion diluent (N_2, CO_2), and operation with or without RFG. We designed the BFB to determine the critical parameter that affects SO_2 behavior using single factor experiments. We concluded that combustion diluent (CO_2, N_2) had negligible effects on SO_2 emissions. We added RFG in a pilot-scale CFB, and replaced N_2 in the air. Inevitably, an RFG stream also recycles pollutants (e.g., SO_x, NO_x, impurities and fly ash), and, therefore, increases concentrations of these species significantly, plus a decrease in overall volume. This explains the higher SO_2 concentration under oxy firing conditions. Because of the increasing concentrations of SO_x and fly ash, RFG will enhance the SO_x removal by fly ash. The SO_2 emission with RFG is lower in terms of total mass.

3.3.4. SO_2 emission estimated by an equilibrium model

We used the CEA programs developed by NASA to calculate SO_2 emissions under various conditions. A wide range of temperatures (600-1100 ^{o}C) was selected, as well as 2 combustion diluents of CO_2/O_2 or N_2/O_2. Illinois #6 coal was investigated, whose

elemental composition is shown in Table 7. The gas flow rate is selected as 4 liters/minute, and the reaction time is taken as 1 minute. Coal particle weight is 0.12 gram. O_2 concentrations are selected as 10, 20, and 30%, balanced with N_2 or CO_2.

Figure 27—Figure 29 show that SO_2 and SO_3 emission data superimpose on each other for oxy and air firing cases. The temperature effect on SO_2 emissions was also examined using the CEA programs. SO_2 emissions increase with an increasing temperature at the temperature range of 600-1100 ^oC, while SO_3 emissions decrease with increasing temperature in this temperature range. However, combustion diluent (N_2 or CO_2) has no apparent effect on SO_2 or SO_3 emissions in terms of equilibrium model calculations. For the temperature range (600-1100 ^oC), the explanation for SO_2 increasing with an increasing temperature is because SO_3 is decreasing with an increasing temperature.

3.4. Summary

Some conclusions can be made after analyzing data from a bench-scale BFB, a pilot-scale CFB, and an equilibrium model.

i. The bench-scale experiments without RFG show no effect of combustion diluent on SO_2 formation.

ii. In the pilot-scale CFB, SO_2 concentrations are higher when oxy firing, but SO_2 emissions in terms of mass (lbs/MMBtu) are lower when oxy firing. The difference results from RFG.

iii. The CEA equilibrium model shows no effect of combustion diluent (N_2, CO_2) on SO_2 emissions.

iv. The model also shows a positive correlation between temperature and SO_2 emission.

v. At 26% O_2 concentration (wet basis with RFG) during oxy firing, the average temperature in the fluidized bed matches very well the air firing reference. Therefore, we used a 26% O_2 concentration for oxy firing operation to match air firing.

Table 7 Ultimate and proximate analyses of Illinois #6 coals (wt.%).

Loss on drying	Ash	C	H	N	S	O	Volatile matter	Fixed carbon	HHV (Btu/lb)
9.65	7.99	64.67	5.59	1.12	3.98	16.65	36.78	45.88	11598

Table 8 Analysis of ash from Illinois #6 coal (wt.%).

Al	Ca	Fe	Mg	Mn	P	K	Si	Na	S	Ti
Al_2O_3	CaO	Fe_2O_3	MgO	MnO	P_2O_5	K_2O	SiO_2	Na_2O	SO_3	TiO_2
17.66	1.87	14.57	0.98	0.02	0.11	2.26	49.28	1.51	2.22	0.85

Table 9 Experimental matrix for SO_2 formation in air vs. oxy combustion

Experimental parameters	
Temperature in BFB (℃)	765, 835, 874, 902
O_2 concentration (vol %)	10, 20, 30
Combustion	Air firing (N_2/O_2), oxy firing (CO_2/O_2)
A total flow gas rate (liter/min)	4
Coal	Illinois #6 (~4.0% S)
Coal particle weight (grams)	0.12 (avg.)
Coal particle size (mm)	3.4−4.6
Bed materials	zirconium silicate (BSLZ-3)
The weight of bed material (grams)	300

Note: each experimental condition was repeated 5 times

Table 10 Simulation matrix for SO_2 formation in air vs. oxy firing

Simulation parameter	
Type of coal	Illinois #6
The weight of coal (grams)	0.12
Total gas volume (liter)	6
Temperature in BFB(℃)	600,700, 800,850,900,950,1000
O2 concentration (vol %)	10, 20, 30
Type of combustion	air firing (N_2/O_2), oxy firing (CO_2/O_2)

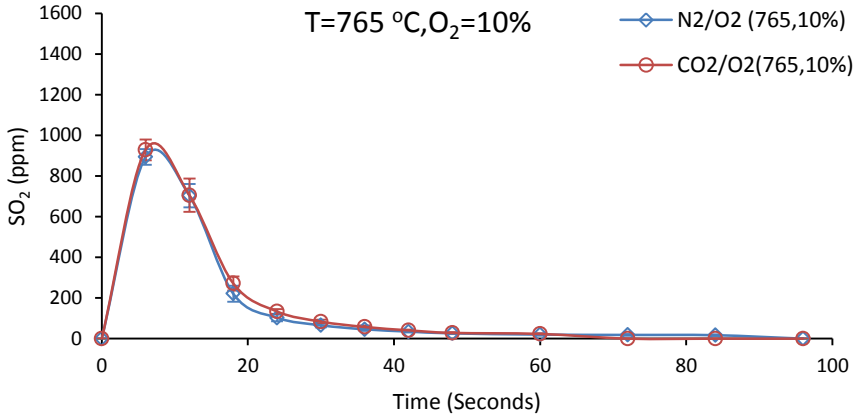

Figure 11 SO_2 emission in oxy vs. air firing (T=765 °C , O_2=10%)

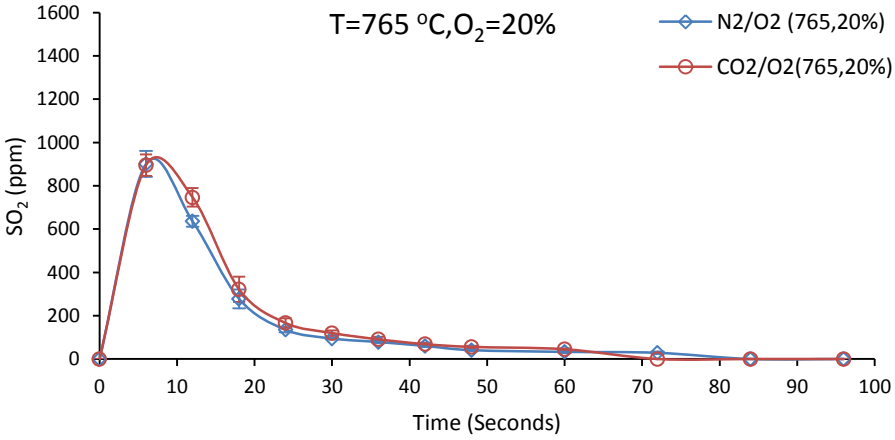

Figure 12 SO_2 emission in oxy vs. air firing (T=765°C, O_2=20%)

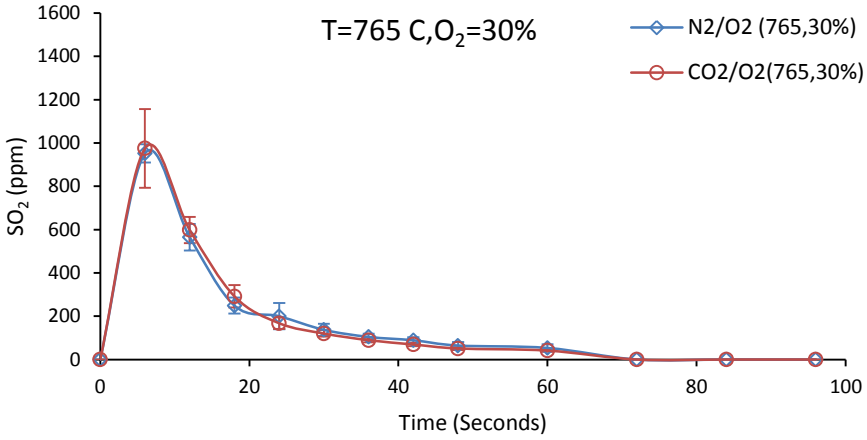

Figure 13 SO_2 emission in oxy vs. air firing (T=765℃, O_2=30%)

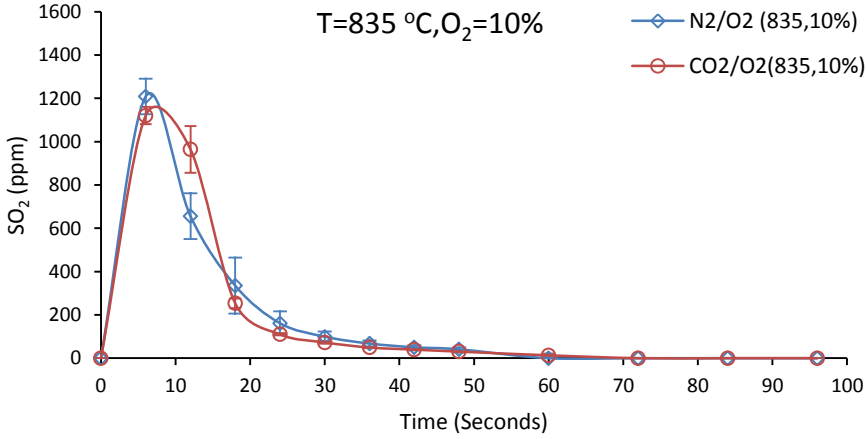

Figure 14 SO_2 emission in oxy vs. air firing (T=835℃, O_2=10%)

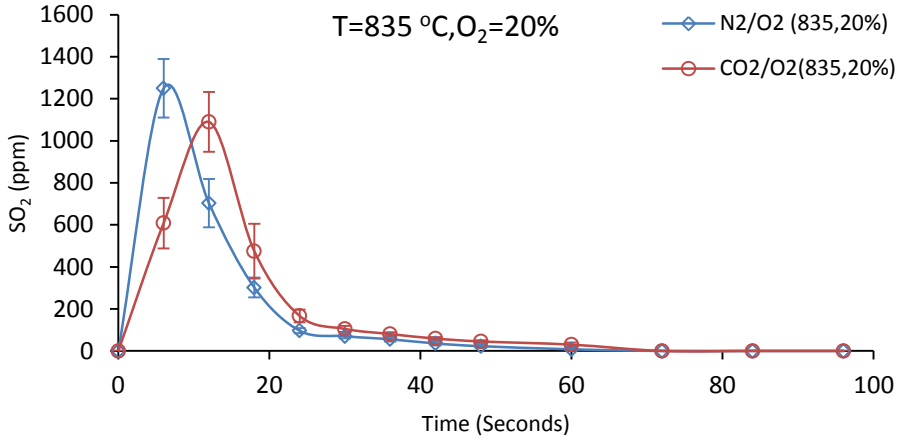

Figure 15 SO_2 emission in oxy vs. air firing (T=835°C, O_2=20%)

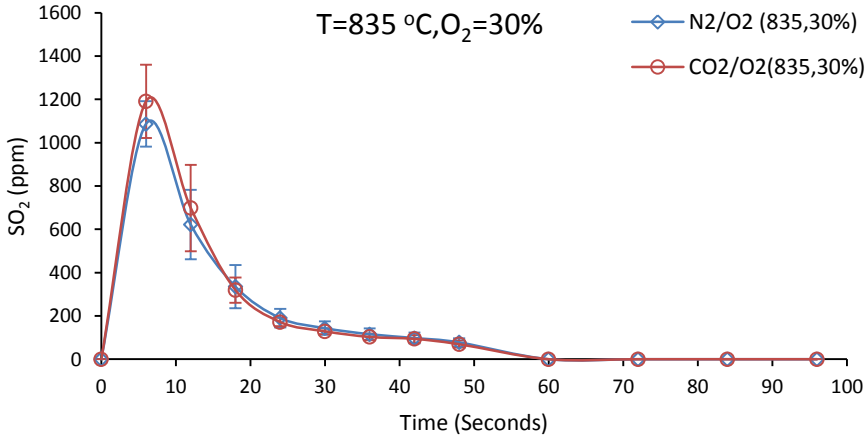

Figure 16 SO_2 emission in oxy vs. air firing (T=835°C, O_2=30%)

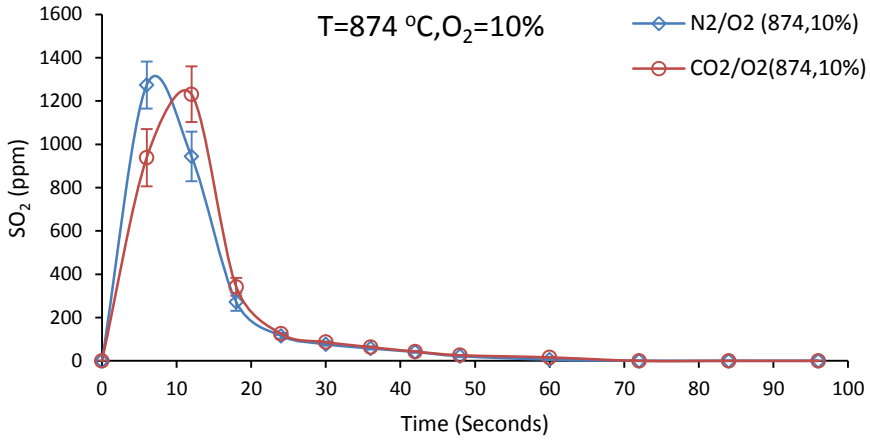

Figure 17 SO_2 emission in oxy vs. air firing (T=874°C, O_2=10%)

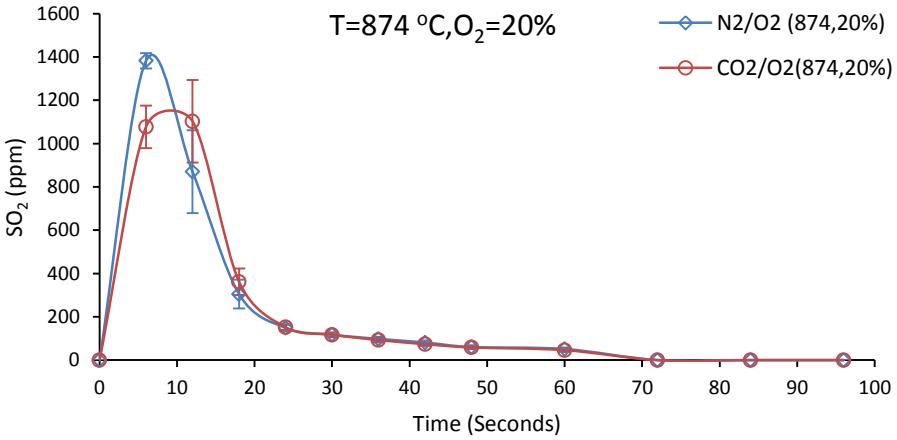

Figure 18 SO_2 emission in oxy vs. air firing (T=874°C, O_2=20%)

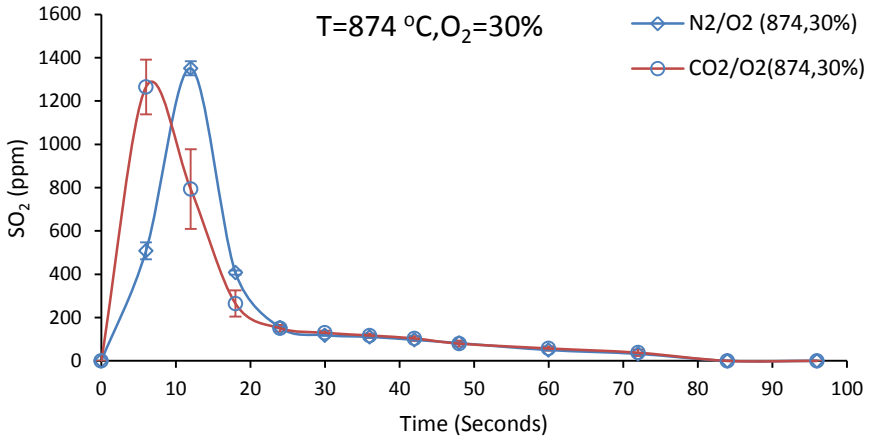

Figure 19 SO_2 emission in oxy vs. air firing (T=874°C, O_2=30%)

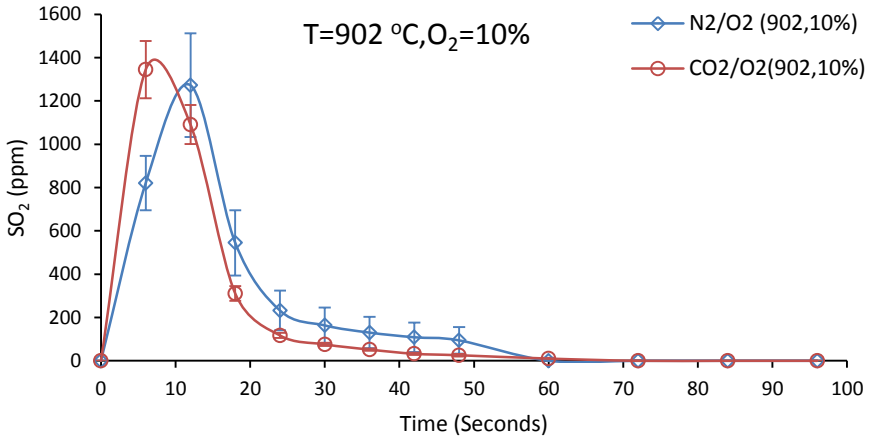

Figure 20 SO_2 emission in oxy vs. air firing (T=902°C, O_2=10%)

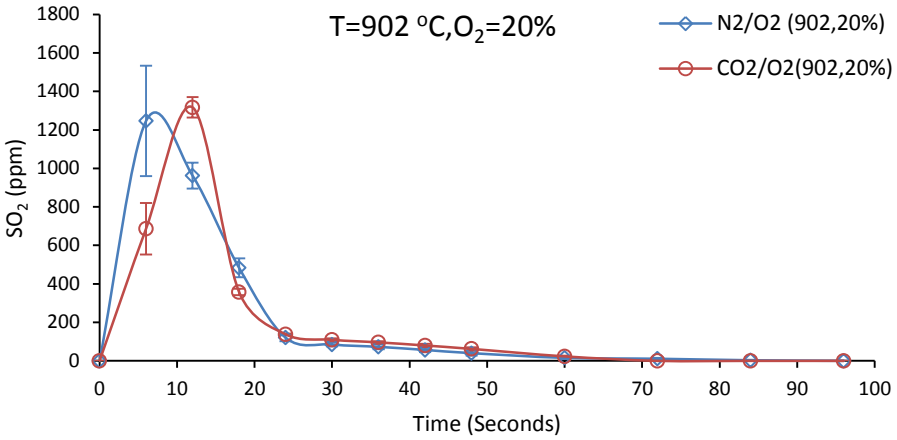

Figure 21 SO_2 emission in oxy vs. air firing (T=902°C, O_2=20%)

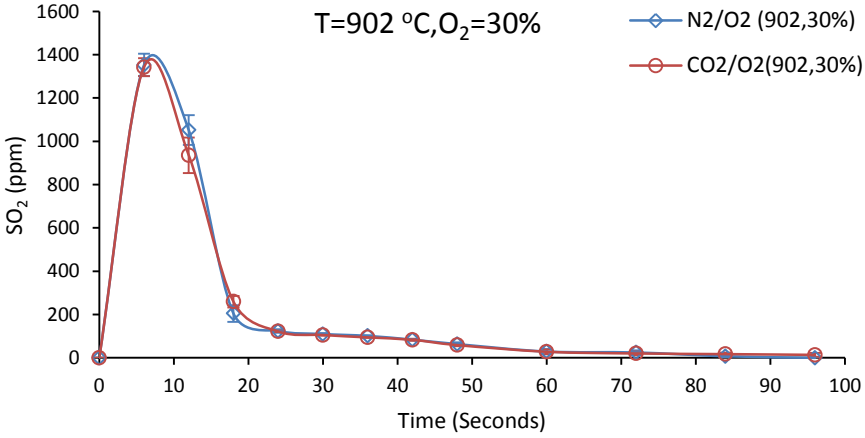

Figure 22 SO_2 emission in oxy vs. air firing (T=902°C, O_2=30%)

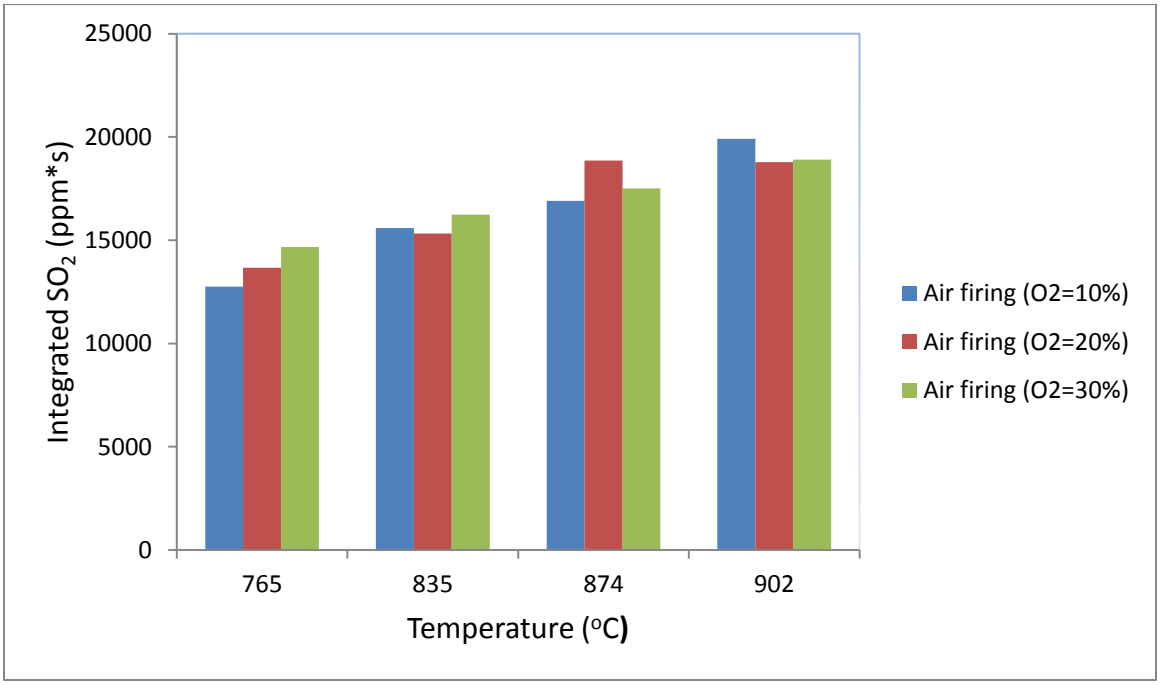

Figure 23 Integration SO_2 emission in air combustion (O_2:10, 20, 30 %)

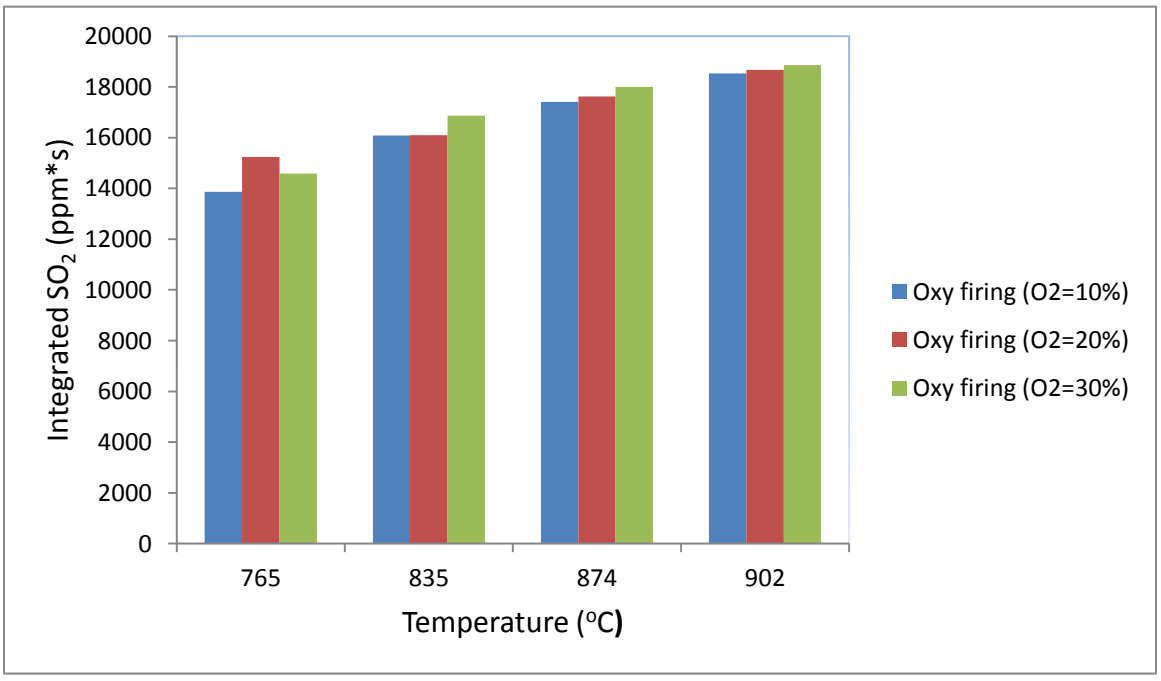

Figure 24 Integration SO_2 emission in oxy combustion (O_2:10, 20, 30 %)

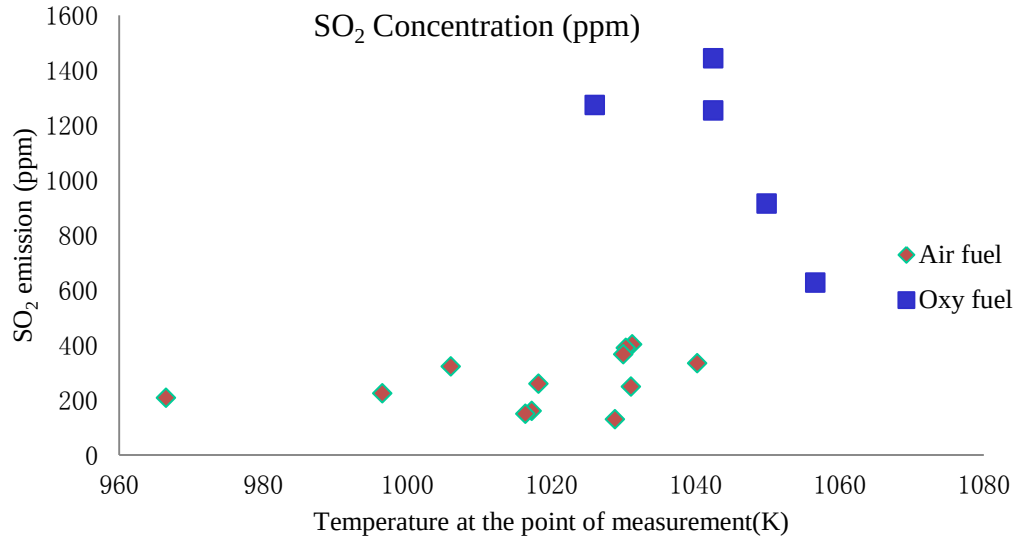

Figure 25 A comparison of SO_2 concentration (in ppm) in a pilot-scale CFB

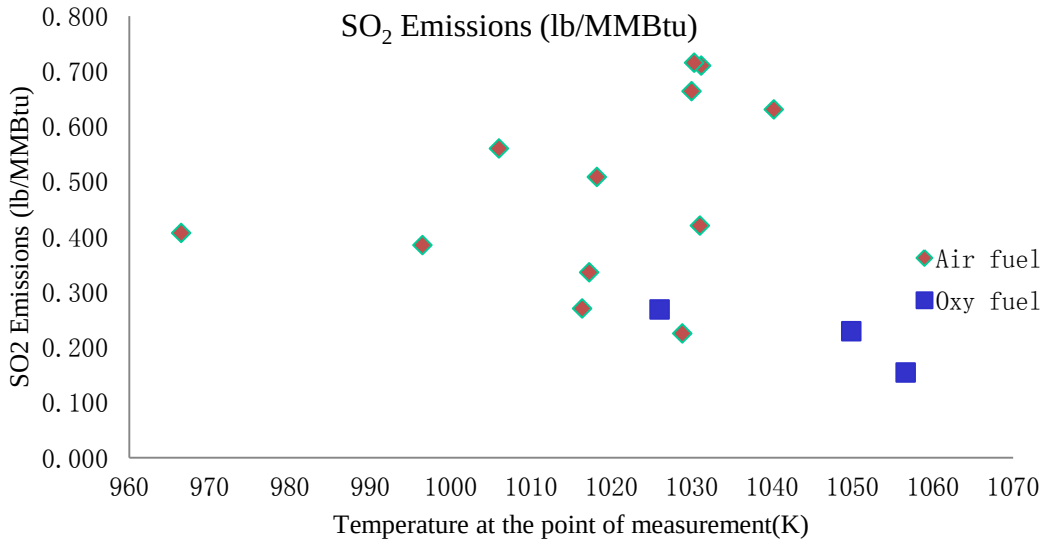

Figure 26 A comparison of SO_2 emission in terms of mass (lb/MMBtu) in a pilot-scale CFB

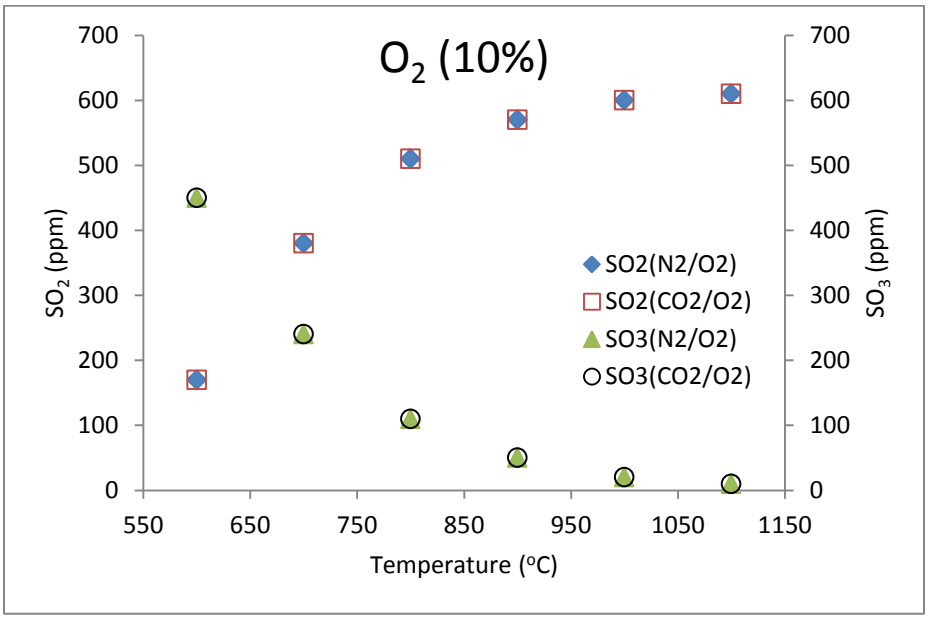

Figure 27 SO_2 and SO_3 emission in oxy and air firing (O_2=10%)

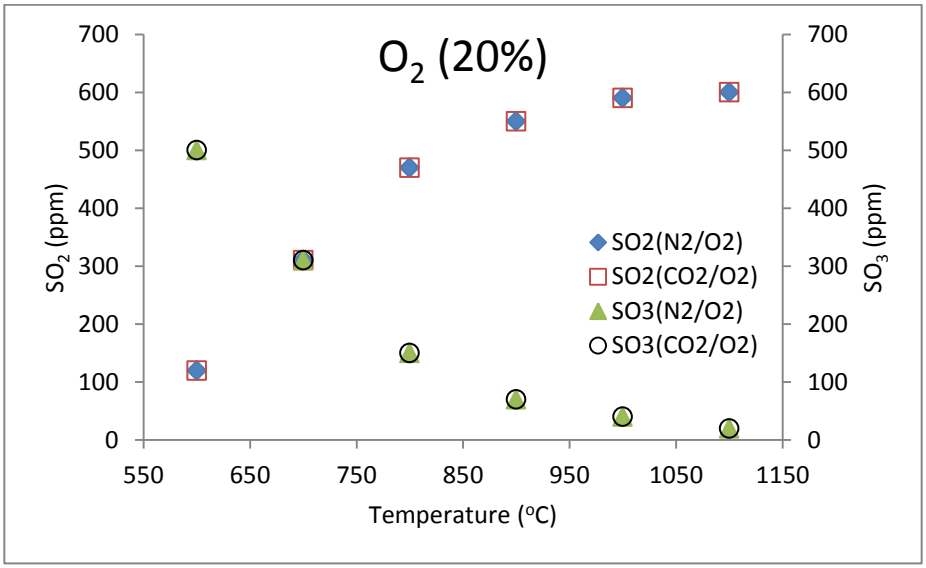

Figure 28 SO_2 and SO_3 emission in oxy and air firing (O_2=20%)

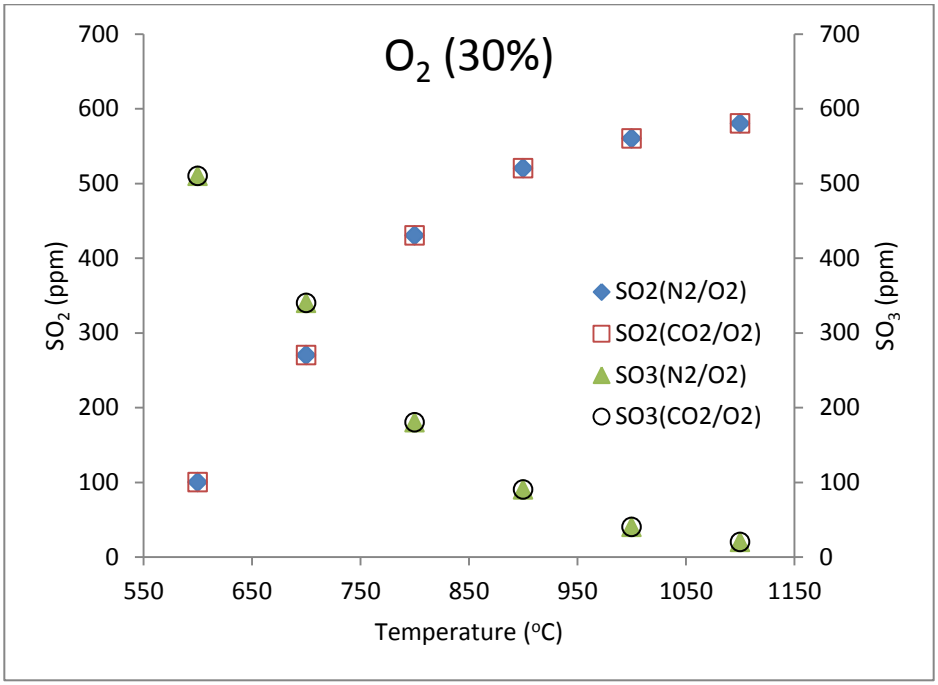

Figure 29 SO_2 and SO_3 emission in oxy and air firing (O_2=30%)

CHAPTER 4

SO_2 REMOVAL BY LIMESTONE DURING COAL COMBUSTION

Coal combustion generated SO_2 can be removed by limestone. This method of direct removal is relatively cheap and convenient, because it occurs inside the fluidized beds. An alternative using an external flue gas desulfurization (FGD) (e.g., wet scrubbing, spray-dry, wet sulfuric acid process) will be relatively expensive due to the cost of construction, maintenance, operation, and repairs. Direct limestone injection into FBC has been investigated earlier [66, 153, 157, 158, 165, 168-188]. Two important transition temperatures were reported, at which calcium carbonate ($CaCO_3$) or calcium sulfate ($CaSO_4$) decomposes. The former determines whether it is a direct sulfation or an indirect sulfation; the latter decides whether SO_2 can be removed by limestone.

A direct sulfation reaction takes place in an uncalcined condition for the limestone while an indirect sulfation reaction happens in a calcined state. Calcination is the decomposition of limestone and the reaction has been studied extensively [90, 102, 112, 115, 116, 118-121, 123, 189, 190]. Under a constant pressure, the temperature for calcination depends on the CO_2 partial pressure [102, 111, 112]. And it increases with CO_2 partial pressure.

4.1. Objectives

In Chapter 3, we found a negligible effect on SO_2 emissions from combustion diluent. It provided a reference to investigate whether there is any difference using limestone to remove SO_2. The effect of combustion diluent on desulfurization ability of limestone was evaluated under the same experimental conditions (e.g., the weight of reactants, environmental temperature, O_2 concentration, gas stream flow rate).

The sulfation behavior of limestone should be quite different between oxy firing and air firing. In oxy firing cases, the calcination of limestone is usually inhibited due to high CO_2 concentrations. A huge Ca/S ratio would be employed to ensure enough contact between limestone and SO_2 released from coal particles. The following issues will be addressed after the experimental matrix is done: Is SO_2 removal by limestone different between air and oxy firing cases? If there is a difference, which scenario benefits more from the presence of limestone? What is the reason behind the difference? What are the recommendations for industrial fluidized bed applications?

4.2. Materials and methods

We carried out SO_2 removal experiments by limestone in the bench-scale BFB and the pilot-scale CFB. The experimental apparatus and installation were described in Chapter 3. The only difference is the addition of limestone.

4.2.1. Experimental installation

We used the bench-scale BFB described in Chapter 3 to investigate the effect of combustion diluent on SO_2 removal by limestone. Because it took some time to heat up

the limestone, limestone was added into the preheated reactor for about 10 minutes. The treatment also eliminates temperature gradient inside limestone particles. Usually, a longer heating up time is required for a larger particle. We also wanted to make sure a complete calcination occurred in air firing FBC, which requires some time, especially for larger particles at lower temperatures.

For the second experimental setup, coal and limestone were fed into a pilot-scale CFB. The mass flow rate of limestone was adjusted to obtain various molar ratios of Ca:S, ranging from 0 to 10. The SO_2 concentration in the flue gas was acquired using a continuous gas analyzer, as described in Chapter 3.

4.2.2. Preparation of limestone particles

Limestone chunks were smashed into small pieces, and particles between 0.6 and 1 mm were obtained by use of sieves. The selected particles were stored in a sealed plastic bottle to prevent the adsorption of moisture from the air. Coal particles were prepared as described in Chapter 3.

4.2.3. Design of experimental matrix

The experimental matrix in the BFB is given in Table 11. A wide range of fluidized-bed temperatures ($765 - 902\,^{\circ}C$) and O_2 concentrations ($10 - 30\%$) was selected. Each experiment was repeated 5 times to reduce observation errors.

4.3. Results and discussion

We studied SO_2 removal by limestone during air and oxy firing combustion in a bench-scale BFB and a pilot-scale CFB. The combustion diluent (N_2, CO_2) showed a significant effect on limestone desulfurization, observed in both reactors. Limestone showed a weaker desulfurization capacity during the oxy firing case. In addition, SO_2 concentrations in the flue gas with or without limestone were compared.

4.3.1. SO_2 removal by limestone during oxy and air firing combustion

Sulfur removal by direct addition of limestone is not easy in a bench-scale BFB. If we had used a small amount of limestone with single coal particles (0.12 grams), combustion generated SO_2 would have very little chance to react with limestone. Therefore, a large amount of limestone particles (10 grams) was used in the bench-scale BFB with Ca:S ratio over 2000. Figure 30—Figure 37 show experimental results for SO_2 emissions under various conditions (10, 20, and 30 % O_2 concentrations, 765—902℃). It is clear that SO_2 removal by limestone is inhibited during oxy firing combustion. For example, in Figure 30, SO_2 concentration reaches 700 ppm in the oxy firing case, in comparison with about 200 ppm in the air firing case.

Because the CO_2 concentration is very high, it may lead to suppression of the limestone decomposition, and in turn, reduce the efficiency of sulfur removal. Direct sulfation likely took place under these conditions. The residence time of SO_2 is short in these experiments, which prevents it from diffusing into limestone particles to have a

direct sulfation reaction. A further investigation will be discussed in Chapter 5 “Indirect sulfation and direct sulfation”. We will talk about the control mechanism: kinetically controlled, diffusion controlled, pore diffusion, product layer diffusivity, etc. In addition, the intrinsic rate and effective diffusivity will be discussed in Chapter 5 as well.

4.3.2. With and without limestone

The limestone addition reduces SO_2 dramatically (Figure 38—Figure 43). For example, in Figure 38, SO_2 emission reaches almost 1000 ppm in both air and oxy cases. Under the same conditions, limestone addition limits SO_2 peak concentration to around 700 ppm in the oxy case, and about 200 ppm in the air case. SO_2 removal by limestone during oxy combustion is not as effective as in the air firing case. It indicates a lower intrinsic kinetic rate for direct sulfation, which would result in an inhibition from CO_2 in RFG. Enhancing SO_2 removal with limestone is a huge challenge for oxy FBC’s applications.

4.3.3. SO_2 removal by limestone in an oxy firing CFB

A Utah coal was used in an oxy firing CFB; O_2 was mixed with a RFG stream before the mixture was split into two streams: one passing through the distributor plate (80%) and one injected above the distributor plate (20%). O_2 (26%) on a wet basis was utilized to obtain similar bed temperatures as in air firing cases. About 2% O_2 (wet basis) existed in the RFG before mixing with pure O_2. SO_2 and SO_3 were sampled at the transition section. SO_2 was measured by an on-line NDIR gas analyzer and SO_3 by a controlled condensation method.

The effectiveness of limestone addition was also investigated. As discussed earlier, SO_2 concentrations are significantly higher under oxy firing conditions than under air firing conditions. In oxy firing cases, not only is N_2 is removed, resulting in a lower volumetric flow rate, but also SO_2 is recycled by RFG. SO_2 concentrations are 2-6 times higher when oxy firing. SO_2 emission depends on operation conditions, the type of coal, furnace, and RFG conditions (wet or dry)[5, 130]. As shown in Figure 44, SO_2 concentrations when oxy firing with no limestone addition (Ca:S=0) is almost 4.5 times as much as air firing. SO_2 concentrations are higher using a wet RFG, because some SO_x (especially SO_3) dissolve in the H_2O vapor. Wet RFG also leads to acidic condensed water. With a dry RFG, SO_x (ppm) will be lower, especially for SO_3, because some sulfur may be removed with the water.

We carried out experiments with various Ca:S molar ratios ranging from 0 to 10. SO_2 emissions decrease with the Ca:S molar ratio (Figure 44). A strong linear relationship was observed. Compared to the air firing cases, SO_2 emissions appear more sensitive to the molar ratio of Ca:S. When oxy firing, SO_2 (ppm) decreases from 1300 ppm at Ca:S = 0 to 400 ppm at Ca:S =10. When air firing, SO_2 (ppm) decreases from 300 ppm to 200 ppm. The higher SO_2 concentration when oxy firing increases the importance of the use of sulfation by limestone addition.

SO_2 emissions on a normalized mass basis (lbs/MMBtu) are plotted in Figure 45. The mass-based emissions are similar for air and oxy firing cases. The mass-based emissions also decrease with increasing Ca:S molar ratio. Emissions from oxy firing experiments also show a higher sensitivity towards limestone addition, which indicates

that a higher SO_2 concentration due to RFG may enhance the removal effectiveness by limestone.

4.4. Summary

The conclusions of this chapter are summarized:

i. Limestone addition results in a significant reduction in SO_2 emission.

ii. In a bench-scale BFB, limestone addition in the air firing condition shows greater capture efficiency than that in the oxy firing condition.

iii. A strong linear relationship is observed between the Ca:S molar ratio and SO_2 concentration, which decreases with Ca:S.

iv. SO_2 emissions when oxy firing show a higher sensitivity to limestone addition due to the higher SO_2 concentrations resulting from RFG.

Table 11 Experimental matrix for SO_2 formation in air vs. oxy combustion

Experimental parameters	
Temperature in BFB (°C)	765, 835, 902
O2 concentration (vol %)	10, 20, 30
Combustion	air firing (N_2/O_2), oxy firing (CO_2/O_2)
A total flow gas rate (liter/min)	4
Coal	Illinois #6 (~4.0% S)
Coal particle weight (grams)	0.12 (avg.)
Coal particle size (mm)	3.4—4.6
Bed materials	zirconium silicate (BSLZ-3)
The weight of bed material (grams)	300
Limestone weight (grams)	10
Limestone particle (mm)	0.6—1

Note: each experimental condition was repeated 5 times

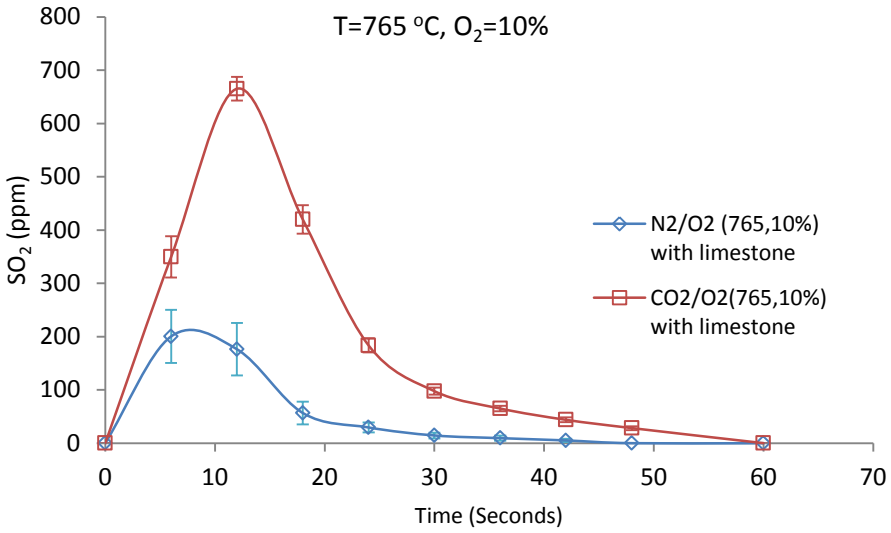

Figure 30 SO_2 removal by limestone during oxy and air firing combustion in a bench-scale BFB (T=765°C, O_2=10%)

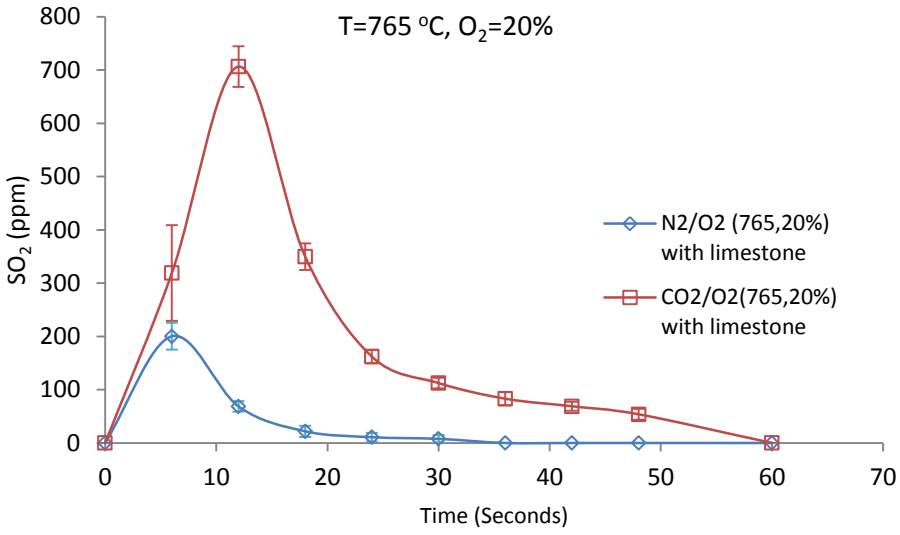

Figure 31 SO_2 removal by limestone during oxy and air firing combustion in a bench-scale BFB (T=765°C, O_2=20%)

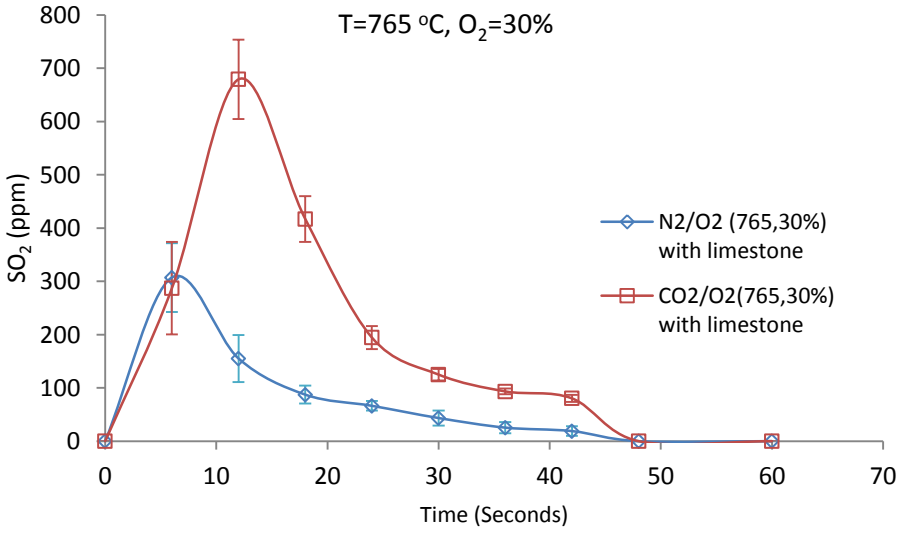

Figure 32 SO_2 removal by limestone during oxy and air firing combustion in a bench-scale BFB (T=765°C, O_2=30%)

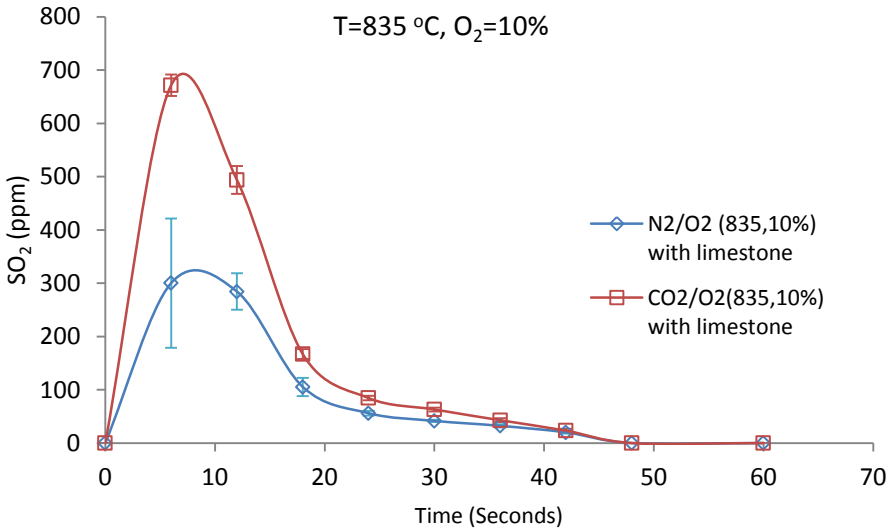

Figure 33 SO_2 removal by limestone during oxy and air firing combustion in a bench-scale BFB (T=835°C, O_2=10%)

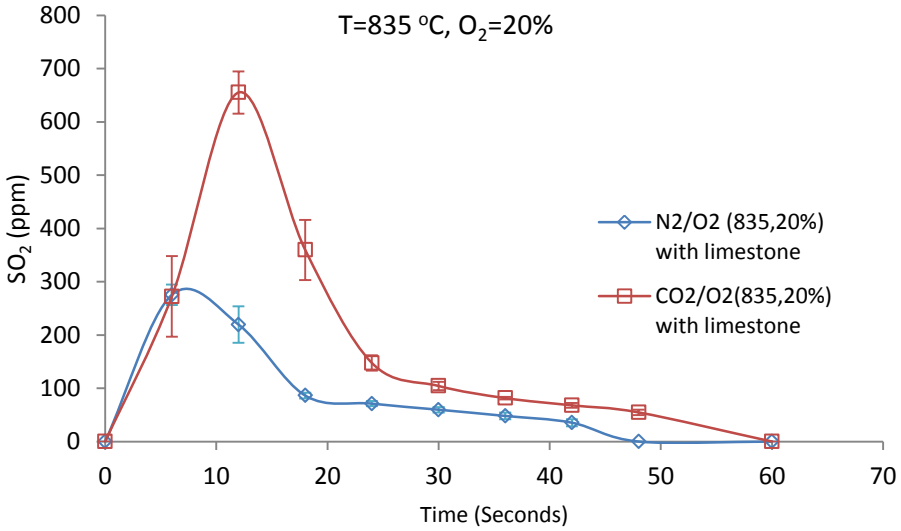

Figure 34 SO_2 removal by limestone during oxy and air firing combustion in a bench-scale BFB (T=835°C, O_2=20%)

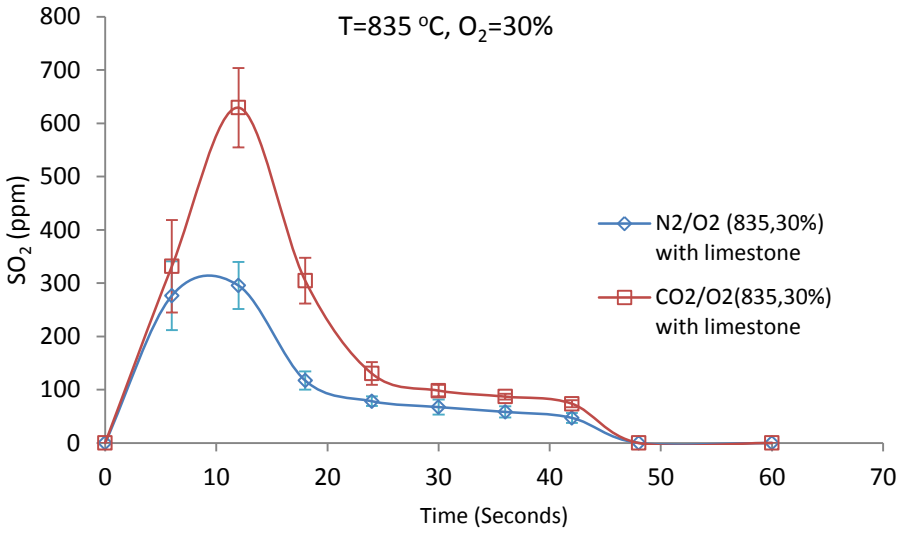

Figure 35 SO_2 removal by limestone during oxy and air firing combustion in a bench-scale BFB (T=835°C, O_2=30%)

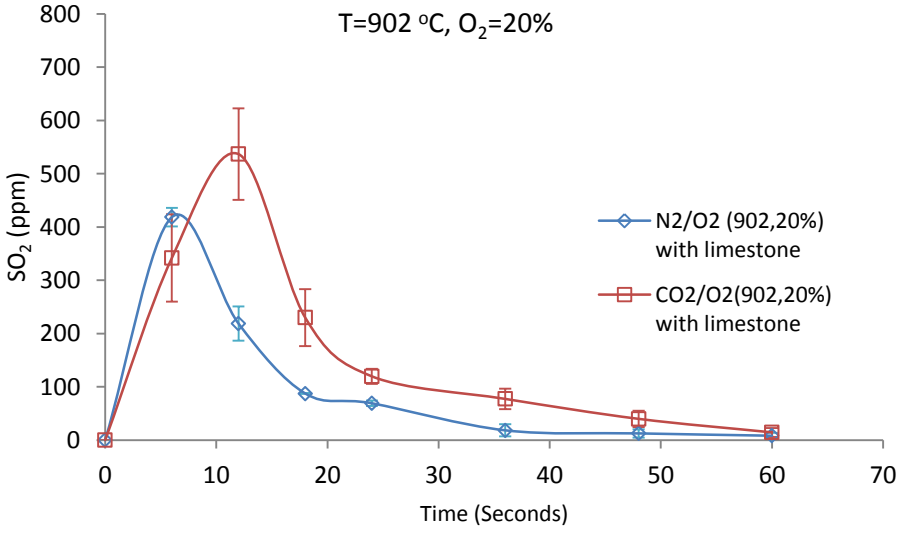

Figure 36 SO_2 removal by limestone during oxy and air firing combustion in a bench-scale BFB (T=902°C, O_2=20%)

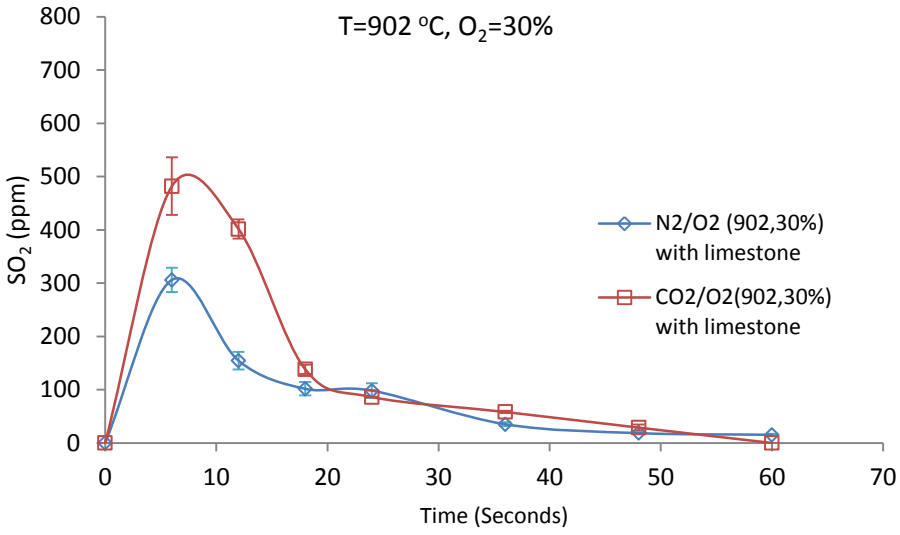

Figure 37 SO_2 removal by limestone during oxy and air firing combustion in a bench-scale BFB (T=902°C, O_2=30%)

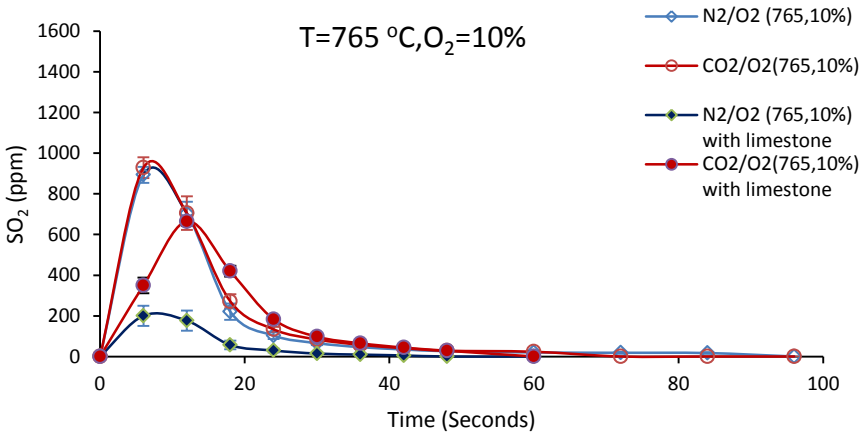

Figure 38 SO_2 behavior with/ without limestone (T=765 °C, O_2=10%)

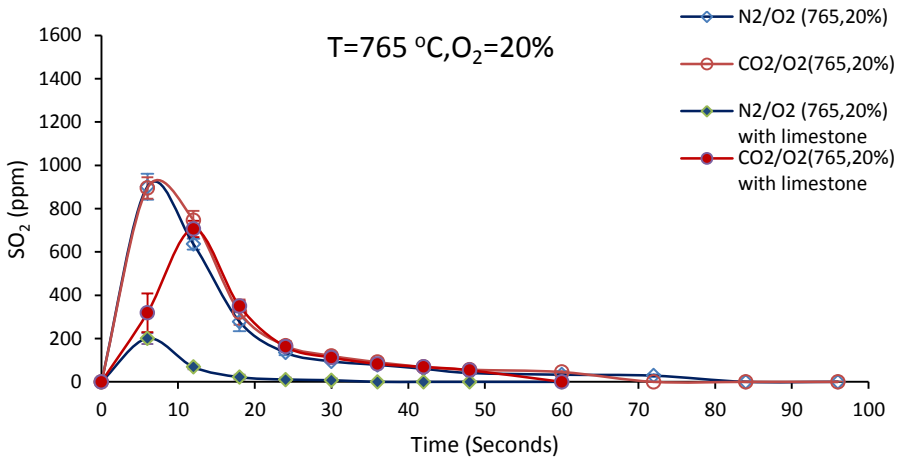

Figure 39 SO_2 behavior with/ without limestone (T=765 ^{o}C, O_2=20%)

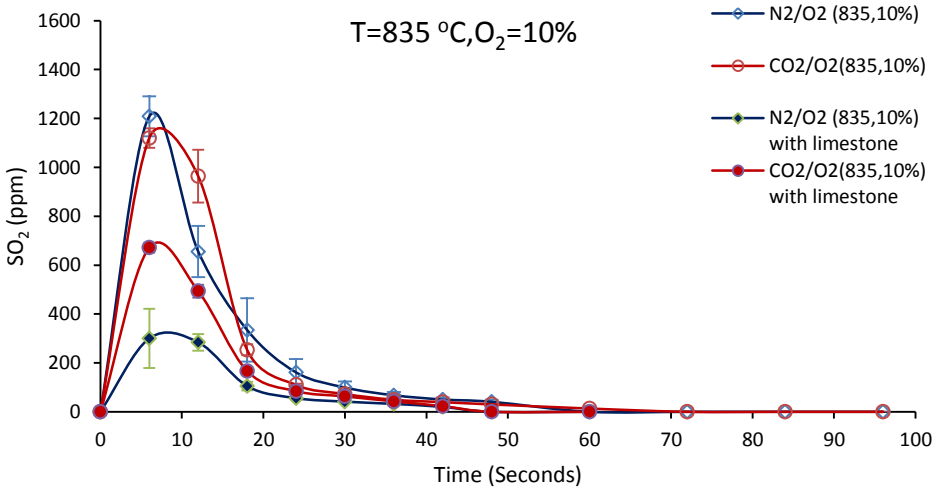

Figure 40 SO_2 behavior with/ without limestone (T=835 ^{o}C , O_2=10%)

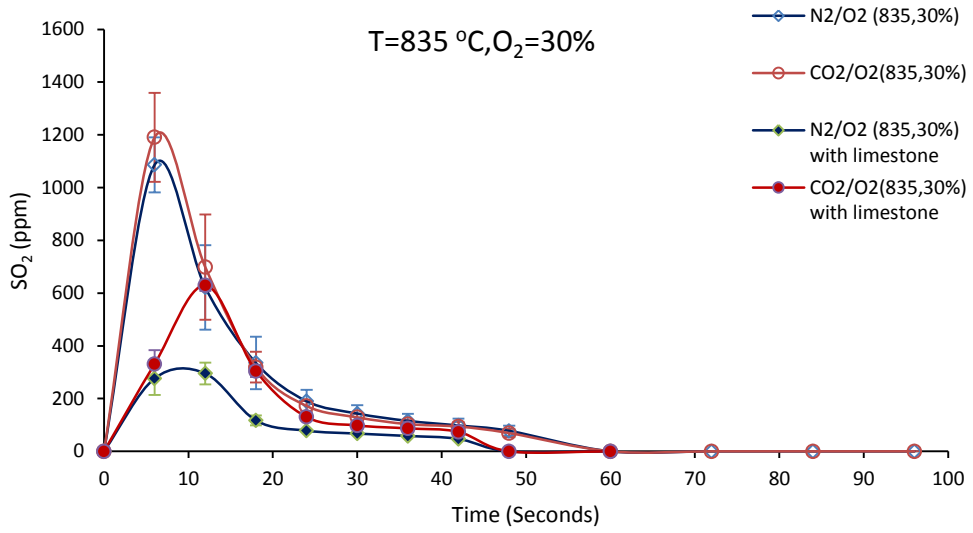

Figure 41 SO_2 behavior with/ without limestone (T=835 ^{o}C, O_2=30%)

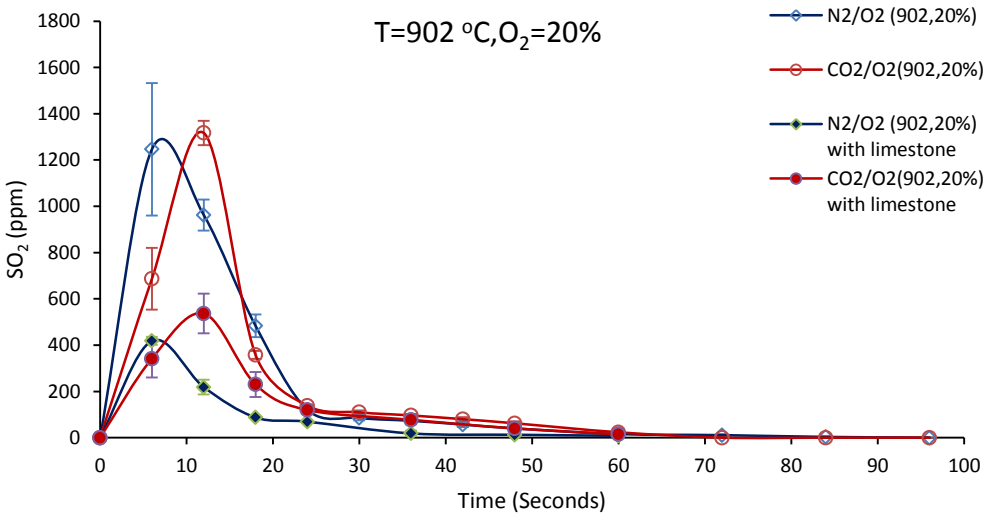

Figure 42 SO_2 behavior with/ without limestone (T=902 ^{o}C, O_2=20%)

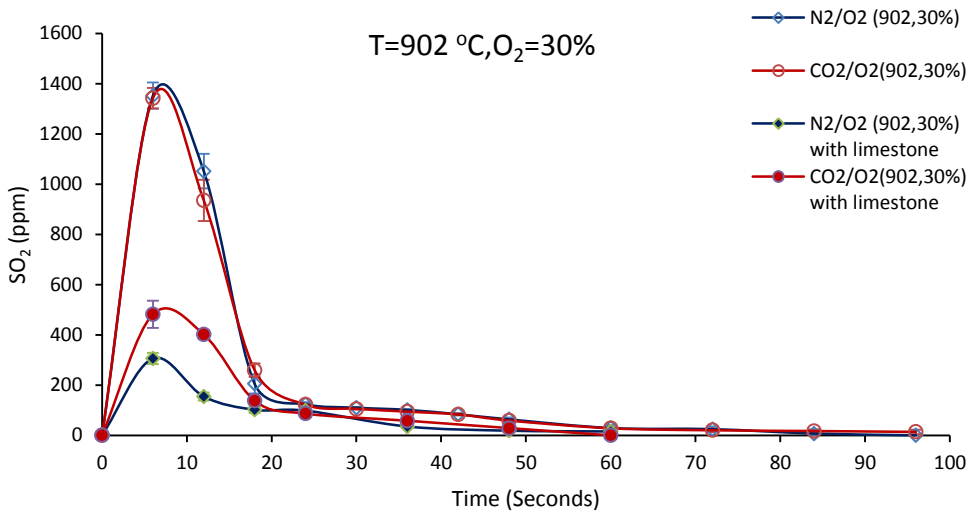

Figure 43 SO_2 behavior with/ without limestone (T=902 °C, O_2=30%)

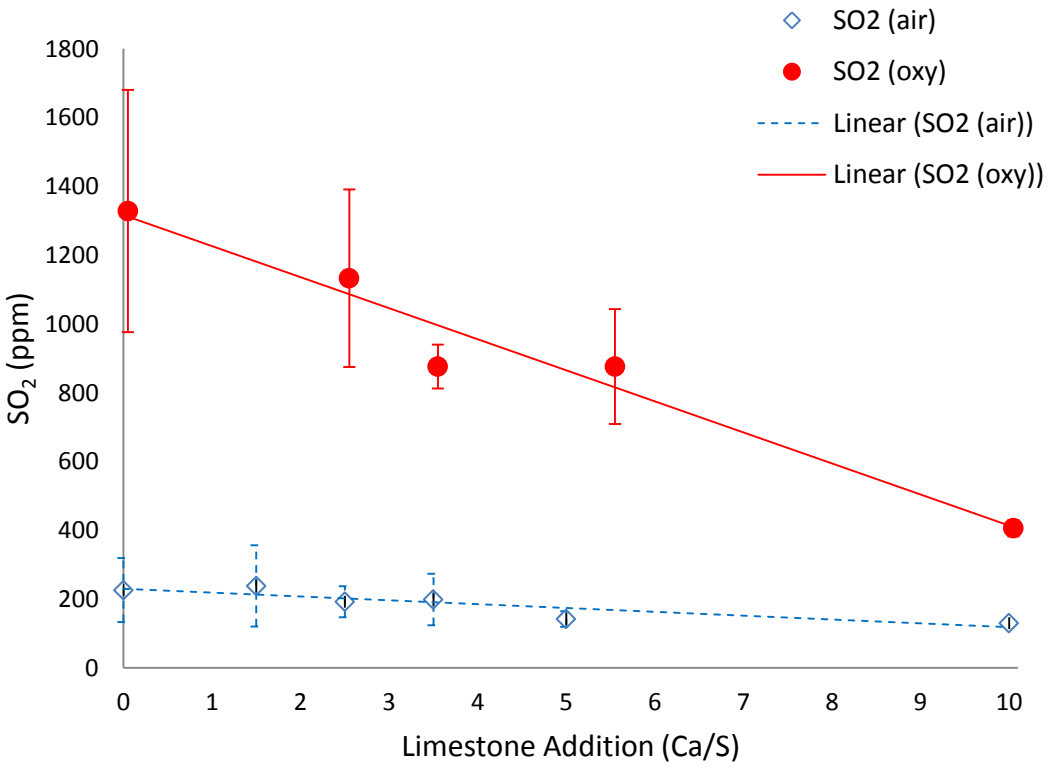

Figure 44 SO_2 concentration (ppm) varies with Ca/S ratio during air firing and oxy firing combustion (50 lbs/hr Utah Coal, 3% excess O_2 in exit flue gas, 80% Primary/20% Secondary)

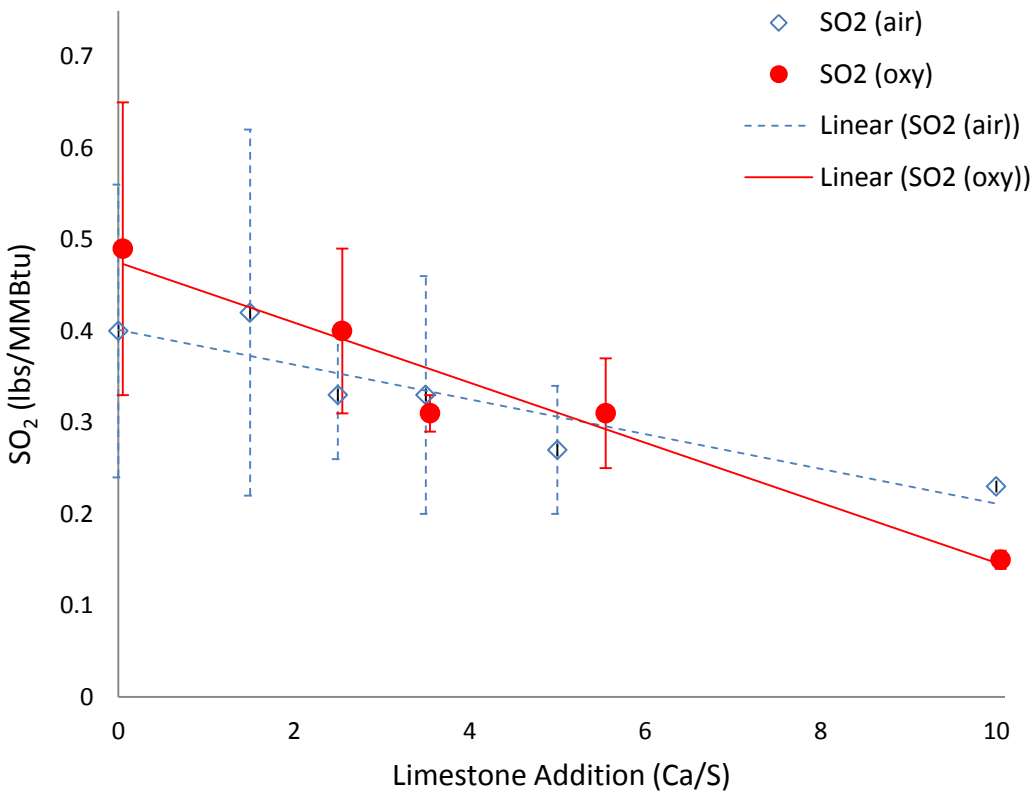

Figure 45 Mass-based SO_2 emission (lbs/MMBtu) varies with Ca/S ratio during air firing and oxy firing combustions (50 lbs/hr Utah Coal, 3% excess O_2 in exit flue gas, 80% Primary/20% Secondary)

CHAPTER 5

INDIRECT SULFATION AND DIRECT SULFATION

5.1. Introduction

Two research objectives were identified in our project: characterizing limestone sulfation and SO_2 removal. In Chapter 4, we mainly focused on SO_2 removal during oxy and air firing combustion. The residence time of SO_2 in the boiler is usually too short for SO_2 to diffuse into the limestone particle core through its product layer. In our experiments, we used an excess of $CaCO_3$ to remove SO_2 to the greatest extent. The molar ratio of Ca:S was over 2000 in the bench-scale BFB, and between 2 and 10 in the pilot-scale CFB. We also wanted to characterize the limestone after use in our experiments. For example, we wanted to know the microstructure and the level of sulfation. To this end, we needed a stable source of SO_2. In order to provide a stable source of SO_2, we replaced SO_2 from coal combustion with a calibration gas.

The sulfation of limestone has been investigated extensively [114, 116, 117, 124, 126, 128, 130, 145, 146, 149, 153, 191-205]. A direct sulfation takes place under an uncalcined condition, while an indirect sulfation happens with calcined limestone. We carried out experiments at various temperatures and CO_2 partial pressures, and then examined the resulting limestone to investigate the calcination process. Earlier studies

were available for CO_2 equilibrium pressure over limestone [111, 112], which is described by the following equation [111] as a function of temperature:

$$\log_{10} p^{e}_{CO_2} = -\frac{8308}{T} + 7.079$$

where $p^{e}_{CO_2}$ is given in atmospheres (1 atm), and T is given in Kelvin.

If the operating temperature is lower than the transition temperature of calcination at a certain CO_2 partial pressure, direct sulfation dominates. Otherwise, indirect sulfation can occur. Generally speaking, direct sulfution occurs during oxy firing combustion, while indirect sulfation takes place in air firing combustion. However, direct sulfation can go forward at low temperatures (≤ 600℃) under the air firing condition; however, the reaction rate would be very low. Similarly, indirect sulfation occurs at high temperatures (≥ 920℃) when oxy firing.

Several mechanisms of direct sulfation were proposed in the literature [101, 102, 124-127]. Tullin [129] observed an inhibiting effect due to high CO_2 concentrations on direct sulfation. In general, the understanding of the direct sulfation is limited and highly speculative. Not much can be confirmed except for $CaSO_4$ as the final product [128]. Direct limestone addition is one of the most attractive options to reduce SO_x emissions when oxy firing. The performance of limestone sulfation with a high CO_2 concentration greatly differs from that in N_2.

5.2. Objectives

In this chapter, we will focus on sulfation reactions of limestone. We are interested in discovering:

i. Behaviors of simultaneous recarbonation and calcination reactions under various operating temperatures and CO_2 concentrations.

ii. Behavior of sulfation under various conditions (e.g., temperature, CO_2, N_2).

iii. The microstructure of sulfated limestone using SEM and EDS.

The investigation of calcination is a prerequisite step for study of the fundamentals of indirect and direct sulfation reactions. A TGA Q600 is used in these experiments to identify the relationship among calcination, temperature, and CO_2 partial pressure. Sulfation of limestone in air is quite different from that in oxy firing cases. The concept of a "$CaSO_4$ product layer" has been previously proposed to explain a direct sulfation mechanism, which fits well with a shrinking core particle model [124, 125]. This proposal leads to the assumption that the reaction is diffusion controlled due to the product layer. We would like to address whether the $CaSO_4$ product layer is similar in direct or indirect sulfation.

The $CaSO_4$ product layer formed during indirect sulfation will inhibit SO_2 penetration into the particle, as shown in Figure 46. Therefore, the sulfation reaction will be very slow. We have made three hypotheses for direct sulfation, as shown in Figure 47. Hypotheses 1 and 2 build on the "product layer" concept, and hypothesis 3 is included as a kinetics control alternative. The difference between hypothesis 1 and 2 lies

in the structure of the product layer. A nonporous product layer will prevent SO_2 from diffusing into the core and effectively stops the sulfation reaction. A porous product layer will allow for diffusion and continued sulfation. Since a diffusion-limiting product layer does not form in hypothesis 3, sulfation reaction is active. Only hypothesis 1 leads to a very similar result as in indirect sulfation.

Snow and Sarofim et al. [126] observed a lower inhibition effect from a diffusion layer when oxy firing. They found a porous product layer under oxy firing conditions. A hypothesis was made that CO_2 is generated by reactions among $CaCO_3$, SO_2, and O_2, and keeps pores open and delays pore closure or shrinking. The hypothesis has been cited repeatedly as the explanation of a highly porous product layer during a direct sulfation. Hu and Dam-Johansen et al. [128] disagreed with this hypothesis. However, they argued that 1.5 moles of gaseous reactants are consumed to generate 1 mole of CO_2, thus the direction of net flux points from the particle surface towards the inner core. They doubted that the porosity observed during direct sulfation results from CO_2.

We would like to investigate the effect of temperature on the calcination with a wide range of CO_2 concentrations. We would like to find out whether sulfation is diffusion or kinetics controlled when air or oxy firing. We also wanted to observe whether a tough-structure product layer exists.

5.3. Materials and methods

Calcination and carbonation experiments were performed using a TGA Q600. The sulfation behavior of limestone was studied using a bench-scale BFB and a FTIR. The

microstructure and sulfur distribution of sulfated limestone was explored by SEM and EDS.

5.3.1. Experimental installation

In previous chapters, we presented results obtained from a bench-scale BFB coupled with FTIR. We interpreted the data using kinetic analysis. In this chapter, we will study microstructures (pore size, formation, percent of void, alignment, sulfur distribution) of sulfated limestone to identify the fundamental mechanisms of indirect and direct sulfation.

A constant SO_2 concentration was necessary in our experiments, and was achieved by use of a calibration gas. We would like to reveal a relation between the Ca/S ratio and the sulfation ability of limestone, as well as the existence of a $CaSO_4$ product layer. Experiments were performed in a bench-scale BFB, which was described in the previous section. 1.0 g of limestone was loaded into the reactor, which contained approximately 300 g of bed material. The limestone was given plenty of time to attain a complete calcination under a N_2 atmosphere. The premixed gas flow is then switched to a sulfur-containing gas stream ($N_2/O_2/SO_2$, or $CO_2/O_2/SO_2$). The total reaction time was about 1 hour.

Sulfated limestone for microstructural examination was prepared in a bench-scale BFB at various temperatures (765, 835, and 874℃) for both oxy and air firing cases. The SO_2 concentration was kept constant in the gas phase. Limestone samples were mounted, cut in half, and polished gently to expose the inner microstructure for

examination. We characterized microstructures in terms of pore structure, size, formation, alignment, etc. The structural information provides useful evidence of the controlling mechanism in indirect or direct sulfation reactions. Two magnifications of SEM (20K×, 3.272K×) were carried out. The lower magnification gives an overview of the particles, while the higher magnification provides more details of local spots.

5.3.2. Design of experimental matrix

TGA measurements can record changes in weight of the limestone as a function of temperature. A TGA Q600 was used to study the calcination and carbonation of limestone using a consistent operating temperature profile. We used a limestone size fraction between 600-1000 μm. The limestone sample (70 mg) was loaded into a ceramic cup in the furnace. The environmental gases were mixtures of N_2 and CO_2 from gas cylinders, and the mixture was controlled by gas rotameters. The CO2 concentration was adjusted to 0, 1.6, 50, 81.9, and 100%.

The operating temperature profile of the TGA was set as follows:

i. The operating temperature increased to 910 ℃ with a heating rate of 5℃/min.

ii. Then, the temperature was maintained at 910 ℃ for 60 minutes.

iii. After that, the temperature dropped from 910℃ to 700℃ with a heating rate of 5 ℃/min.

We anticipated observing a diffusion limited layer, if a large particle size and high reaction temperatures were used. Therefore, a large size limestone particle (600−900

μm) was used to remove SO_2 at various temperatures (765, 835, and 874℃). The experimental matrix designs are reported in Table 12.

5.4. Results and discussion

The effect of CO_2 concentration on calcination and carbonation is studied under the same experimental conditions. Experimental results reveal a close correlation among carbonation, calcination, CO_2 concentration, and operating temperature. The preferential conditions for calcination include high temperatures (endothermic) and low CO_2 concentrations. Carbonation is the reverse reaction of calcination, which happens at low temperatures and high CO_2 concentrations. When oxy firing, limestone sulfation depends on the temperature for both direct and indirect sulfation. By contrast, the temperature shows a less insignificant effect on sulfaction when air firing. This was further confirmed by SEM; the product layer shows a porous structure when oxy firing, and nonporous when air firing.

5.4.1. Preliminary experiment: calcination and carbonation

Sulfation starts with calcination and carbonation that are reverse competing reactions. The reaction rates vary with CO_2 concentration and particle temperature. As Figure 49 shows, it is quite clear that limestone calcination occurs with 100% N_2. The limestone weight loss starts around 620℃. Limestone loses 44% of the initial weight, and the calcination is almost 100% completed, since CO_2 weighs 44% of the total weight of $CaCO_3$. No change is observed after 44% of the weight is lost even if the temperature

increases for several minutes. Because reaction-generated CO_2 is purged in TGA, no sign of carbonation is observed, even during the cooling-down period.

If CO_2 increases from 0 to 50%, as shown in Figure 48, the weight change of limestone is different from the previous 100% N_2 example (Figure 49). The temperature at which calcination starts is higher due to increased CO_2 partial pressure.

Because of the existence of CO_2, carbonation competes favorably with calcination. As the temperature increases, the rate of calcination becomes greater than that of carbonation, and a weight loss is observed. When the final temperature of 910 ℃ is reached, about 44% of the total weight is lost, indicating a completion of calcination. The temperature is held for 1 hour and no further weight loss is observed. During the temperature ramp-down, carbonation eventually becomes possible and the sample weight starts to increase again. The weight increases from 56% to 76%, before a third weight platform forms.

It is not exactly clear what causes the first step in the weight loss profile observed in Figure 48. There are two possible explanations. We used natural limestone, not 100% pure, and some impurities (such as $MgCO_3$) could cause the first step. Another possible explanation is the competition between carbonation and calcination reactions. The calcination process begins at a lower temperature, similar to what is observed with 0% CO_2, but soon the competition with the recarbonation reaction effectively balances the calcination rate. The temperature continues to rise and once a high enough temperature is reached, the calcination rate begins to exceed that of the recarbonation reaction, and we again see continued weight loss, as shown in Figure 49.

When we use a higher CO_2 concentration (81.9%), carbonation becomes more competitive. An initial phase of calcination is seen in Figure 50 before it levels off at about the same temperature as in the 50% CO_2 case. A further weight loss follows, but starts at a higher temperature (898 ℃) than that in the 50% CO_2 case (862 ℃). The higher starting temperature is the result of a higher CO_2 concentration. Carbonation and calcination compete with each other and the relative contribution of each rate depends upon the temperature. At a high enough temperature, the rate of calcination exceeds that of carbonation, and the limestone decomposes until reaching another weight platform. It is considerably longer for calcination to complete, and the steep slope seen in Figure 48 is no longer seen due to competition with the reverse reaction. As the temperature decreases, the weight of limestone increases from 59 to 82% because carbonation becomes more competitive again.

When we use 100% CO_2, as shown Figure 51, carbonation becomes even more favorable. As at T = 910 ℃, the calcination rate still exceeds that of carbonation, and the advantage is so small that after 60 minutes, only a 15% weight loss is recorded. The weight of limestone increases from 79 to 88% during the cooling-down period.

We can regroup the experimental data presented in Figure 49—Figure 51, and the data are presented in Figure 52 and Figure 53 to faciliate comparisons. Apparently, as shown in Figure 52, calcination starts at a higher temperature when a higher CO_2 concentration is used. In addition, calcination does not go forward to 100% completion. The temperature at which carbonation exceeds calcination in Figure 53 increases with CO_2 partial pressure (recall that the tempeature is decreasing with time at this stage). In

summary, carbonation competes with calcination under various CO_2 concentraions. Higher CO_2 concentrations delay calcination and promote carbonation even at high temperatures. Equilibrium calculation is used through a CEA program. The conditions of equilibrium calculation are shown as Table 13; the results of equilibrium calculations are shown in Table 14. At higher temperature (910 ^oC), $CaCO_3$ is decomposed into 100% CaO at the range of CO_2 concentration (0, 50, 81.9, 100%). At lower temperature (750 ^oC), 100% $CaCO_3$ is existing in CO_2 concentrations (50, 81.9, 100%), while 100% CaO is formed at the CO_2 concentration (0%).

5.4.2. Indirect sulfation and direct sulfation in TGA

The degree of sulfation is calculated by the following equation:

$$f_t = \frac{PM_{CaCO_3}}{RTm^0_{CaCO_3}} \int_0^t Q \bullet \left(c_o - c_t\right) * 10^{-6} dt$$

f_t	The degree of sulfation at t time
P	Pressure in the reactor (Pascal)
T	Temperature in the reactor (Kelvin)
M_{CaCO_3}	Molecular weight of $CaCO_3$
$m^0_{CaCO_3}$	Initial mass of $CaCO_3$ (kg)
Q	Total flow rate (m^3/s)
c_o	Initial SO_2 concentration (ppm) before reacting with limestone
c_t	SO_2 concentration (ppm) after reacting with limestone at t time

The degree of sulfation as a function of time for air and oxy combustion cases is illustrated in Figure 54 and Figure 55. When air firing, the reactor temperature shows no

significant effect on the degree of sulfation between 765 and 874°C. The degree of sulfation is quite low at 15% after 1 hour. It is well established that significant pore plugging will limit the degree of sulfation because of the larger molar volume of $CaSO_4$. Therefore, the reaction will take place at the particle surface, and will be inhibited below a thin outer layer. The low degree of sulfation shown in Figure 54 is consistent with this hypothesis. In addition, the very limited dependence on temperature also suggests a diffusion-controlled regime.

The degree of sulfation is shown in Figure 55, which reveals a clear dependence on temperature when oxy firing. Similar to the air case, the level of sulfation is quite low. A more detailed comparison between air and oxy cases is provided in Figure 56 and Figure 57. At 765℃, the rate of sulfation in the presence of CO_2 is much less than that in the presence of N_2. After 1 hour, the sulfation degree when oxy firing is about 12%, and that when air firing is about 15%. By contrast, a higher degree of sulfation is observed for oxy combustion at 874℃. The conversion of limestone reaches more than 17%, higher than 14% obtained in the air case. Different mechanisms dominate in air or oxy cases. Most likely, the indirect mechanism dominates when air firing, and the direct mechanism dominates in oxy combustion. Also, it appears that the mechanism during air combustion is diffusion controlled as discussed earlier. We suspect that the direct sulfation mechanism is kinetically controlled, since the temperature dependence is much more significant. The SO_2+$CaCO_3$ reaction is slow under oxy firing. This will allow the formation of $CaSO_4$ over a larger surface area and allow a longer reaction window prior to pore plugging. Therefore, SO_2 can be transported more deeply inside the

particle without the diffusion limitation; the $SO_2/CaCO_3$ reaction rate will be higher at high temperatures.

In addition, equilibrium calculations of CaCO3/CaO-SO2 were performed using the CEA code. The parameters for the equilibrium model are shown in Table 18. In the following equilibrium calculations, there was an excess of SO_2, compared with $CaCO_3/CaO$. The equilibrium calculation results show that for all conditions, the solid Ca species is 100% $CaSO_4$ (II).

5.4.3. Mechanism identification by microstructure

Our hypothesis of fundamental sulfation mechanisms in oxy vs. air combustion can be evaluated using analysis of microstructures (pore size, percent of void, alignment, sulfur distribution). This analysis complements the kinetics analysis in the previous section. In this chapter, sulfated limestone was examined using SEM and EDS.

5.4.3.1. Microstructure of sulfated limestone by SEM and EDS

Temperature dependence of sulfur emission suggests a very different mechanism during air firing (O_2/N_2) and oxy firing (O_2/CO_2) combustions. We made one hypothesis. When air firing (indirect sulfation), a rapid formation of $CaSO_4$ near the surface will plug pores and inhibit sulfation of the inner portion of the particle. Direct sulfation shows a low temperature sensitivity that suggests the process would be diffusion-controlled.

Oxy firing combustion shows strong temperature sensitivity, which indicates a kinetically controlled process. A high concentration of CO_2 is an inhibiting factor to the

formation of CaO by calcination. Therefore, the process will proceed via direct sulfation. We believe the overall rate may be kinetically limited but not diffusion limited. SO_2 will penetrate deeper into the particle and will not plug pores due to $CaSO_4$ formation. If this is true, we will expect an absence of a product layer, and a more uniform distribution of $CaSO_4$ as a function of radius.

In this section, we will provide evidences to examine our hypothesis with regard to sulfation mechanisms during air and oxy firing combustion. Figure 58 presents SEM photomicrographs of a sulfated limestone with a magnification of 3.272K×. It provides a rough view of a particle. The sample in Figure 58 (a) was sulfated after calcination in the presence of N_2, and represents an indirect sulfation mechanism. The image in Figure 58 (b) is taken from a direct sulfation in the presence of 80% CO_2. The air combustion generated limestone (Figure 58 (a)) appears to have a distinct product layer ($CaSO_4$), while the oxy combustion sample (Figure 58 (b)) does not show an obvious product layer that could prevent SO_2 from penetrating deeper into the particle.

We also examined microstructures using a higher magnification level (20K×). A higher magnification enables us to make a further comparison between the edge and the center of a particle. As shown in Figure 59 (air firing) and Figure 60 (oxy firing), the edge and the center of a particle were examined in greater details. A surface $CaSO_4$ layer (Figure 59 (a)) demonstrates a compact pore structure, while porous structures of CaO (Figure 59 (b)) appear to be available in the center because of the initial calcination followed by a subsequent evolution of CO_2 gas. According to our hypothesis, in the presence of $N_2/O_2/SO_2$, pores will be blocked very quickly because of the formation of

an outer $CaSO_4$ product layer, which prevents gaseous diffusion into the particle, and would thus impose a typical diffusion-controlled regime.

In contrast, SEM microstructure from oxy firing experiments (direct sulfation) supports our hypothesis. As shown in Figure 60 (a), no clear product layer is observed on the particle surface. The particle surface is as porous as the center of the particle (Figure 60 (b)). A different mechanism is needed to describe the observations for oxy firing cases. In the presence of a high CO_2 concentration, the kinetic rate for $SO_2/CaCO_3$ (direct sulfation) reaction is slower compared to that of SO_2/CaO (indirect sulfation). Pore diffusion is not the limiting factor and the reaction occurs throughout the particle. $CaSO_4$ will cover a larger surface area and yield a longer reaction time prior to pore plugging. Based on the SEM analyses of sulfated limestone particles under air and oxy firing conditions, it is apparent that the product layer formed under $CO_2/O_2/SO_2$ is more porous, compared to that formed under $N_2/O_2/SO_2$.

Sulfur distribution in a limestone particle was scanned by EDS. The sulfur distributions are shown in Figure 61 (oxy firing) and Figure 62 (air firing). Elemental sulfur is represented by the green color. An EDS photomicrograph of sulfated limestone was prepared with a magnification rate of 3.272K×.

The sulfur distribution is very similar for both cases. Sulfur exists mainly at the edge of the particle or in cracks of the particle. A clear sharp $CaSO_4$ product layer is seen in both cases. Thus, our hypothesis to explain the difference in sulfur emission becomes debatable.

5.5. Summary

In this chapter, we discussed sulfation mechanisms and our hypothesis for the reaction of SO_2 with limestone. The major points are summarized here:

i. The starting temperature for calcination increases with the CO_2 concentration. The degree of calcination decreases at a higher CO_2 partial pressure. The temperature of recarbonation increases with the CO_2 partial pressure.

ii. A significant temperature effect on sulfation of limestone was seen when direct sulfation proceeds. No significant temperature effect was seen for indirect sulfation. One possible explanation is that the particle size of limestone we used is very large (600-1000 micron), where it is possible to form a thick product layer for these particles relative to fine limestone particles. In indirect sulfation, the product layer showed no porosity, and thus, the sulfation process was strongly limited by diffusion, which has a lower temperature sensitivity than a kinetically-controlled process.

iii. A sharp layer is seen in SEM images for the air firing condition that blocks gas transport into pores. No distinct sharp layer is seen when oxy firing. It is anticipated that the competition between calcination and carbonation reactions in the presence of CO_2 inhibits calcination and promotes more emphasis towards the direct sulfaction reaction. Lower reaction rates for the direct sulfation reaction led to less product layer formation and thus less of a diffusion barrier, such that SO_2 could penetrate more effectively into the particle and provide a

more uniform $CaSO_4$ conversion throughout the particle, instead of high conversion only near the surface resulting in the dense surface layer. The direct sulfation produced a higher “activity” than the indirect sulfation after a long reaction time under the conditions we tested due to the ability of SO_2 to continue to diffuse into the particle at longer times in the absence of the dense surface product layer.

Table 12 Experimental matrix for known SO_2 concentration in N_2/CO_2 with limestone.

Experimental Parameters	
Temperature of fluidized bed (°C)	765, 835, 874
O_2 concentration (vol. %)	20
Calibration gas (vol. %)	80
SO_2 concentration in calibration gas (ppm)	1000
SO_2 concentration in final mixture (ppm)	800
Bed material	300 g of zirconium silicate (BSLZ-3)
Limestone	Lab grade, calcium carbonate, chips (471-34-1), >99%
Limestone weight (g)	1
Limestone size (mm)	0.6-0.991mm
Total gas flow rate (liter/min)	3

Table 13 The conditions of equilibrium calculation for $CaCO_3$-CaO

	Conditions
Gas phase concentration (moles)	0 (100 mole N_2), 50 (50 mole CO_2+50 mole N_2), 81.9 (81.9 mole CO_2+18.1 mole N_2), 100 (100 mole CO_2)
Temperature (°C)	750, 800, 850, 910
$CaCO_3$	1 mole

Table 14 The results of equilibrium calculation for $CaCO_3$-CaO

CO_2 concentration (%)		0	50	81.9	100
Temperature (°C)	750	CaO (100%)	$CaCO_3$ (100%)	$CaCO_3$ (100%)	$CaCO_3$ (100%)
	800	CaO (100%)	$CaCO_3$ (100%)	$CaCO_3$ (100%)	$CaCO_3$ (100%)
	850	CaO (100%)	CaO (100%)	$CaCO_3$ (100%)	$CaCO_3$ (100%)
	910	CaO (100%)	CaO (100%)	CaO (100%)	CaO (100%)

Table 15 The parameters of equilibrium calculation for $CaCO_3$/CaO-SO_2

Parameter	
SO_2 (mole)	8
O_2 (mole)	20000
N_2 or CO_2 (mole)	80000
$CaCO_3$ or CaO (mole)	2
Temperature (^oC)	765, 835, 874

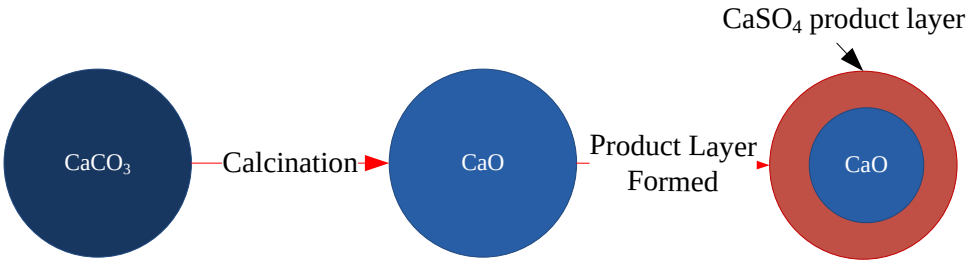

Figure 46. Indirect sulfation mechanism of limestone

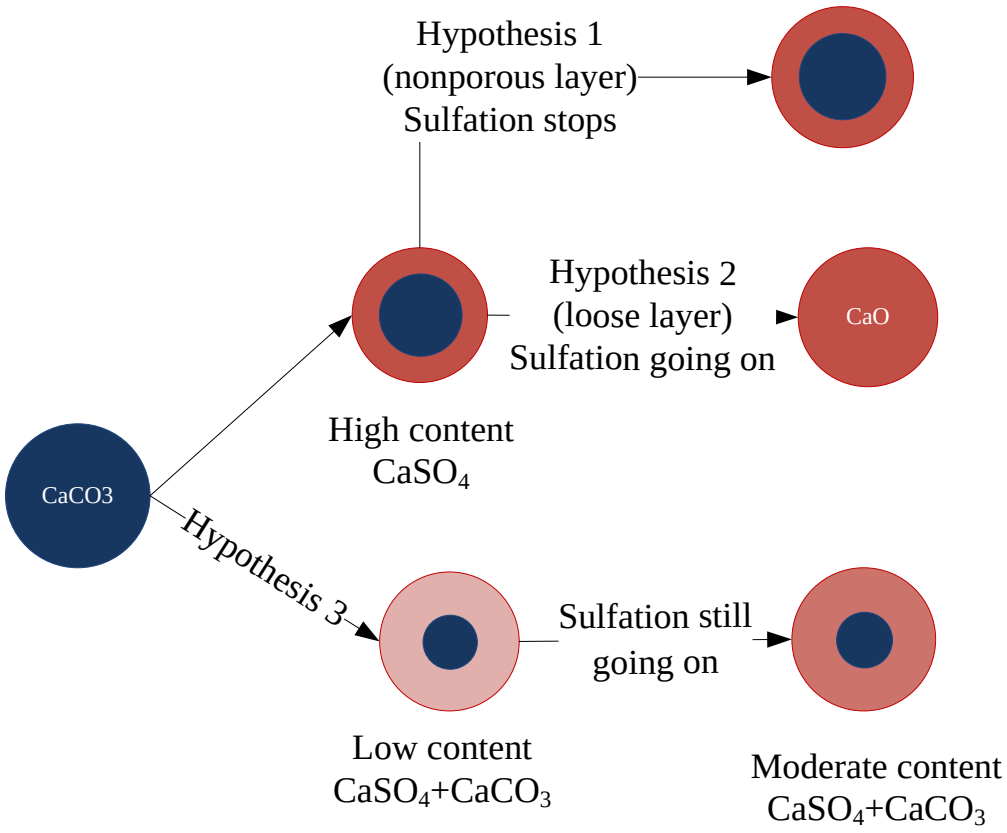

Figure 47. Hypotheses of direct sulfation mechanisms

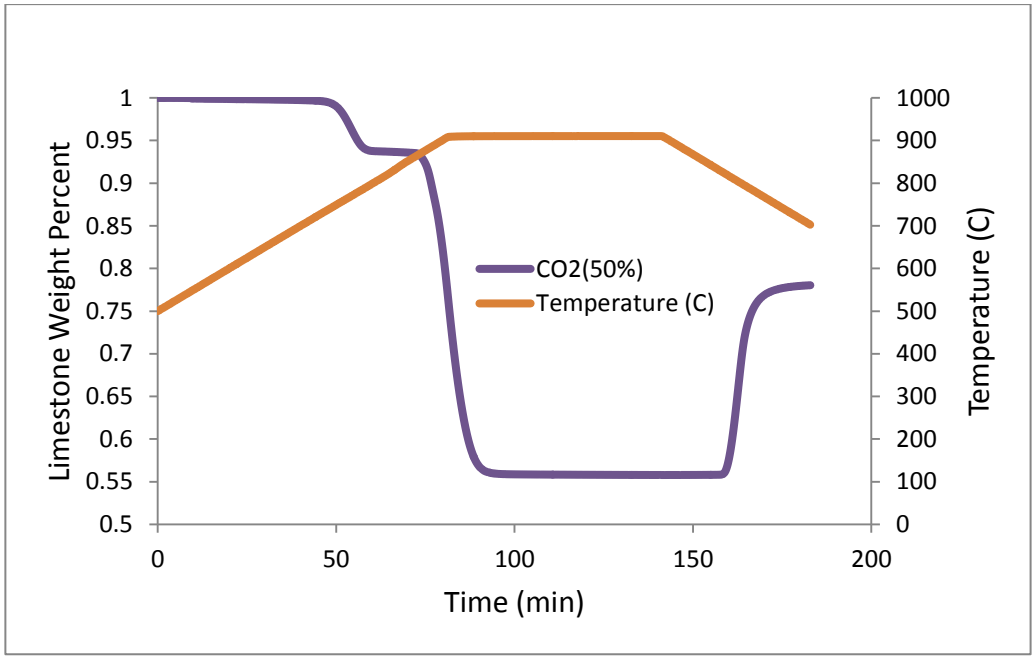

Figure 48 Calcination and carbonation of limestone at 50% CO_2 +50% N_2

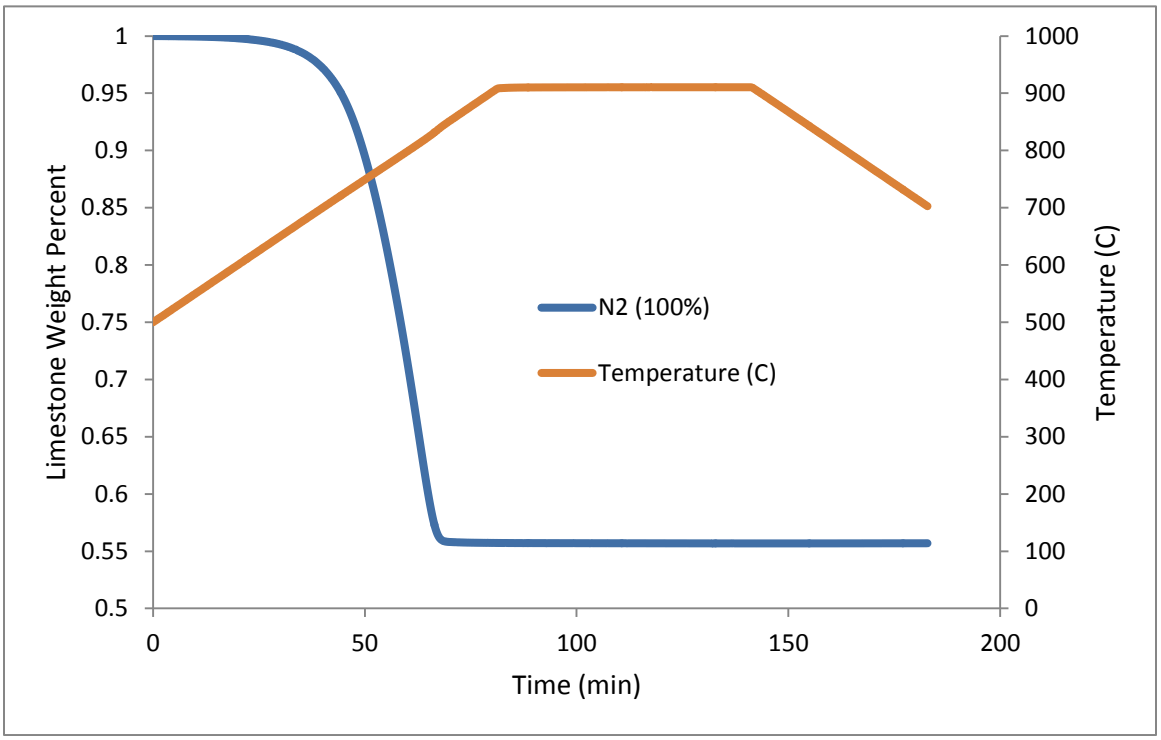

Figure 49 Calcination of limestone at 0% CO_2+100% N_2

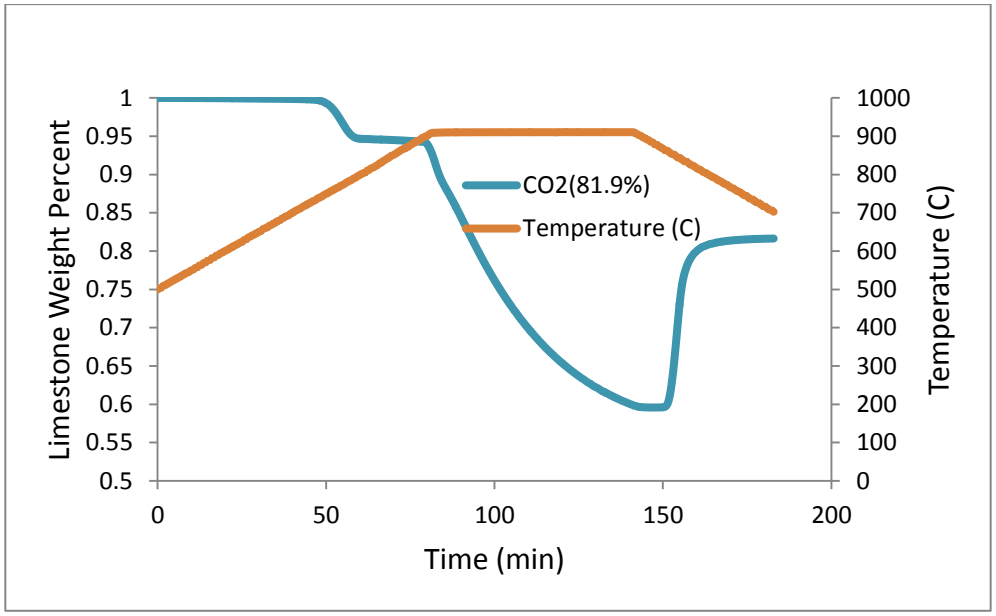

Figure 50 Calcination and carbonation of limestone in 81.9% CO_2+18.1% N_2

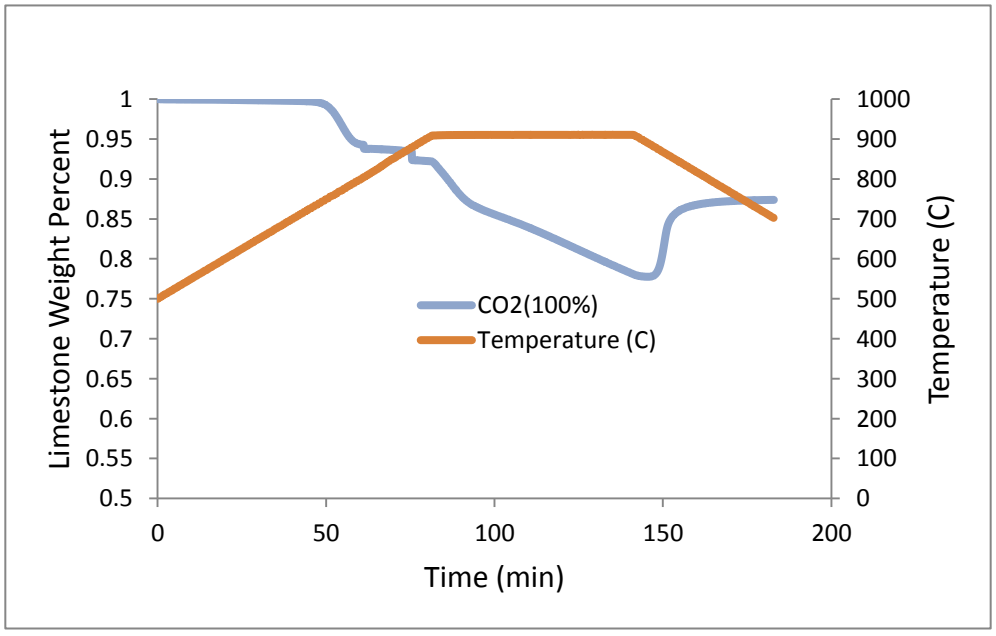

Figure 51 Calcination and carbonation of limestone in 100% CO_2.

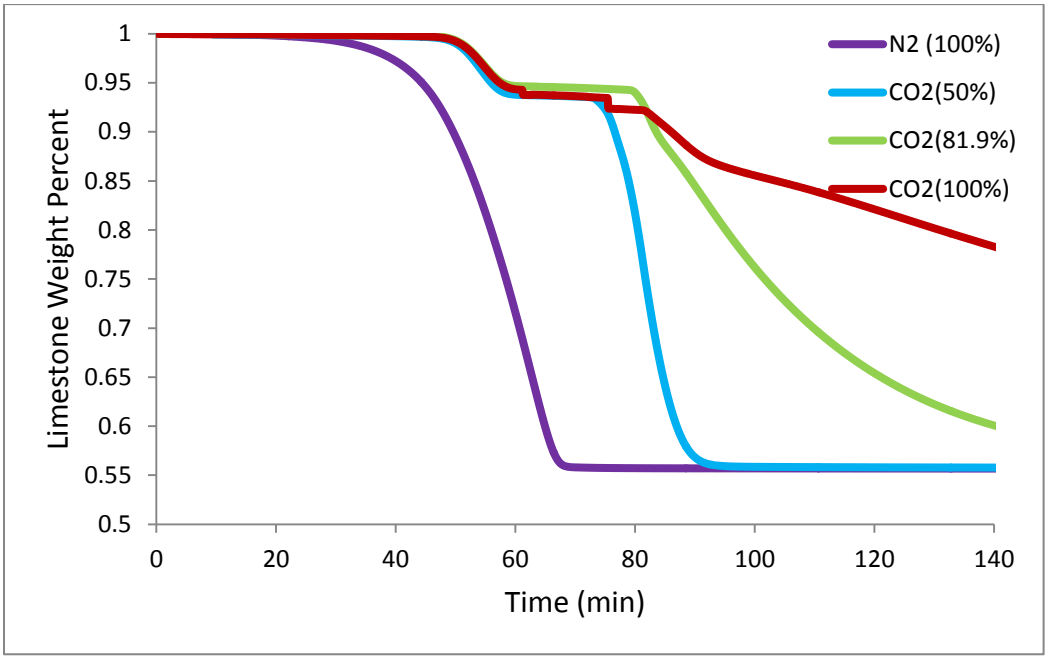

Figure 52 Effect of CO_2 partial pressure on onset of calcination of limestone.

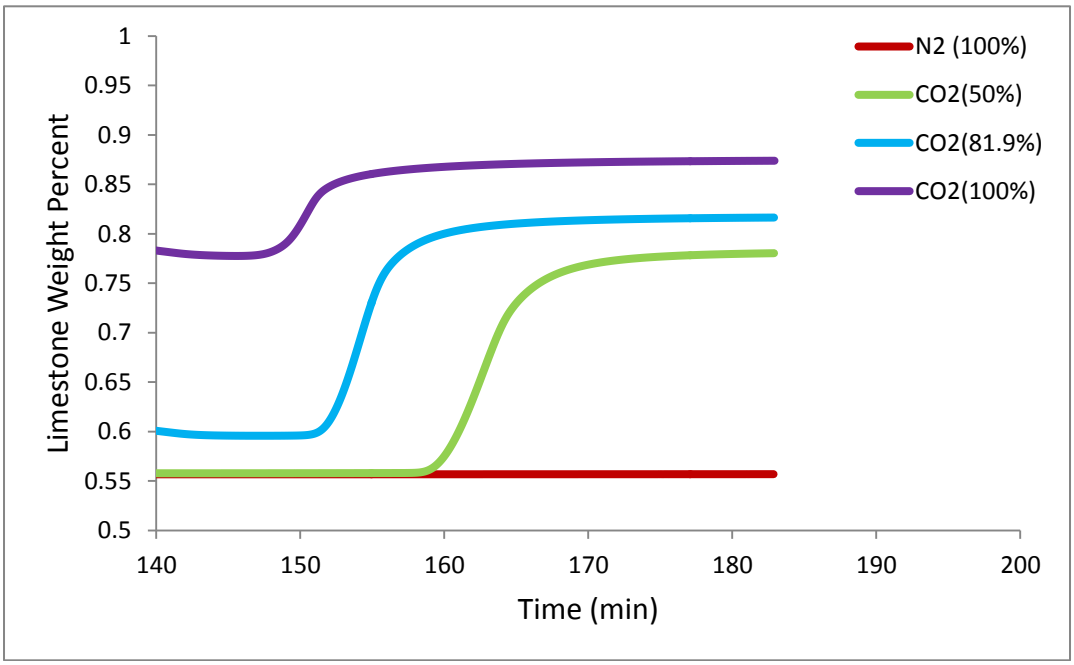

Figure 53 Effect of CO_2 partial pressure on recarbonation of limestone

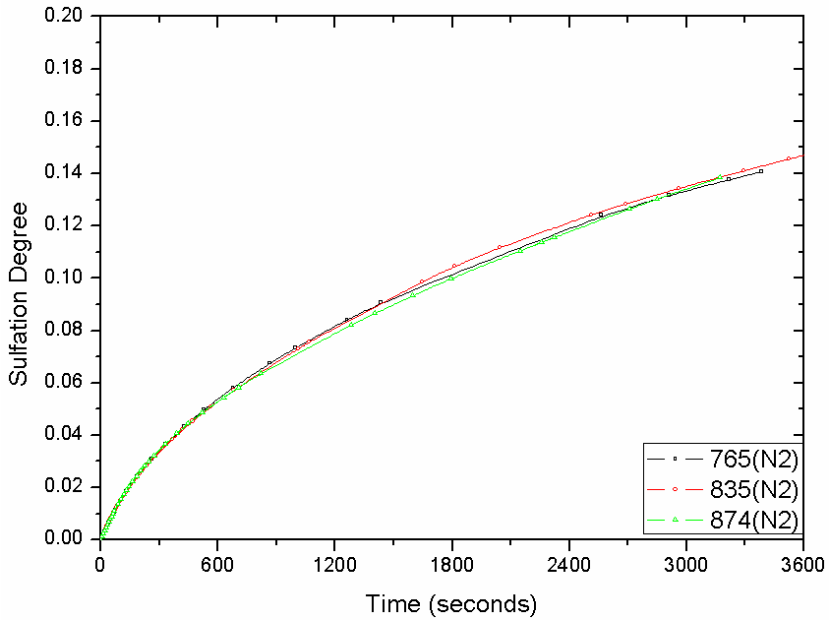

Figure 54. Effect of temperature on the sulfation degree of limestone (air firing).

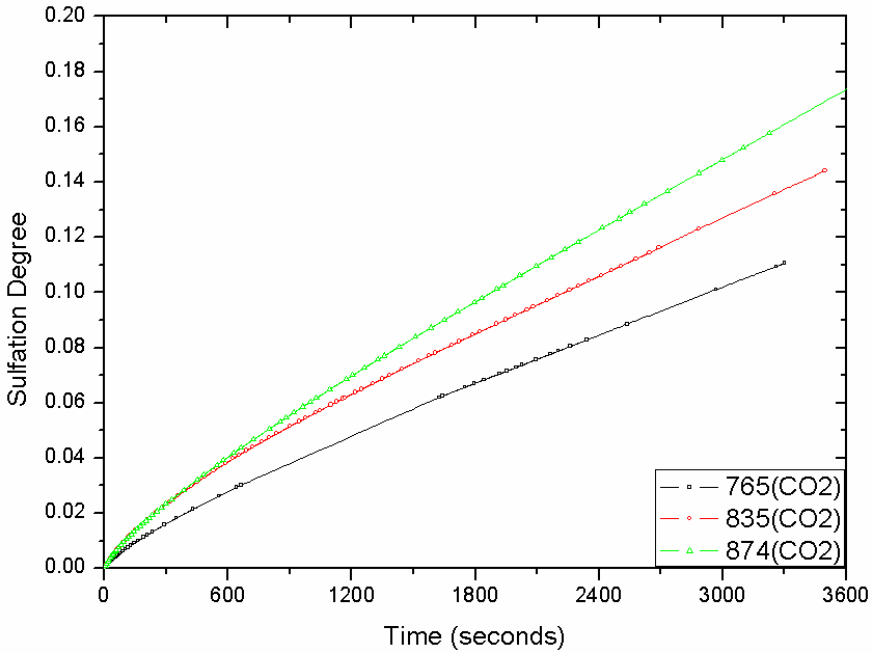

Figure 55. Effect of temperature on the sulfation degree of limestone (oxy firing).

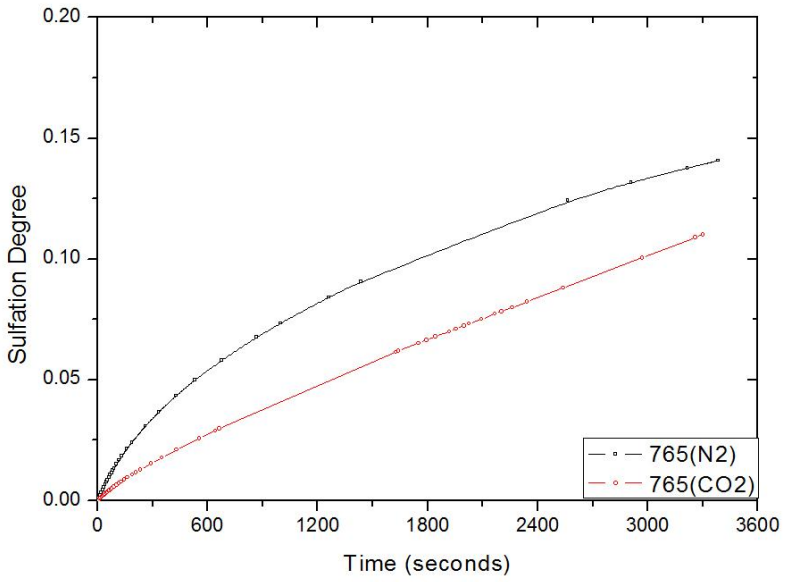

Figure 56. Comparison of sulfation degree of limestone between $N_2/O_2/SO_2$ and $CO_2/O_2/SO_2$ at T=765℃.

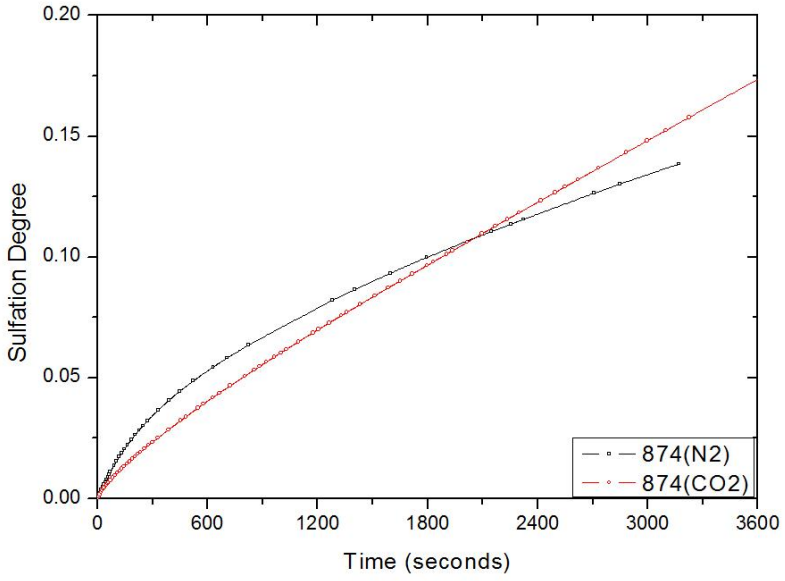

Figure 57. Comparison of the sulfation degree of limestone between $N_2/O_2/SO_2$ and $CO_2/O_2/SO_2$ at T=874℃

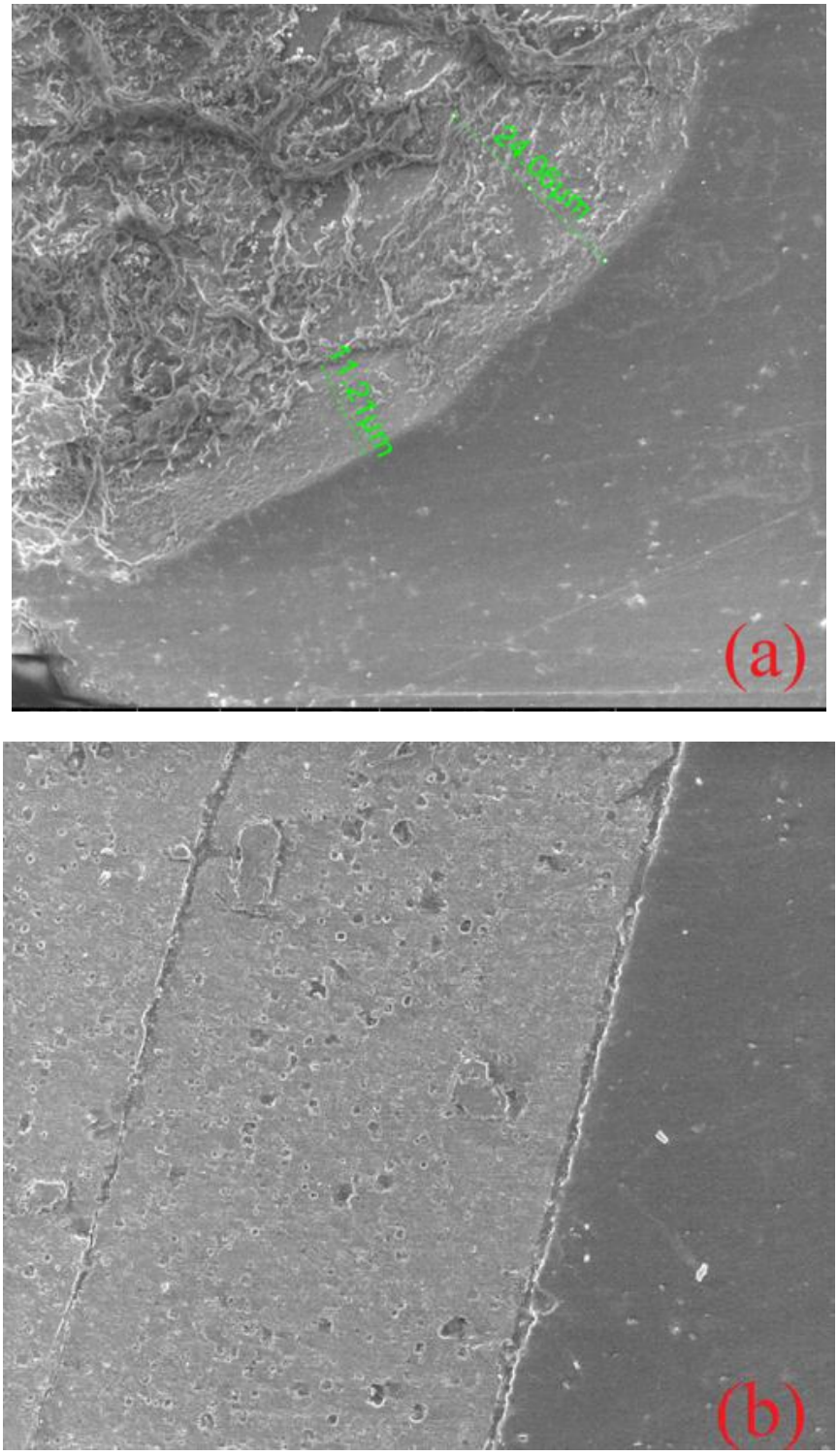

Figure 58. SEM photomicrograph of a sulfated limestone with a magnification rate (3.272K×), T=874 ℃. (a) 800 ppm SO_2, 20% O_2 and 80% N_2; (b) 800 ppm SO2, 20% O_2 and 80% CO_2.

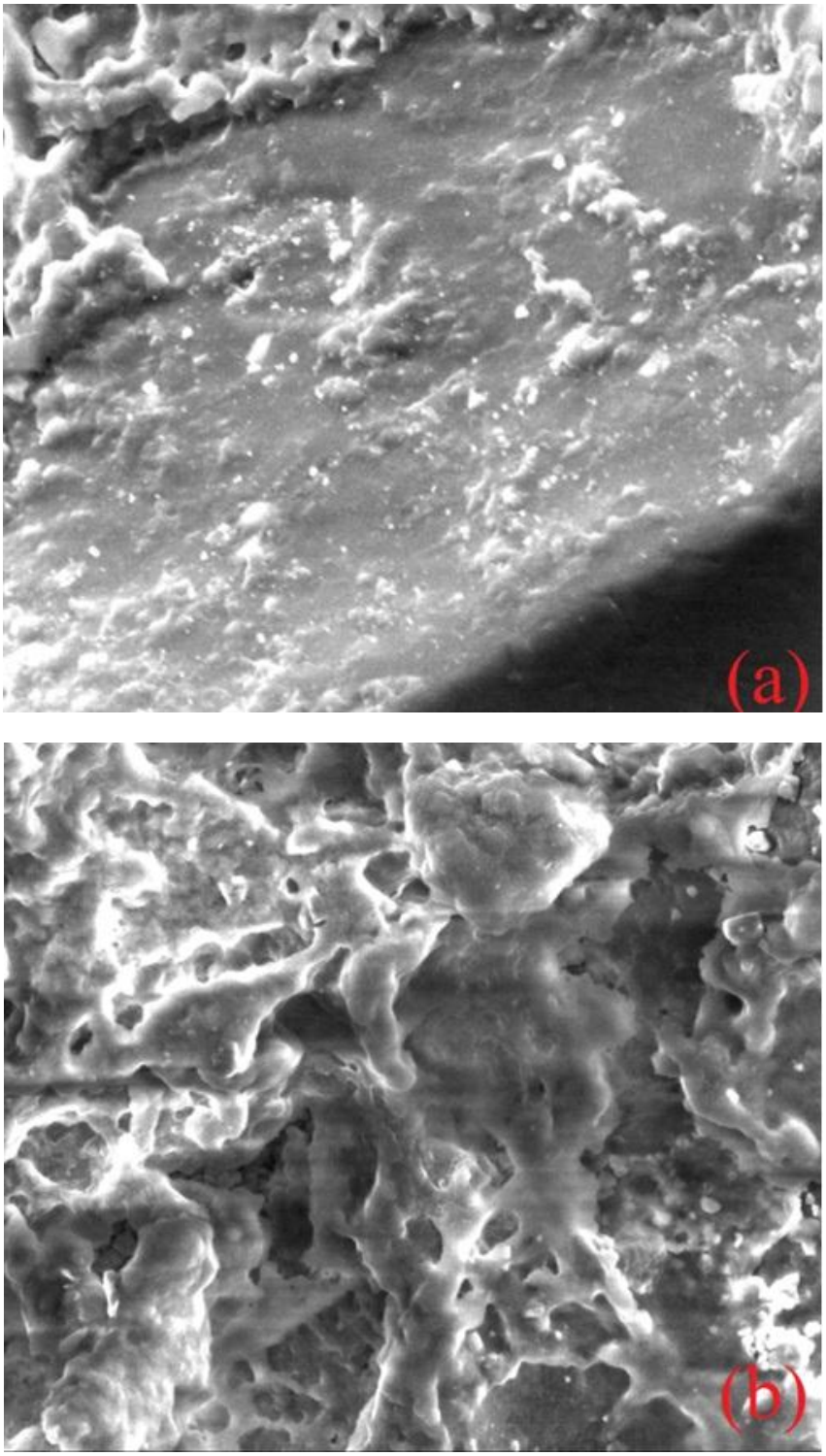

Figure 59. SEM photomicrograph of sulfated limestone with a magnification rate (20,000×) with 800 ppm SO_2, 20% O_2 and 80% N_2, T=874℃. (a) At the edge of a particle; (b) In the center of a particle.

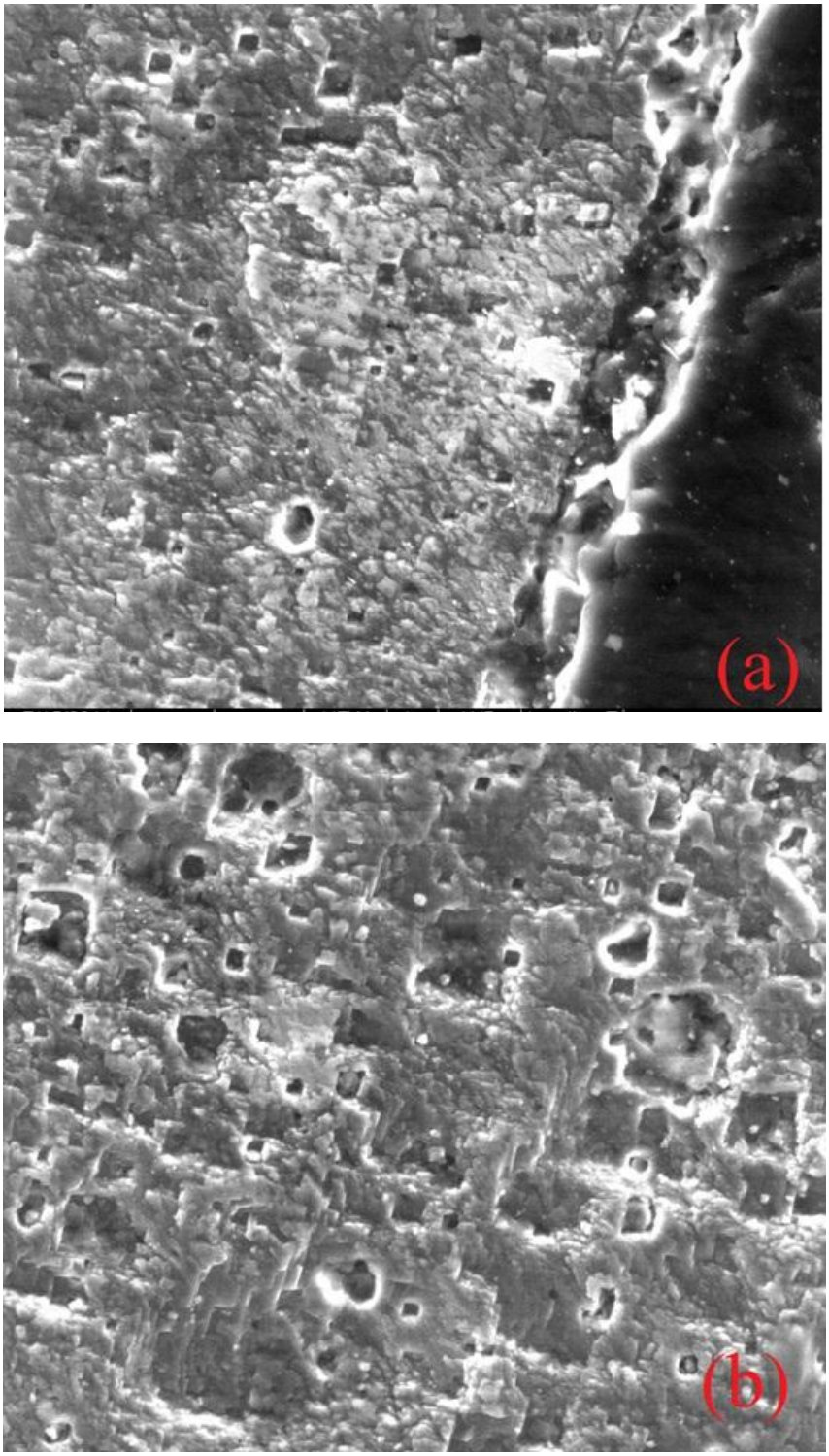

Figure 60. SEM photomicrograph of sulfated limestone with a magnification rate (20,000×) with 800 ppm SO_2, 20% O_2 and 80% CO_2, T=874°C. (a) At the edge of a particle; (b) In the center of a particle.

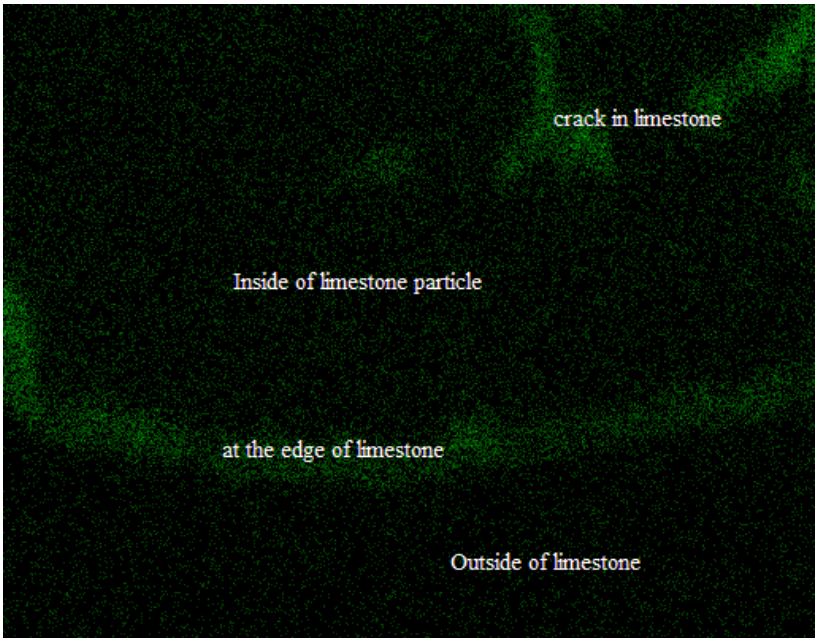

Figure 61 EDS photomicrograph of sulfated limestone at the magnification rate (3.272K×), T=874℃. 800 ppm SO_2, 20% O_2 and 80% CO_2

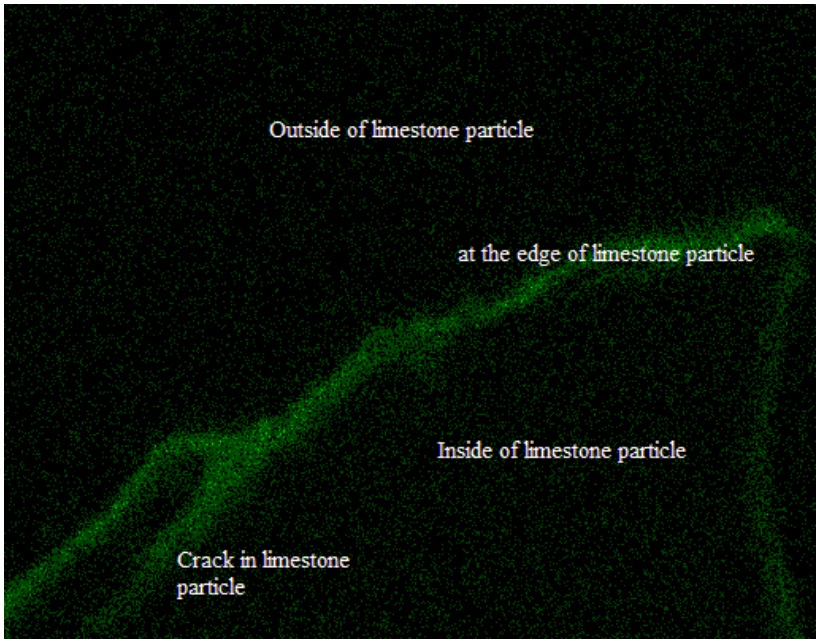

Figure 62 EDS photomicrograph of sulfur distribution at the magnification rate (3.272K×), T=874 ℃ 800 ppm SO_2, 20% O_2 and 80% N_2

CHAPTER 6

DEVELOPMENT AND APPLICATION OF A SINGLE PARTICLE MODEL

6.1. Introduction

Single particle models have been applied to many industrial and research problems, such as coal particle combustion, limestone-SO_2 system, catalyst pellets, and chemical vapor deposition (CVD), etc. Although there are different applications of the single particle model, there are some common features. First, they are a gas-solid system. Second, they are associated with reaction and diffusion. The common scheme for these types of procedures is shown in Figure 63.

Usually, the process of char particle combustion is strongly dependent on the particle temperature and its size. As suggested by Biggs [134], char particle temperature is associated with the external heat and mass transfer coefficients between a char particle and the bulk gas, the char combustion kinetics, and the particle-related CO/CO_2 product ratio. If char particle temperature is low and its size is small, it would be expected to be kinetically dominated. On the contrary, it is likely to be diffusion controlled at a high temperature and large particle size. The difference is whether mass species and temperature gradients exist inside the particle. The shrinking core particle model can be applied to the diffusion controlled case, and it divides the

particle into a reacted zone and an unreacted zone. There is evidence that particle size influences the reaction rate at higher temperatures, whereas at lower temperatures, the rate could be essentially independent of particle size [135-137].

The single particle model can also be applied to the limestone-SO_2 capture process. In most previous formulations, it is a simplified model for gas-solid reaction, which assumes a sharp boundary between the unreacted core and the formed product layer. It is often valid for nonporous particles but not for porous particles [114, 148].

The low chemical conversion during the sulfation process of limestone is due to the following issue. The solid volume expands significantly with the formation of $CaSO_4$, since its molar volume is 172% larger than that of CaO and 34.5% larger than that of $CaCO_3$. Expanding solid volume could block the pores, preventing SO_2 from diffusing into the particle.

6.2. Objectives

A shrinking core particle model is used to deal with large size particles at a high temperature. Fine size particles at a low temperature are kinetically controlled, and the whole particle is homogenous. A computational framework for a single particle is developed, which can handle both kinetic and diffusion controlled scenarios. The research objective is described as the following:

i. Develop a single coal particle model based on a computational framework.

ii. Develop a single particle model for limestone-SO_2 interactions.

6.3. Single particle model methodology

In this model section, we present a mathematical framework for a generalized gas-solid and reaction-diffusion single particle model. The mathematical framework presented in this study is based on “multiple grains”. This particle model originates from a series of governing equations that couple effective diffusivity inside pores, external mass convection in the bulk gas, internal heat conduction, external heat convection, radiation, and chemical reaction heat generation. The governing conservation equations include one energy equation and several mass equations (the number is determined by how many mass species are in the system, including both gaseous and solid species). All the mass conservation equations and the energy equation are coupled through reaction and heat generation terms. Numerical methods to solve the stiff problem are used, such as implicit time integration and dynamic time stepping.

Before the generalized gas-solid and reaction-diffusion single particle model is set up, three points will be made: First, a philosophical idea behind the model is given. The philosophy of a model provides a consistent approach to solving a particular problem, in much the same way that a person’s mind governs the actions they take. Second, a series of transport equations will form the mathematical framework, just as a skeleton forms a physical framework for a human body. Finally, discretization techniques, numerical methods, and computer code must be combined together to solve the governing equations.

A complete model for a single particle was developed. This work will provide a tool for academic and industrial research and development, and is widely applicable to problems such as chemical vapor deposition, coal combustion, catalyst pellets, and polymer material drying.

6.3.1. Classification of particle models

There are three types of single particle models: the shrinking core particle model, multigrains model, and fine single particle model. Shrinking core particle models and multigrains models are used to model particles with internal gradients. A single particle model is suitable for these model particles without internal gradients. Shrinking core particle models are based on an assumption of a nonporous reactant, even if the solid reactant has considerable porosity. Chemical reaction and external mass diffusion are coupled during the reaction of nonporous solids. The surface shows up as one of the boundary conditions where the chemical reaction happens at the plane surface of a solid.

Three different regimes are identified by Szekely et al. [206] as a function of different ranges of temperature. The intrinsic reactivity of the solid is slow at low temperatures; hence, at low temperatures, the concentration of gaseous species is uniform throughout the particle. The overall rate is dominated by the intrinsic chemical reaction. There is not any gradient of gaseous species throughout the particle.

With an increase of temperature, the intrinsic solid reactivity becomes greater, and most reactions occur near the external surface of the particle. Both diffusion within

the pores and chemical reactions are dominated by the progress of the reaction. At higher temperatures, the solid reactivity will be so fast that gaseous species will react with the solid when they reach the particle surface. Consequently, the progress of reaction is dominated by external mass transfer.

6.3.2. Single coal particle combustion model

The mathematical framework of the generalized model is based on governing equations, including one energy equation and several mass equations. The energy equation provides the profile of temperature in time and space. Also, these mass equations can provide species concentrations in time and space. Mass equations are coupled with the energy equation by the Arrhenius equation, which gives the connected bridge between reaction rate constant and temperature. Also, the temperature of a coal particle is associated with external heat convection and internal heat conduction, radiation, and chemical heat generation. Moreover, the chemical heat generation is relative to mass species, which couples the energy and mass equations. At the same time, the profiles of mass species are also dependent on the temperature due to the kinetics rate constant. During the computing process, all of the parameters are coupled. The model nomenclature is shown in Table 16.

The energy conservation equation given by (6.1) describes the temperature profile along with time and space.

$$c_p \frac{\partial(\rho_s T)}{\partial t} = \frac{1}{r^2}\frac{\partial}{\partial r}\left(r^2 \lambda_{eff,s} \frac{\partial T}{\partial r}\right) + \sum \Delta H_i \hat{r}_i \qquad (6.1)$$

There is net flux when stoichiometry is not 1 in the reaction. Thus, the convective term should be included in equation (6.1). For a particle model, there are typically some general assumptions made to allow us to neglect the convective term for certain model applications:

i. For a coal particle combustion model, the overall reaction is $C+O_2—CO_2$. There is no net flux since stoichiometry is 1, so the convective term is zero.

ii. For the sulfation model, since the sulfation process is very slow for a large particle, and the net flux is very small, then we can ignore it.

Two boundary conditions are located in the particle center and at the particle surface. Heat flux is zero in the center of the particle. Also, another boundary condition at the particle surface is associated with radiation and external heat convection, which allows the exchange of thermal energy between the particle and the external environment.

Boundary condition 1 in the center of the particle is represented by the formula

$$\left.\frac{\partial T}{\partial r}\right|_{r=0} = 0$$

Boundary condition 2 at the particle surface is shown by the following equation:

$$\lambda_{eff}\left.\frac{\partial T}{\partial r}\right|_{r=R}=\varepsilon_r h\left(T_s-T_b\right)+\delta\left(T_s^4-T_w^4\right)$$

The convective heat transfer coefficient between particle and bulk gas is given as:

$$h=\frac{Nu\bullet\lambda_f}{d}$$

As well, the mass conservation equations for gas species will be written in the following general forms:

$$\varepsilon_s\frac{\partial c_j}{\partial t}=\frac{1}{r^2}\frac{\partial}{\partial r}\left(r^2 D_{eff,j}\frac{\partial c_j}{\partial r}\right)+\sum\nu_{i,j}\hat{r}_j \qquad (6.2)$$

Boundary condition 1 is located in the center of particle:

$$\left.\frac{\partial c_j}{\partial r}\right|_{r=0}=0$$

Boundary condition 2 lies at the particle surface:

$$D_{eff,j}\left.\frac{\partial c_j}{\partial r}\right|_{r=R}=k_j\left(c_{j,s}-c_{j,b}\right)$$

And the mass transfer coefficient between single particle and bulk gas is given by the following expression:

$$k_j = \frac{Sh \bullet D_j}{d}$$

Robin boundary condition is one highlight in my computational framework, which represents the exchange of mass or energy between internal particle and external environment. For example, how does it account for CO_2 to cross the system boundary? Does CO_2 diffuse out of the particle or is it forced out by decomposition? According to the boundary condition, $c_{CO_2,s}$ is updated with each time step. If $c_{CO_2,s}$ is higher than $c_{CO_2,b}$, then CO_2 diffuses out; otherwise, it diffuses in.

Mass conservation equations should also include equations for solid species. An assumption of the solid phase is that the solid phase is unmovable. Consequently, the solid mass equations do not have boundary conditions, unlike the gas mass equations, just an initial condition.

$$\varepsilon_j \rho_j \frac{\partial \omega_j}{\partial t} = \sum \nu_{i,} \hat{r}_j M_j \tag{6.3}$$

Two types of reactions (heterogeneous reactions and homogenous reactions) link all mass equations. Moreover, the reaction constant is associated with temperature, which links to the energy equation. Depending on the rate law, a chemical reaction is also a function of the concentrations of the various species.

Every parameter (i.e., molecular diffusivity coefficient, heat capacity, effective diffusivity, solid phase porosity, thermal conductivity) can be a function of other factors (such as temperature, mass species concentrations, and solid species content). Considering the effective diffusivity of component j as an example, multicomponent effects will be considered. The diffusivity (molecular diffusion coefficient) of the gas species in the particle will be calculated by the Chapman–Enskog equation [207].

$$\mathcal{D}_{AB} = CT^{3/2}\frac{\sqrt{\left\{\left(M_A + M_B\right)/\left(M_A M_B\right)\right\}}}{P\sigma_{AB}^2\Omega_D} \tag{6.4}$$

$$\Omega_D = \frac{A}{\left(T^*\right)^B} + \frac{C}{\exp\left(DT^*\right)} + \frac{E}{\exp\left(FT^*\right)} + \frac{G}{\exp\left(HT^*\right)}$$

$$T^* = \frac{k_b T}{\varepsilon_{AB}}$$

$$\sigma_{AB} = \frac{\sigma_A + \sigma_B}{2}$$

$$\varepsilon_{AB} = \sqrt{\varepsilon_A \varepsilon_B}$$

Gas species diffusivity's mixing rule comes from the Stefan-Maxwell diffusion equation. The diffusion coefficient of species A to the remaining mixture, containing B, C, D, and other species equations, is given by the following equation:

$$D_{A,m} = \frac{1 - X_A}{\frac{X_B}{D_{AB}} + \frac{X_C}{D_{AC}} + \frac{X_D}{D_{AD}} + \cdots} \tag{6.5}$$

The effective diffusion coefficient of gaseous components within the particle pores are calculated considering both molecular diffusion and Knudsen diffusion, which should consider particle porosity and a tortuosity factor.

$$D_{A,M}^{K} = D_{A,M} \frac{\varepsilon}{\varepsilon_0} \frac{\tau_0}{\tau} \tag{6.6}$$

$$\frac{\varepsilon}{\varepsilon_0} = 1 - \frac{(Z-1)(1-\varepsilon_0) X}{\varepsilon_0} \tag{6.7}$$

From equations (6.4) through (6.7), the value of effective diffusivity of each location at one time can be obtained, and it is very dependent on the temperature, gas species concentrations, and a variety of other factors (i.e., porosity, tortuosity factor, and conversion rate). All variables are updated at each mode and each time step. At the same time, the effective diffusivity will affect gas species transport, which is an

important factor to determine the gas species concentration distribution at the next time step. From the above example of effective diffusivity, we have the same strategy for the thermal conductivity, porosity of solid matter, density of overall solid matter, and reaction rate constants.

6.3.3. SO_2 limestone particle model

Silcox [208] developed a mathematical model to predict the behavior of sulfated limestone. His grain model coupled the gas mass transport equation (SO_2) with a solid reactant (CaO) kinetics equation, associated with the change of thickness of the product layer ($CaSO_4$). One of his assumptions was that SO_2 mass transport was at a steady state. Another important assumption was that SO_2 concentration at the particle surface was equal to that in the bulk gas stream. In my sulfation model, the following assumptions were given in the development of the limestone-SO_2 mathematical model:

i. The limestone particle is fully converted into CaO for the indirect sulfation mechanism; alternatively, limestone particles cannot be formed into CaO by the calcination reaction for the direct sulfation mechanism.
ii. The system is isothermal.
iii. The sulfation reaction is irreversible.
iv. The product layer is made of $CaSO_4$.
v. The particle is spherical.
vi. The diffusivity inside the product layer is uniform.
vii. There is no reaction inside the unreacted core.

viii. The overall particle is unchangeable during reaction.

ix. The effect of O_2 concentration is negligible.

All nomenclatures are in Table 17. The unsteady-state mass conservation for SO_2 is shown as the following expression (in the product layer):

$$\frac{\partial C_{SO_2}}{\partial t} = \frac{1}{r^2}\frac{\partial}{\partial r}\left(r^2 D_{eff,SO_2} \frac{\partial C_{SO_2}}{\partial r} \right) \tag{6.8}$$

One boundary condition is located at the particle surface (r=R), another lies where the chemical reaction occurs at the plane surface of the solid ($r=r_f$).

$$\left.\frac{\partial C_{SO_2}}{\partial r}\right|_{r=r_f} = k_s C_{SO_2}$$

$$\left. D_{eff,j} \frac{\partial C_{SO_2}}{\partial r}\right|_{r=R} = h_{SO_2}\left(C_{SO_2,s} - C_{SO_2,b} \right)$$

The total mass balance for solid reactants (CaO, $CaCO_3$) depends on indirect or direct suflation.

$$\frac{dr_f}{dt} = -\frac{M}{\rho} k_s C_{SO_2,f}^{\alpha} \tag{6.9}$$

The effective diffusivity is proposed to be varying with conversion according to the following expressions [209], where $\tau=1/\varepsilon$ and $\tau_o=1/\varepsilon_o$ are taken from the paper written by Reyes [210]:

$$D_e = D_{eo}\frac{\varepsilon}{\varepsilon_o}\frac{\tau_o}{\tau} \tag{6.10}$$

$$\frac{\varepsilon}{\varepsilon_0} = 1-\frac{(Z-1)(1-\varepsilon_0)X}{\varepsilon_0} \tag{6.11}$$

$$D_e = D_{eo}\left[1-\frac{(Z-1)(1-\varepsilon_0)X}{\varepsilon_0}\right]^2 \tag{6.12}$$

6.4. Results and discussion

Using the same computational framework, an unreacted shrinking core particle model is developed. The multigrains model is applied to char particle combustion, and the shrinking core particle model is used for the investigation of the limestone-SO_2 system.

6.4.1. Multigrains model in single char particle combustion

The multigrains model of single char particle combustion is performed at different particle sizes (50 μm, 3000 μm), as in Figure 64 —Figure 66. The simulation

results show the evolution of fixed carbon with reaction time and char particle space. Fine particles (50 μm) are typically kinetically dominated, while large particles are more likely to be diffusion controlled. Generally, fine particles are considered to be a uniform point, with no gradients in temperature or gaseous species inside the char particle. On the contrary, large particles are usually modeled using a shrinking core particle model due to the gradients in temperature and mass species inside the char particle. However, the fine particle model and shrinking core particle model are two special applications of the multigrains model. Figure 64 shows the evolution of fine char particle (50 μm) combustion over 1 second, while Figure 65 represents that of large char particle (3000 μm) combustion for the same time period. Their performances are totally different. Fixed carbon consumption is much faster in a fine char particle than in a large char particle. The whole particle “burns” when the char particle is fine, unlike with large char particles. In other words, fixed carbon burns more evenly for fine char particles, eliminating gradients of temperature and mass species.

If a longer reaction time is selected for the large particle, the characteristic of a shrinking core particle model is acquired. As Figure 66 shows, the evolution of fixed carbon shows clear evidence of diffusion control. Obviously, the fixed carbon is burned out layer by layer from outside to inside. The combustion front of fixed carbon has a sharp layer, which is a well-known assumption in the shrinking core particle model. Hence, the shrinking core particle model is only one of the special applications for the general gas-solid model.

6.4.2. SO_2 limestone model

The SO_2 limestone model is based on the single particle computational framework. The validation of the temperature dependence of the degree of sulfation for an indirect and direct sulfation mechanism is accomplished using the proposed sulfation mechanism. This sulfation model can help identify the difference between direct and indirect sulfation mechanisms. Sulfation behavior of limestone has a distinct performance in oxy and air firing conditions.

For direct sulfation, $CaCO_3$ is directly reacted with SO_2 to form $CaSO_4$. For indirect sulfation, an assumption is given that calcium carbonate is decomposed to 100% calcium oxide. Then, CaO is reacting with SO_2 to form $CaSO_4$ in the absence of the calcination process. The main parameters in the sulfation model are given in Table 18.

6.4.2.1. Direct sulfation mechanism

At the beginning of the sulfation reaction, the product layer of a limestone particle is so thin that the sulfation process is considered to be kinetically dominated. Our experimental data on sulfation degree were utilized to obtain the apparent reaction constant, as shown in Figure 67. At the beginning of the reaction (the degree of sulfation ≤0.03), the product layer is so thin that the sulfation process is considered as kinetically controlled [127]. Consequently, the effect of the product layer can be neglected. An Arrhenius expression for the reaction constant, k_s=0.087*exp (-5416/T), is obtained for direct sulfation of limestone, as shown in Figure 67. The diffusion processes within the particle during sulfation of limestone are so complex that the formula merely represents

an empirical, mathematical relationship that fits the data, but has no clear physical meaning [127]. The constants for the model of effective diffusivity of SO_2 in the limestone are obtained through fitting of the experimental results using a proposed sulfation model.

The effective diffusivity of SO_2 in the particle was obtained through fitting of the experimental results by using the above-mentioned model. In order to be consistent, the experimental data before 2500 seconds were used to fit both indirect sulfation and direct sulfation. If enough reaction time or sulfation degree is selected during the sulfation process, the sulfation process is considered as diffusion controlled due to the thickness of the product layer [127]. An Arrhenius form relationship was used to obtained a regressed formula of $D_{eff}=8.62*10^{-6}\exp(-13590/T)$, as shown in Figure 68. Due to the complexity of the fluidized system, an apparent reaction order must be obtained through fitting experimental data. The best fit occurs with an apparent reaction order of 0.1. The modeling results can predict experimental data quite well, as shown in Figure 69. The degree of sulfation is a strong function of operating temperature with direct sulfation, and this effect is accurately predicted by the model.

In addition, the effect of gas film diffusion on sulfation behavior under the direct sulfation mechanism can be explored based on the proposed sulfation model. Silcox [208] made an important assumption, ignoring SO_2 diffusion through the gas film. Thus, Silcox indicated that SO_2 concentration is equal to that in the bulk gas stream. The expression for the mass transfer coefficient (h_D) is shown as the following equation (6.13). The Sherwood number represents the ratio of convective to diffusive mass

transport. With an increase of Sherwood number, the mass transfer coefficient of SO_2 in the gas film is increasing. The Sherwood number can also be further defined as a function of the Reynolds number and Schmidt numbers, as it is expressed by the equation (6.14). There is an increase in the Sherwood number with an increase in Reynolds number. There is a question as to whether the change in Sherwood number at a fixed particle size will have an effect on the sulfation process. Or, as suggested by Silcox, can we ignore the diffusion through the gas film?

There are two limiting conditions for Sherwood number. One is the minimum Sherwood number value equal to 2. Another condition is that the value of Sherwood number is infinitely large, which means the SO_2 concentration on the particle surface is equal to that in the bulk gas stream. Simulation results are shown Figure 70, where it is apparent that there is no difference when Sherwood number is 2 or infinitely large. It suggests that Silcox's assumption is correct, and the process of SO_2 diffusing through the gas film can be considered negligible.

$$h_D = \frac{Sh \bullet D_{SO_2,gas}}{d} \tag{6.13}$$

$$Sh = 2 + 0.6\,\mathrm{Re}^{\frac{1}{2}}\,Sc^{\frac{1}{3}} \tag{6.14}$$

6.4.2.2. Indirect sulfation mechanism

The above-mentioned pore diffusion model was also used to explain the sulfation degree in indirect sulfation. The effective diffusivity in the particle for CaO-SO_2 was supposed to be varying with conversion according to equation (6.10) to equation (6.12) . Constant kinetics rate is obtained when the sulfation degree is less than 0.3%. The effect of the product layer can be neglected when the product diffusion layer is thin. An Arrhenius expression for the reaction constant, $k_s=1.976*10^{-3}$ exp (-201/T), is obtained for indirect sulfation of limestone, as shown in Figure 71. Our experimental data for sulfation degree were also used to obtain the estimated effective diffusivity for a reaction time of 2500 seconds, as in the previous discussion. The effective diffusivity of the product layer ($D_{eff}=1.42*10^{-12}$) was obtained through fitting the experimental data. The effective diffusivity of the product layer under indirect sulfation is constant, and not a function of operating temperature. The effective diffusivity of the product layer in direct sulfation was dependent on the temperature, instead of that in indirect sulfation. Since the effective diffusivity is obtained through fitting experimental data using the above-mentioned single particle sulfation model, then that should be consistent with the experimental data. The effective diffusivity in direct sulfation is a function of temperature because the sulfation degree in direct sulfation is dependent on temperature. However, that in the indirect sulfation is not associated with temperature since the sulfation degree in the indirect sulfation is not a function of temperature.

Due to the complexity of the fluidized system, an apparent reaction order must be obtained through fitting my experimental data. The best fit occurs with an apparent reaction order of 0.2. The modeling results can fit my experimental data quite well, as shown in Figure 72. Note that the degree of sulfation is not a function of operating temperature with indirect sulfation, and this effect is accurately reflected by the model.

6.5. Summary

A singe particle model was developed, which was applied as a single particle coal combustion model and a single limestone particle sulfation model.

i. For the single coal particle model, a shrinking core particle model and pulverized coal particle were demonstrated as two specific cases of my general single particle model.

ii. The single particle limestone sulfation simulation results are consistent with my experimental results.

iii. The degree of sulfation under direct sulfation conditions is quite sensitive to changes in operating temperature for the temperature ranges studied.

iv. The degree of sulfation under indirect sulfation conditions is not sensitive to change in operating temperature for the temperature studied.

v. Simulation results show that we can neglect SO_2 diffusion through the gas film.

Table 16 Nomenclature for single char particle combustion model

Nomenclature	Definition	Unit
A	Pre-exponential factor	1-mol/(m^2.s); 2-m^3/(mol.s)
c	Gas concentration	ppm
C	Mole concentration	mole/m^3
d	Diameter of particle	m
$D_{i,eff}$	Effective diffusivity of gas component i	m^2/s
D^K	Knudsen diffusivity	m^2/s
E	Activation energy	J/mol
ΔH	Heat of chemical reaction	J/mol
k	Reaction rate constant	
k_m	External mass transfer coefficient	m/s
M	Molecular weight	g/mol
m_c	Mass of fix carbon	kg
R_g	Universal gas constant	J/(mol.K)
$\hat{r}$	Reaction rate	mol/(m^3.s)
r	Particle radius	m
s	Pore surface area	m^2/m^3
T	Char temperature	K
X_c	Carbon conversion degree	
Z	Ratio of molar volume of solid phase	
Greek letters		
ρ	Particle density	kg/m^3
λ	Thermal conductivity	J/(m.s.K)
ε_s	Solid char porosity	
δ	Boltzmann constant	$J/m^2.s.K^4$
η	Stoichiometric coefficient ratio for CO/CO_2 for a given reaction	
σ	Characteristic length	
Ω_D	Diffusion collision integral	
ε	Molecular energy parameter	
ψ	Pore parameter	
τ	Tortuosity	
ν	Stoichiometric coefficient	
Subscript		
o	Initial	
C	Fixed carbon	
eff	Effective	
j	Component	
g	Gas	

Table 17 Nomenclature for sulfation model

Nomenclature	Definition	Unit
C	SO_2 molar concentration at same radius	mol/m^3
D	Diffusivity of SO_2	m^2/s
E	Activation energy	J/mol
H	Mass transfer coefficient of SO2 in gas film	m/s
k_s	Reaction rate constant on apparent area basis	m/s
r	Particle radius	m
R	Initial particle radius	m
R_g	Universal gas constant	J/(mol.K)
Sh	Sherwood number	
t	Reaction time	s
T	Particle temperature	K
X	Sulfation degree of sorbent (CaO, CaCO3), mole fraction	
Z	Ratio of molar volume of solid phase (reactant and product)	
Greek letters		
E	Porosity	
P	Particle density	mol/m^3
τ	Tortuosity	
Subscripts		
e	Effective	
f	Interface between product layer and unreacted core	
o	Initial	
s	Particle surface	

Table 18 The parameters in the sulfation model

Nomenclature& Unit	Definition	Value
C_{SO2} (ppm)	SO_2 concentration in bulk gas	800
$D_{SO2\text{-}air}$ (m^2/s)	Molecular diffusivity of SO_2 in air/CO_2	$1*10^{-5}$
M_{CC}	Molecular weight of $CaCO_3$	100
M_{CO}	Molecular weight of CaO	56
R (m)	Initial limestone radius	0.0004
R_g(J/(mol.K)	Universal gas constant	8.3142
Sh	Sherwood number	2-unlimited
T (K)	Reaction temperature	1038,1138,1147
ρ_{CC} (kg/m^3)	Density of $CaCO_3$	2910
ρ_{CO} (kg/m^3)	Density of CaO	3350
Z	Ratio of molar volume of solid phase ($CaSO_4$/CaO)	2.74
Constant kinetic rates	Calculated from experimental data (Arrhenius form)	
Effective diffusivity	Fitting experimental data using my above-mentioned model	
Apparent reaction order	Fitting experimental data using my above- mentioned model	

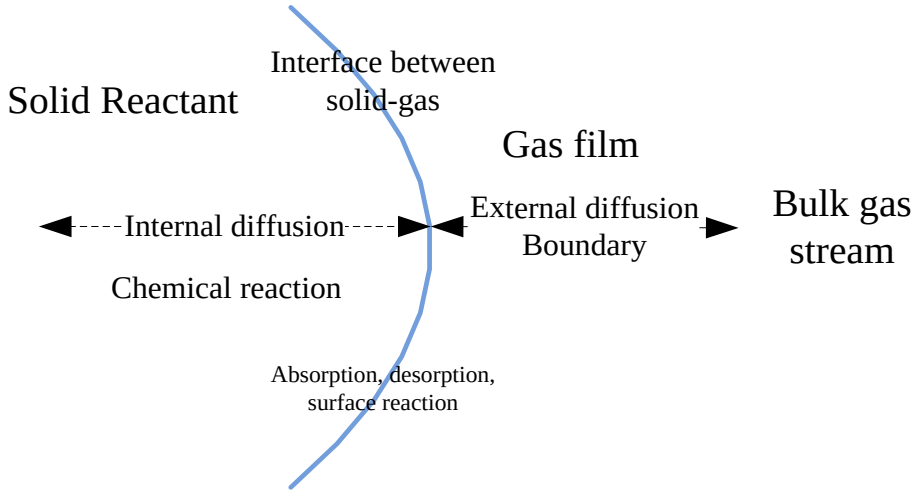

Figure 63 Scheme of general solid-gas and reaction-diffusion single particle system

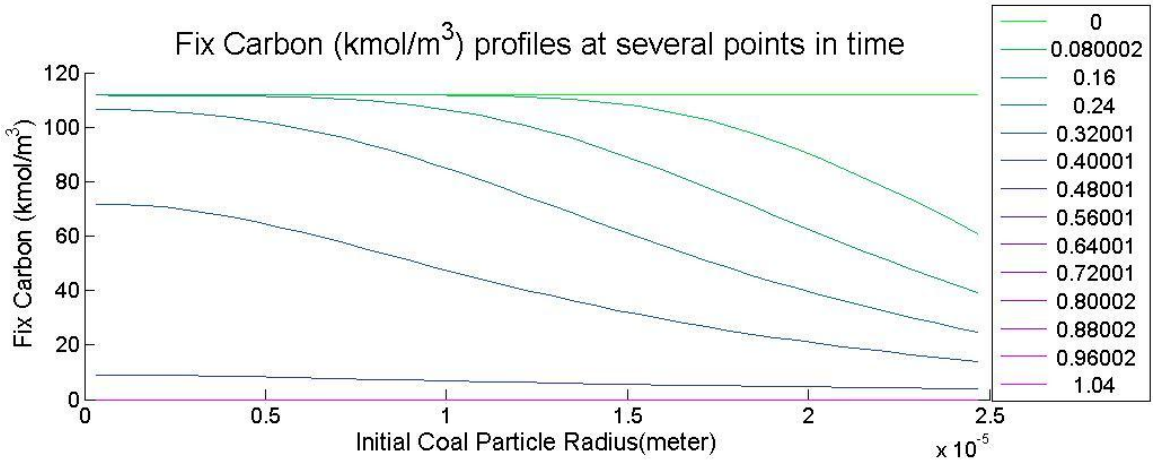

Figure 64 The evolution of fixed carbon in single coal particle (50µm) combustion model during 0-1 second

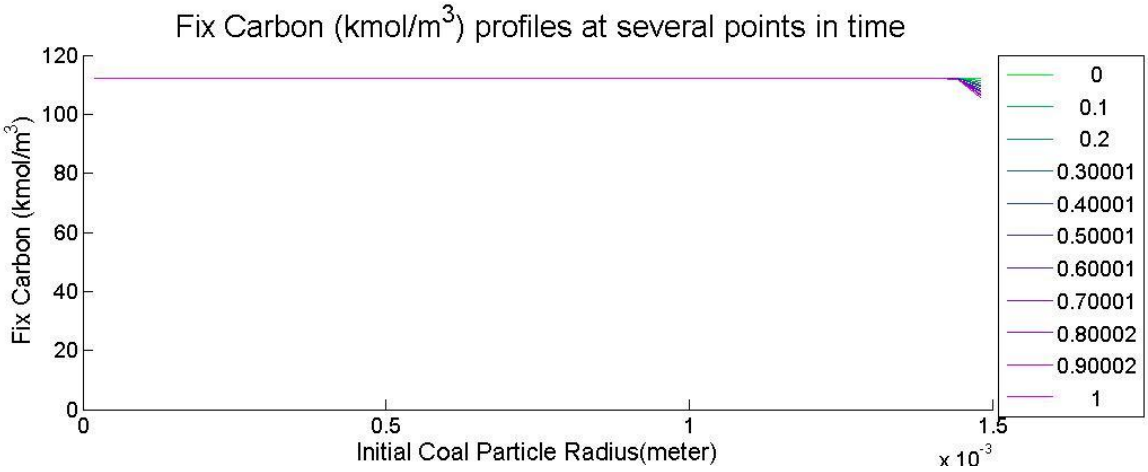

Figure 65 The evolution of fixed carbon in single coal particle (3000 µm) combustion model during 0-1 second

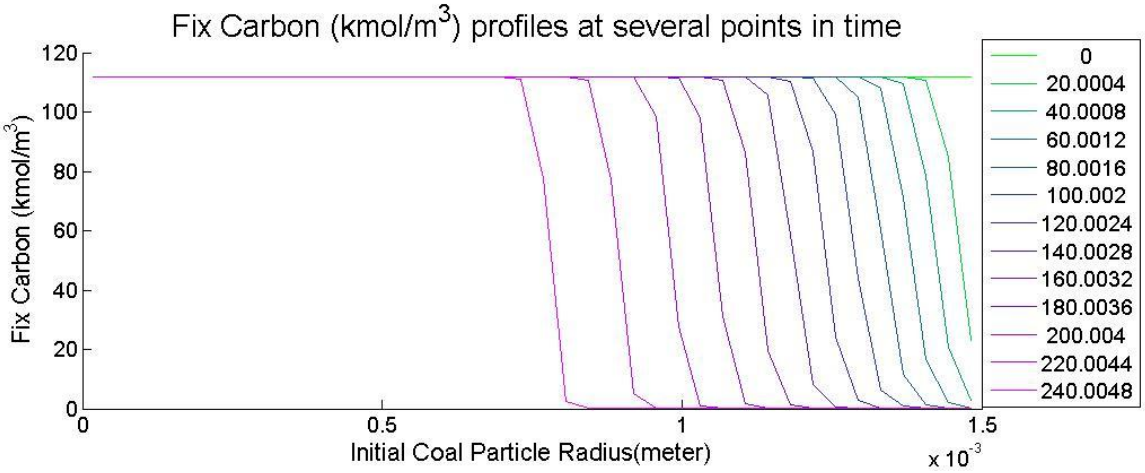

Figure 66.The evolution of fixed carbon in single coal particle (3000 µm) combustion model during 0-240 seconds

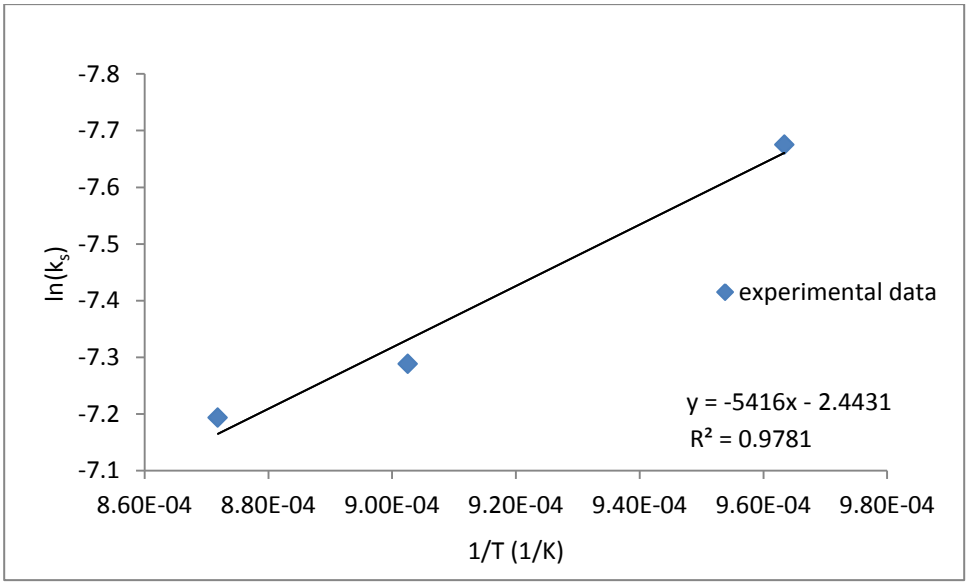

Figure 67 Arrhenius plot of ln(ks) vs. 1/T in an atmosphere of 20% O2, 80% CO_2, and 800 ppm SO_2 balanced with CO_2 (average limestone particle size: 800 µm)

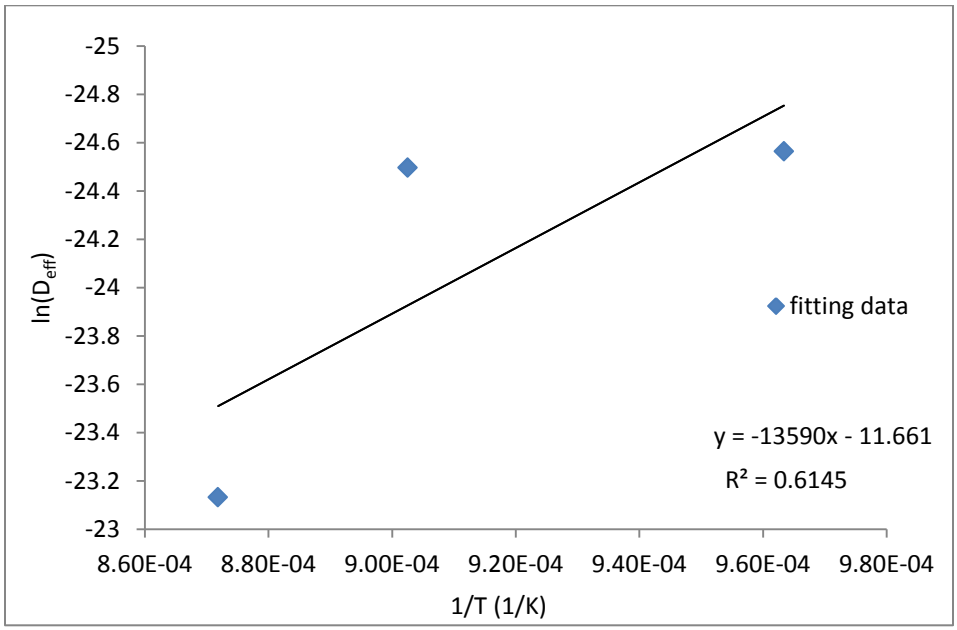

Figure 68 Arrhenius plot of ln(D_{eff})vs. 1/T in an atmosphere of 20% O_2, 80% CO_2, and 800 ppm SO_2 balanced with CO_2 (average limestone particle size: 800 µm)

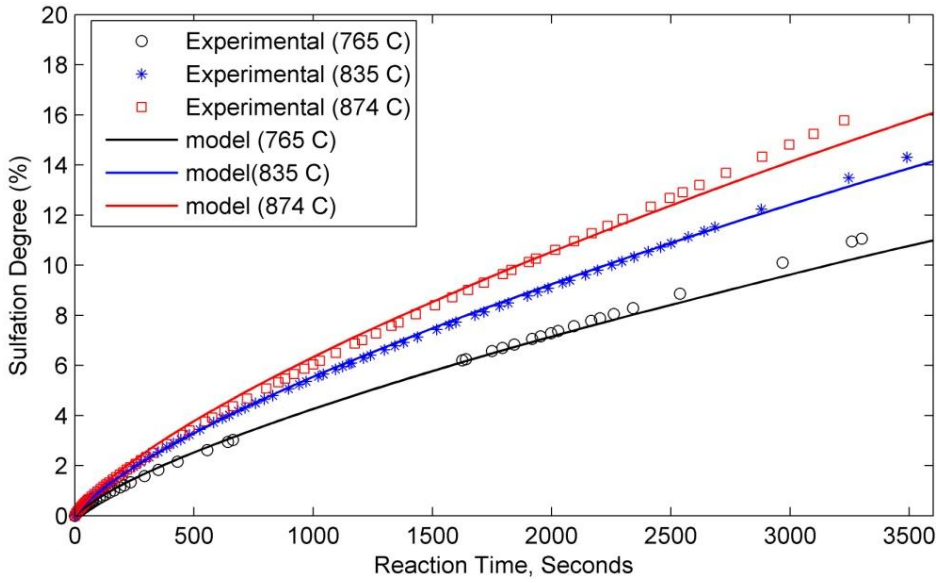

Figure 69 Variation of sulfation degree with time in an atmosphere of 20% O_2, 80% CO_2, and 800 ppm SO_2 balanced with CO_2 (average limestone particle size: 800 µm)

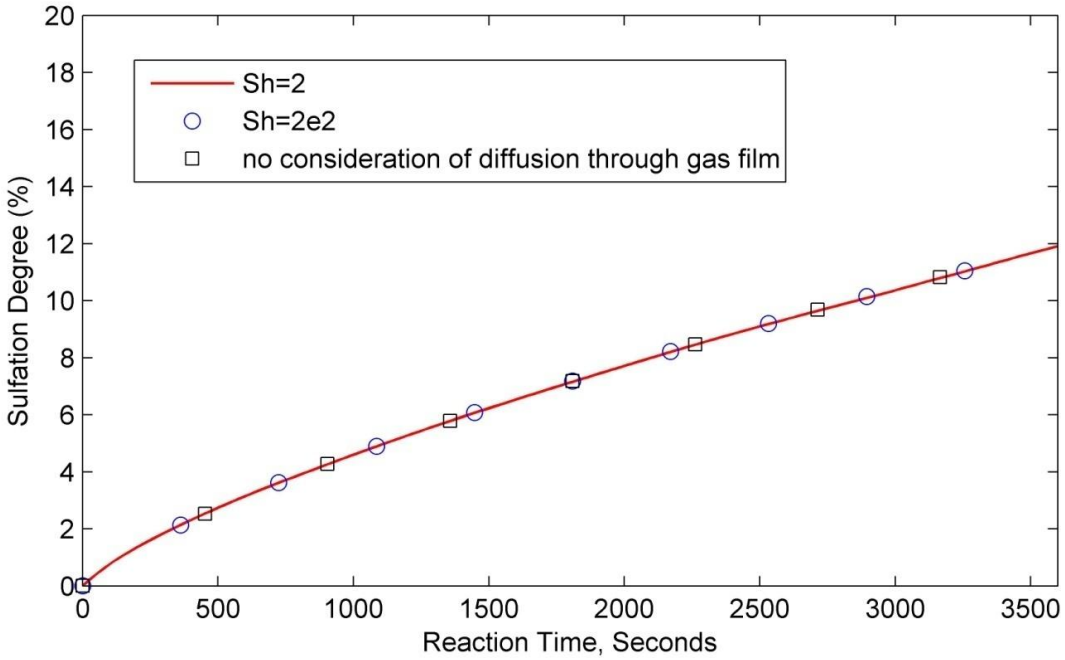

Figure 70 Effect of diffusion in gas film on sulfation behavior of limestone in an atmosphere of 20% O_2, 80% CO_2, and 800 ppm SO_2 balanced with CO_2 (average limestone particle size: 800 µm, 835 C temperature)

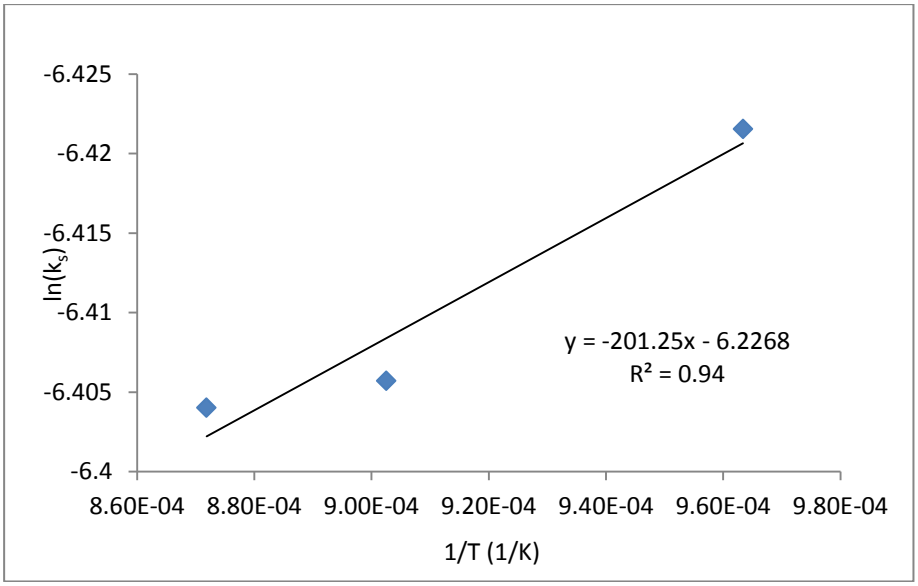

Figure 71 Arrhenius plot of ln(ks) vs. 1/T in an atmosphere of 20% O_2, 80% N_2, and 800 ppm SO_2 balanced with N_2 (average limestone particle size: 800 µm)

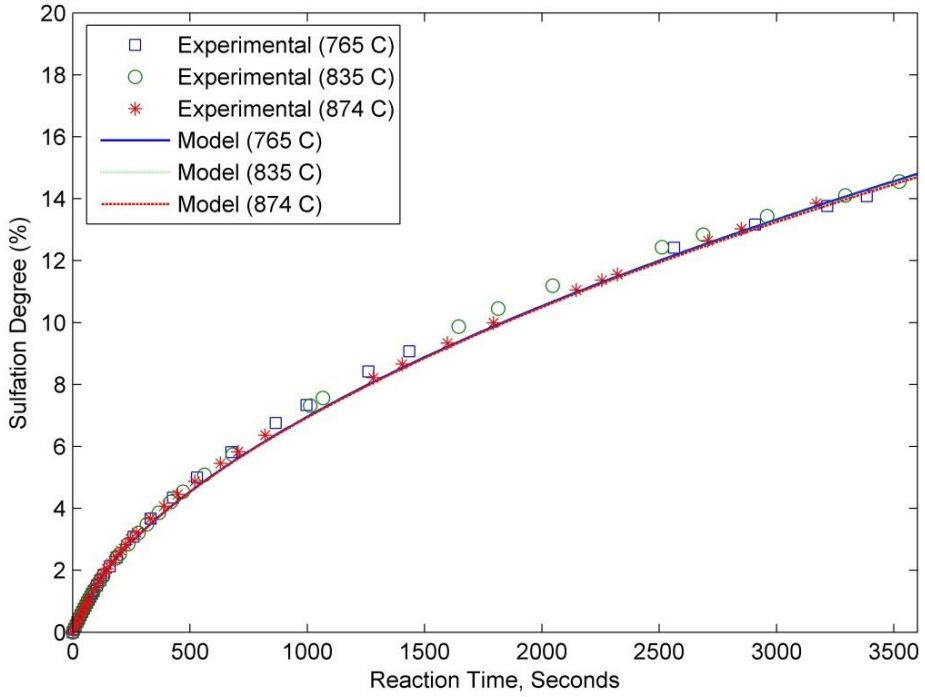

Figure 72 Variation of sulfation degree with time in an atmosphere of 20% O_2, 80% N_2, and 800 ppm SO_2 balanced with N_2 (average limestone particle size: 800 µm)

CHAPTER 7

SUMMARY AND CONCLUSION

7.1. Conclusion

A bench-scale bubbling fluidized (BFB) bed and a 330 KW pilot-scale circulating fluidized (CFB) were used to investigate SO_2 behavior in air and oxy coal combustion. SO_2 releases with and without limestone sorbent were investigated in N_2/O_2 and CO_2/O_2 environments for the following conditions: temperature range (765-902℃), O_2 concentration range (10-30%), and a wide range of Ca/S ratios.

The bench-scale experiments without recycled flue gas (RFG) and the equilibrium calculations of NASA Chemical Equilibrium with Applications (CEA) show no effect of combustion diluent (N_2, CO_2) on SO_2 emissions. In the pilot-scale CFB, SO_2 emissions (ppm) based on concentration are higher when oxy firing, but SO_2 emissions in terms of mass (lbs/MMBtu) are lower when oxy firing. The difference results from the use of RFG, which produces significantly higher SO_2 concentrations and thus facilitates sulfur capture by ash minerals. Limestone addition results in a significant reduction in SO_2 emission. SO_2 removal by limestone addition in air fired conditions is much higher than that in oxy fired conditions, in terms of the experimental data from the bench-scale bubbling fluidized bed (BFB).

In addition, sulfation behavior of limestone in $N_2/O_2/SO_2$ and $CO_2/O_2/SO_2$ atmospheres was studied, exploring the mechanisms of indirect and direct sulfation in a wide range of temperatures (765– 874℃). A significant temperature effect on sulfation behavior of limestone was seen during direct sulfation reactions. However, a limited temperature effect was seen for indirect sulfation reactions. A sharp, dense product layer is seen in SEM images under air firing conditions that blocks gas transport into pores. No distinct sharp layer is seen when oxy firing. Also, direct sulfation produced a higher "activity" for sulfur capture than indirect sulfation after a long reaction time under the conditions we tested.

A mathematical and computational framework for a single particle model was developed. The shrinking core particle model and pulverized coal particles are two specific cases of this general single particle model. Also, the simulation results from the sulfation model are consistent with my experimental results.

7.2. Recommendations for future research

Since SO_2 removal by limestone in oxy fired conditions does not produce high efficiencies for sulfur capture, it will be a significant challenge to control SO_2 emissions under oxy fired conditions. In my opinion, the use of limestone as a SO_2 removal sorbent has a great disadvantage when applied to oxy firing conditions. My suggestion is to develop a new type of SO_2 removal sorbent, which would not be affected by the high concentration of CO_2 found in oxy fired conditions.

Based on the experimental data in Chapters 3 and 4, my suggestion for additions to this work would be to develop equations that summarize the rate of sulfur evolution as a function of temperature. Another useful suggestion is to measure SO_3 behavior in the bench-scale BFB, and track all solid forms of sulfur, to close an overall sulfur balance.

APPENDIX A

CALIBRATION CURVES FOR FTIR

The calibration curve for CO_2, CO, and SO_2 is carried out in order to obtain gaseous species concentrations (ppm) from FTIR spectrum peak areas. A typical Fourier transform infrared (FTIR) spectrum of SO_2 is shown in Figure 74. There are two main absorbance regions: one region 1 is located between 1294cm^{-1} and 1421 cm^{-1}, and the other (region 2) is from 1087cm^{-1} to 1209 cm^{-1}. Obviously, the absorbance in region 1 is much stronger than that in region 2. To avoid overlapping with other species, the wavelength region from 1319 to 1363 cm^{-1} is used for SO_2 absorption.

CO_2 spectra have a large absorbance peak area (2281 cm^{-1} to 2404 cm^{-1}), compared with the CO absorbance peak area (2086 cm^{-1} to 2281 cm^{-1}), as shown in Figure 73. There is no overlap area between SO_2, CO and CO_2, thus, their concentrations can be acquired simultaneously. To avoid overlapping, the wavelength region from 2283 to 2397 cm^{-1} and 2076-2223 cm^{-1} are used for CO_2 and CO absorption, respectively. Calibration curves for SO_2 were carried out at room temperature. SO_2 calibration gas flowed through the gas cell, and its concentration is 4050 ppm or 998 ppm balance N_2 or CO_2, respectively, and they were mixed with N_2 or CO_2 by mass flow controller to attain the desired concentrations of SO_2 (0-4050 ppm or 0-998 ppm). Three spectra were taken for each condition to decrease measurement error. Calibration curves of SO_2

balanced with N_2 and CO_2 are shown in Figure 75 and Figure 76, and the calibration equation of SO_2 is obtained. The relation between absorption area and SO_2 concentration (ppm) is exact linearity. R-squared value is more than 0.999. Figure 77 illustrates the calibration curve of SO_2 in N_2 or CO_2 environments. Both calibration curves were highly linear, with an R^2 value greater than 0.999. The calibration curves of SO_2 are very similar for a balanced gas (N_2 or CO_2). In other words, there is no effect of CO_2 or N_2 on the SO_2 absorption spectrum.

In addition, a calibration gas (CO_2 (165900 ppm) + CO (9830 ppm) balanced N_2) is mixed with N_2 to achieve desired CO_2 and CO concentration. The mixed gas is passed through the FTIR gas cell. Each condition is repeated three times. In order to get more details of correlation at low CO_2 levels, a calibration gas (CO_2 (300 ppm) balanced N_2) is used. The calibration curves of CO_2 and CO at higher concentrations are displayed in Figure 78 and Figure 79, while the calibration curve of CO at a lower concentration is shown in Figure 80. All of them show exact linearity, and R-squared values are higher than 0.996.

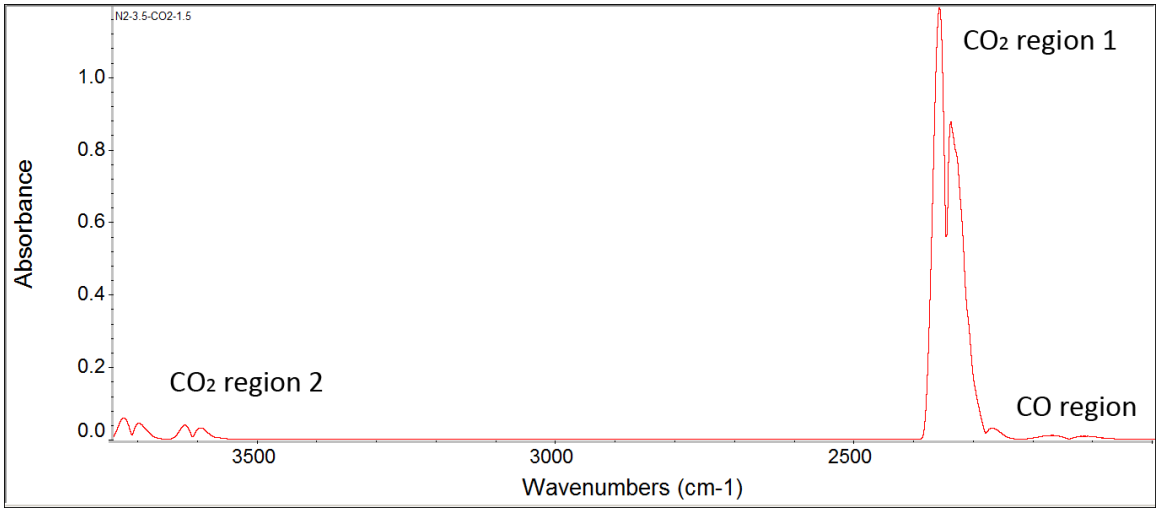

Figure 73. CO_2-CO spectra in FTIR

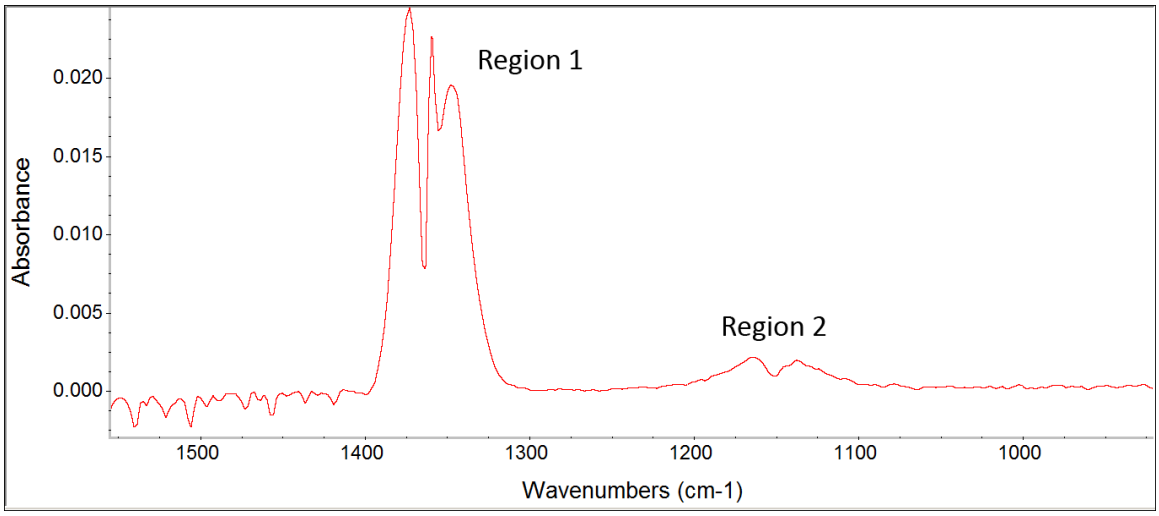

Figure 74. SO_2 spectra by FTIR with SO_2 concentration 1000 ppm

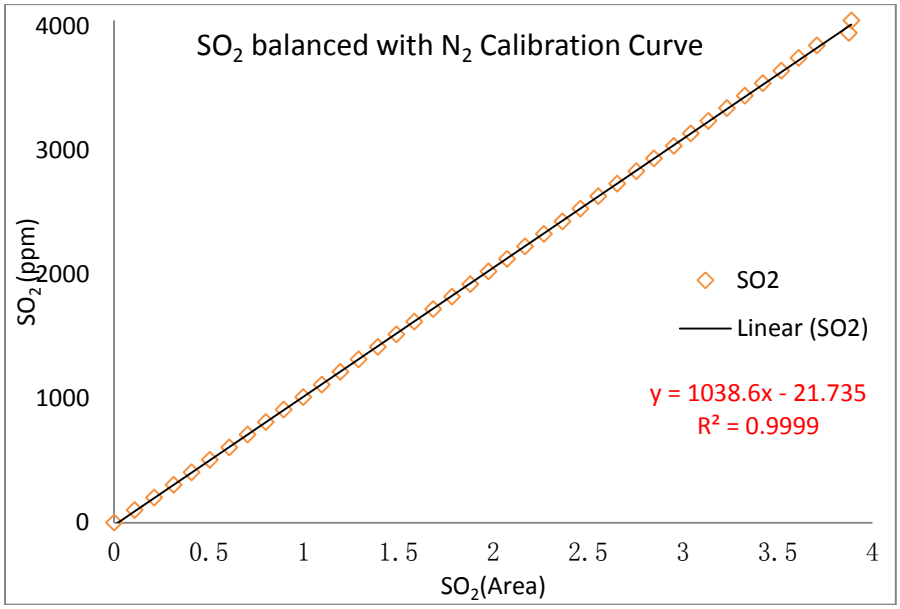

Figure 75 Calibration curve (absorption area vs. ppm) of SO_2 (4050 ppm) balanced with N_2

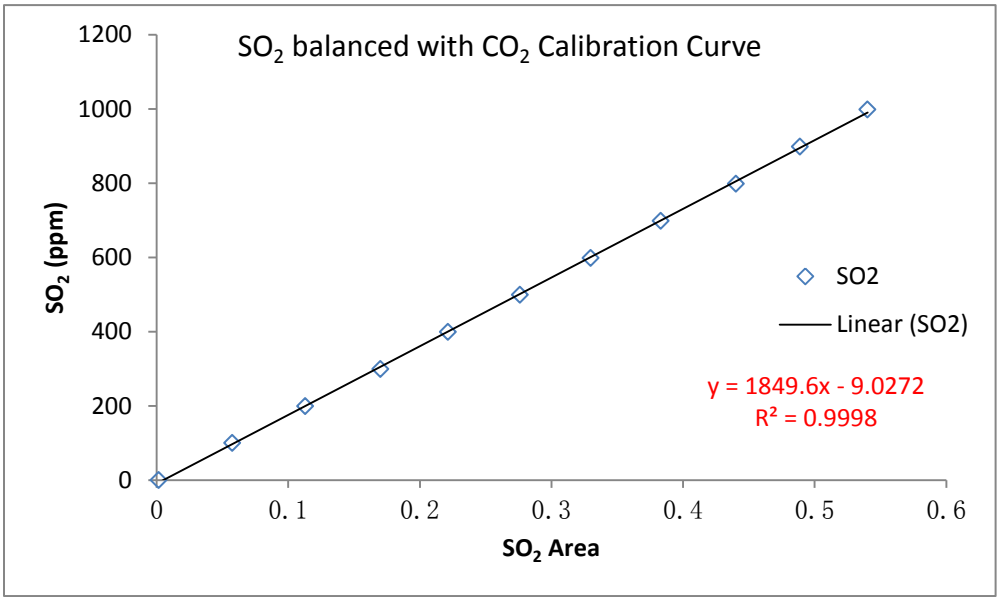

Figure 76 Calibration curve (absorption area vs. ppm) of SO_2 (998 ppm) balanced with CO_2

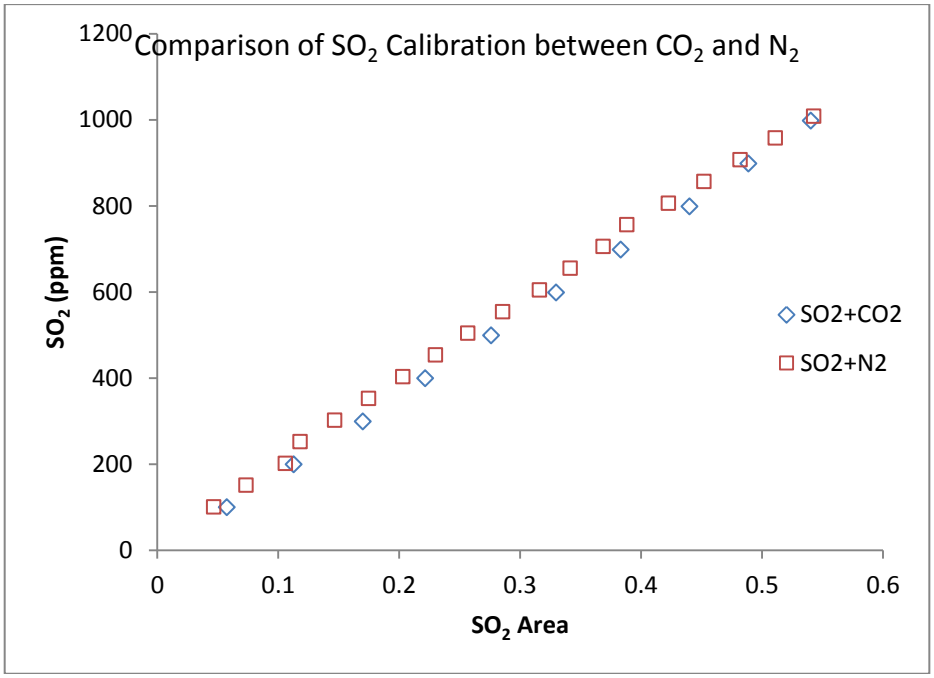

Figure 77 Effect of balanced gas (CO_2, N_2) on SO_2 calibration curve

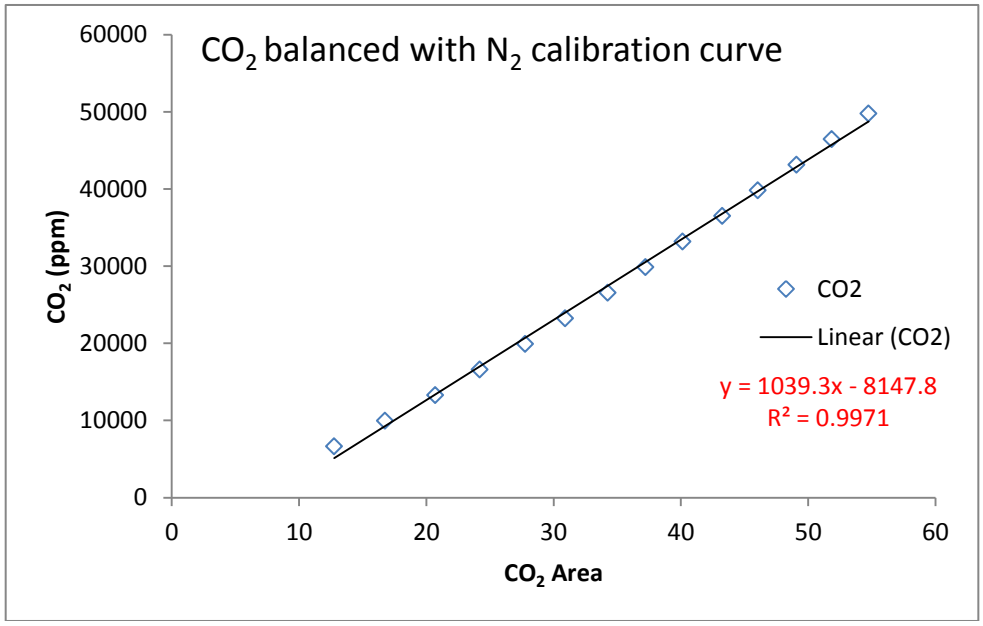

Figure 78 Calibration curve (absorption area vs. ppm) of CO_2 (165900 ppm) balanced with N_2

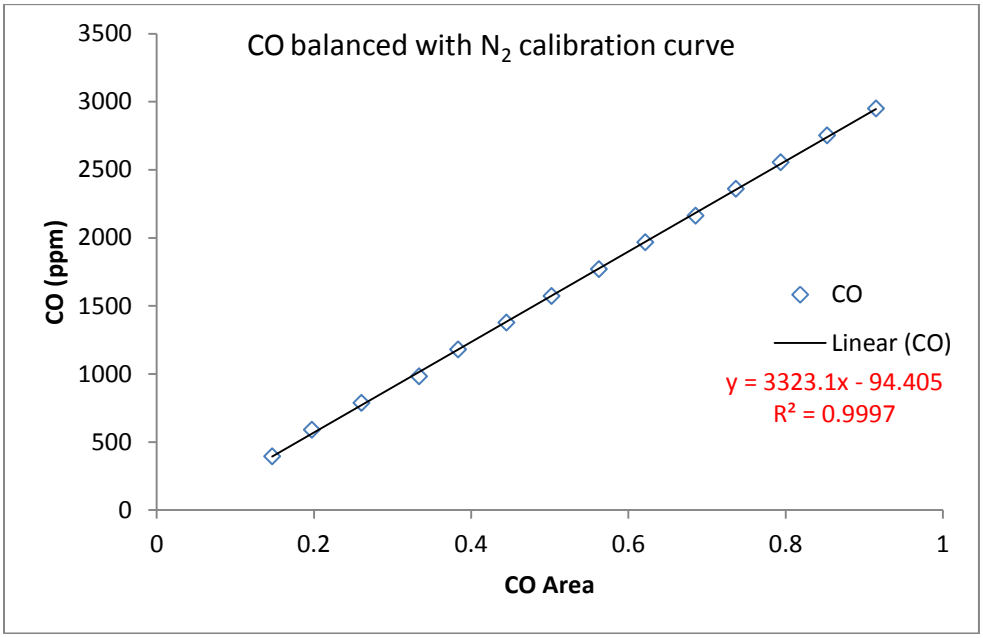

Figure 79 Calibration curve (absorption area vs. ppm) of CO (9830 ppm) balanced with N_2

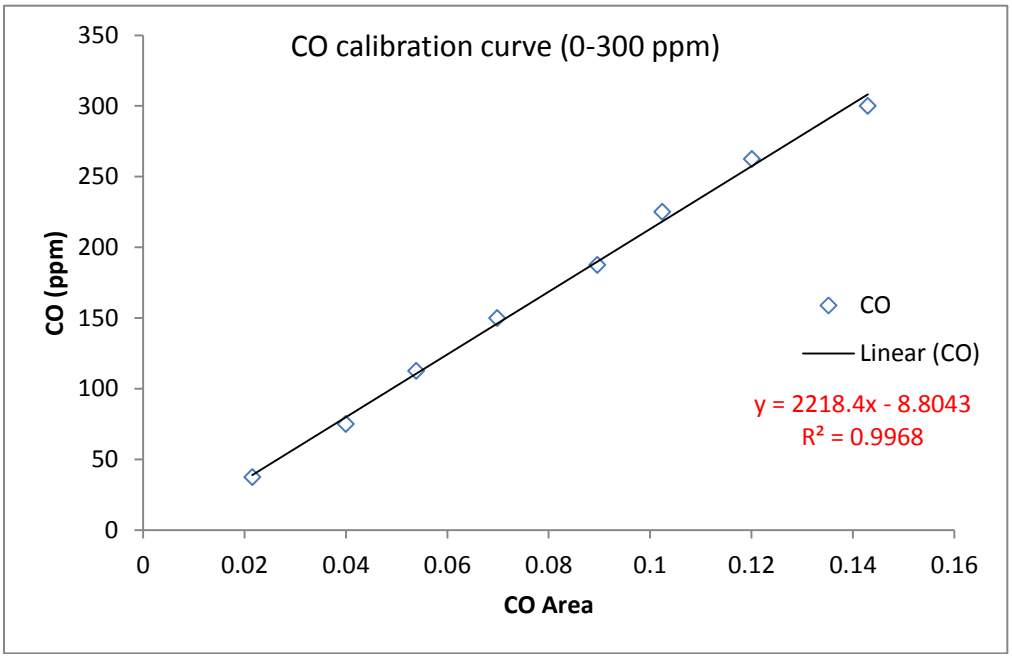

Figure 80 Calibration curve (absorption area vs. ppm) of CO (300 ppm) balanced with N_2

APPENDICES B

MATLAB SULFATION MODEL SCRIPT

```
%--------------------------------------------------------------------------
%                       Author: Liyong Wang
%--------------------------------------------------------------------------
% This model is to predict sulfation degree v.s. time, which is applied to
% indirect sulfation and direct sulfation.
% The sulfation of limestone is a very complicated process.
% Some parameters such as effective diffusivity are very difficult
% to obtain directly. Modeling is also necessary to investigate
% this process. Therefore, a pore diffusion model was
% developed for direct sulfation of limestone.
% The simplifying assumptions are as follows

% i.    The limestone particle is fully converted into CaO in the indirect
%       sulfation mechanism, comparatively, limestone particle can't be
%       formed into CaO by the calcination reaction
% ii.   The system is isothermal
% iii.  The sulfation reaction is irreversible
% iv.   Product layer is made of CaSO4
% v.    The particle is spherical
% vi.   The diffusivity inside the product layer is uniform
% vii.  There is no reaction inside the unreacted core
% viii. The overall particle is unchangeable during reaction
% ix.   The effect of O2 concentration is negligible
%
%
% The mathematical framework includes the unsteady mass conservation equation
% and the total mass balance
%
%
%
%
%
```

```
clear all; clc; close all


% Mesh of time
nt = 2e2;

time_interval = linspace(0,3.6e3,nt);

% Mesh of Space
nr = get_npts();

% The Radius of limestone particle
R = get_length();

% Set the initial mass concentration and initial radius interface between
% product layer and unreacted core
%Initial condition setting up
[Co,Rf] = set_initial_condition();

Co=[Co;Rf];

% solve the problem.  Here we use ode23s because it is faster.  Also,
% if you select ode45 solver, it will be very slow since this is a stiff
% problem
[t,C] = ode15s(@mass_eqn_rhs, time_interval, Co );




X=conversion_degree(C(:,end));


% Load the experimental data of direct sulfation
load T765
load T835
load T874

T765(:,2)=100.*T765(:,2);
T835(:,2)=100.*T835(:,2);
T874(:,2)=100.*T874(:,2);

% Experimental Data
plot(T765(:,1),T765(:,2),'s',T835(:,1),T835(:,2),'o',...
```

```
   T874(:,1),T874(:,2),'*');

hold on;

plot(t,X,'b','LineWidth',2);



% plot(T874(:,1),T874(:,2),'s','MarkerSize',4);
xlabel( 'Reaction Time, Seconds' );
ylabel( 'Sulfation Degree (%)' );
title( 'Sulfation Degree v.s Reaction Time','color','k','fontsize',12 );




axis([0 3600 0 20]);

legend ('Experimental (765 C)','Experimental (835 C)',...
    'Experimental (874 C)','Model (765 C)','Model (835 C)',...
   'Model (874 C)');

%legend ('765 C','835 C','874 C')
%legend ('unlimited','Sh=2e-11','Sh=2e-10','Sh=2','Sh=2e2' )




function C_b=bulk();

C=800e-6;

T=temperature();

C_b=(C)/(22.4e-3)*273/T;

end
```

```
function J = calculate_mass_flux( C )
%
% function q = calculate_heat_flux( T )
%  calculates the heat flux at all points on the staggered mesh, given the
%  temperature on the original (nonstaggered) mesh.
%

R = get_length();

dr = get_spacing(C(end));

cof=coeff();

nr = get_npts();

r=get_radius(C(end));

R_f=C(end);

X=conversion_degree(C(end));

C=C(1:end-1);

D_eff=cof*diffusivity();


if( nr -= length(C) ) error('Inconsistent number of grid points'); end

% since we are staggering the heat flux, it will have nz+1 entries.
J = zeros(nr+1,1);

%
% calculate the heat flux in the interior.
% The "k" index is the index for the heat flux.  Remember that the heat
% flux has nz+1 entries, so we loop from 2 to nr.  The values at 1 and
% nr+1 are obtained via the boundary conditions.
%
for k=2:nr


  % calculate the heat flux from the discretized heat flux expression.
  J(k) = -(r(k).^2).*D_eff.*( C(k)-C(k-1) )./dr;
```

```
end

ks=reaction_constant();

J(1)=-(R_f.^2).*ks.*C(1);


km=mass_tranfer();

C_b=bulk();

J(nr+1)=-(R.^2).*km.*(C_b-C(nr))/dr;

% all done.

end
```

```
function cof=coeff()
%UNTITLED Summary of this function goes here
%

cof=1e-6;
end
```

```
function X=conversion_degree(Rf);

% The radius of limestone particle (unit: m)
R = get_length();

% Rf: radius interface between product layer and unreacted core
X=100.*(1-(  (R+Rf)./R  ).^3);
```

```
end


function D_eff=diffusivity();

% This function is to calculate effective diffusivity of SO2 in product
% layer

T=temperature(); % Unit (K);

%The effective diffusivity of SO2 in the particle during direct sulfation
% of limestone was estimated through fitting of the experimental results by
% using the above-mentioned model.

% The diffusion in particle during
% direct sulfation of limestone is complicated and vague.
% This formula merely represents a semi-empirical, mathematical
% relationship of data but has no clear physical meaning.

% we supposed an exponential relationship and obtained a regressed formula

A=8.62e-6;
E=-13590;

D_eff=A.*exp(E./T);



end


function R = get_length();

% return the domain length in meters
R = 400e-6;

end
```

```
function n = get_npts()
% return the number of grid points in the domain
n = 40;
end


function r=get_radius(Rf);


nr = get_npts();
R = get_length();

% the radius s we should get
r = linspace( R+Rf, 0.9999999*R, nr )';

end


function dz = get_spacing(Rf)
% return the mesh spacing, in meters.
R = get_length();
nr = get_npts();
dz = abs(Rf) / nr;


%   |       |  dr |       |
%   |  o    o    o    o  |
%   |                 |

end


function rhs = mass_eqn_rhs( t, C)
% function rhs = heat_eqn_rhs( t, T )
%  calculate the rhs at each grid point.
%

%
%  NOTE: the grid points start at dz/2 and end at L-dz/2
%
%
%   |       |  dr |       |
%   |   o    o    o    o  |
```

```
%   |                   |
%  r=R+Rf               r=R
%
%

dr = get_spacing(C(end));

nr = get_npts();

r=   get_radius(C(end));

if( nr -= length(C(1:end-1))) error('Inconsistent number of points'); end


% get the diffusive fluxes at all STAGGERED grid points.  This gives us a
% field of length nz+1.

J = calculate_mass_flux(C);

if( nr+1 -= length(J) ) error('Wrong number of points in mass flux'); end


% now we are ready to calculate the rhs at each point.
rhs = zeros(nr,1);


for i=1:nr


  rhs(i) = -1./(r(i).^2).*(J(i+1)-J(i))./dr;

end

%The total mass balance equation is associated with radium
% rhs(nr+1)=0;


ks=reaction_constant();

pho=MV(); % mol/m^3

rhs(nr+1)=-ks./pho.*C(1).^0.1;
```

```
% all done.

end


function km=mass_tranfer();

R = get_length();
Sh=2;

D_air=1e-5;

km=Sh*D_air/(2*R);

end


function ks=reaction_constant();

% At the beginning of the reaction ? sulfation degree = 0:03);
% the product layer of a sorbent particle is so thin that
% the sulfation process is considered to be  chemically
% controlled
% An expression of reaction rate constant was obtained for direct sulfation of
% limestone

T=temperature(); % Unit (K);

% reaction rate constant on apparent area basis (m/s)
A=0.087;

B=-5416;

ks=A.*exp(B./T);



end


function [C,Rf] = set_initial_condition();
%
% function [C,Rf] = set_initial_condition()
```

```
% set the initial temperature field at all points in space.
% returns the mesh as well as the initial mass concentration profile.
%
%
%   |        | dr |       |
%   |   o    o    o    o  |
%   |                    |
%  r=R+Rf                 r=R
%

% length interface between product layer and unreacted core (unit: m)


nr = get_npts();
% The radius of limestone particle (unit: m)
R = get_length();
Rf=-0.000001*R;
% interface between product layer and unreacted core
r=get_radius(Rf); % column vector of spatial points for radius

% column vector of SO2 molar concentration inside the particle (unit: mol/m^3)
C = linspace(0,0,nr)';

end



function z=MV();

pho=2.910e3; % density of CaCO3 g/cm^3
M_cc=100;

z=pho./M_cc*1000; % mole/m^3

end
```

REFERENCES

[1] Recent climate change: atmosphere changes, Climate Change Science Program. United States Environmental Protection Agency. 2007.

[2] Feron P, H.M., Hendriks C, A., CO_2 capture process principles and costs, Oil & Gas Science and Technology - Rev. IFP. 2005; 60 (3): 451-459.

[3] Stefan B, CO_2 storage in geological media: role, means, status and barriers to deployment, Progress in Energy and Combustion Science. 2008; 34 (2): 254-273.

[4] Gozalpour F, Ren S, R., Tohidi B, CO_2 Eor and Storage in Oil Reservoir, Oil & Gas Science and Technology - Rev. IFP. 2005; 60 (3): 537-546.

[5] Toftegaard MB, Brix J, Jensen PA, Glarborg P, Jensen AD, Oxy-fuel combustion of solid fuels, Progress in Energy and Combustion Science. 2010; 36 (5): 581-625.

[6] Terry W, Combustion processes for carbon capture, Proceedings of the Combustion Institute. 2007; 31 (1): 31-47.

[7] John D, Performance and costs of power plants with capture and storage of CO_2, Energy. 2007; 32 (7): 1163-1176.

[8] Notz R, Asprion N, Clausen I, Hasse H, Selection and pilot plant tests of new absorbents for post-combustion carbon dioxide capture, Chemical Engineering Research and Design. 2007; 85 (4): 510-515.

[9] Descamps C, Bouallou C, Kanniche M, Efficiency of an Integrated Gasification Combined Cycle (IGCC) power plant including CO_2 removal, Energy. 2008; 33 (6): 874-881.

[10] Kanniche M, Gros-Bonnivard R, Jaud P, Valle-Marcos J, Amann J-M, Bouallou C, Pre-combustion, post-combustion and oxy-combustion in thermal power plant for CO_2 capture, Applied Thermal Engineering. 2010; 30 (1): 53-62.

[11] Williams TC, Shaddix CR, Schefer RW, Effect of syngas composition and CO_2-diluted oxygen on performance of a premixed swirl-stabilized combustor, Combustion Science and Technology. 2007; 180 (1): 64-88.

[12] Whitty KJ, Zhang HR, Eddings EG, Emissions from syngas combustion, Combustion Science and Technology. 2008; 180 (6): 1117-1136.

[13] Pehnt M, Henkel J, Life cycle assessment of carbon dioxide capture and storage from lignite power plants, International Journal of Greenhouse Gas Control. 2009; 3 (1): 49-66.

[14] Damen K, van Troost M, Faaij A, Turkenburg W, A comparison of electricity and hydrogen production systems with CO_2 capture and storage—Part B: Chain analysis of promising CCS options, Progress in Energy and Combustion Science. 2007; 33 (6): 580-609.

[15] János M B, High efficiency electric power generation: The environmental role, Progress in Energy and Combustion Science. 2007; 33 (2): 107-134.

[16] http://en.wikipedia.org/wiki/Integrated_gasification_combined_cycle.

[17] Schnurrer S EL, Wall T., Influence of oxy-fuel environment on sulphur species in ash from pulverised coal combustion, 7th International symposium on gas cleaning at high temperatures. 2008.

[18] Toporov D, Bocian P, Heil P, Kellermann A, Stadler H, Tschunko S, Kneer R, Detailed investigation of a pulverized fuel swirl flame in CO_2/O_2 atmosphere, Combustion and Flame. 2008; 155 (4): 605-618.

[19] Zanganeh KE, Shafeen A, A novel process integration, optimization and design approach for large-scale implementation of oxy-fired coal power plants with CO_2 capture, International Journal of Greenhouse Gas Control. 2007; 1 (1): 47-54.

[20] Kakaras E, Koumanakos A, Doukelis A, Giannakopoulos D, Vorrias I, Oxyfuel boiler design in a lignite-fired power plant, Fuel. 2007; 86 (14): 2144-2150.

[21] Andersson K, Johnsson F, Flame and radiation characteristics of gas-fired O_2/CO_2 combustion, Fuel. 2007; 86 (5-6): 656-668.

[22] Tan Y, Croiset E, Douglas MA, Thambimuthu KV, Combustion characteristics of coal in a mixture of oxygen and recycled flue gas, Fuel. 2006; 85 (4): 507-512.

[23] Murphy JJ, Shaddix CR, Combustion kinetics of coal chars in oxygen-enriched environments, Combustion and Flame. 2006; 144 (4): 710-729.

[24] Buhre BJP, Elliott LK, Sheng CD, Gupta RP, Wall TF, Oxy-fuel combustion technology for coal-fired power generation, Progress in Energy and Combustion Science. 2005; 31 (4): 283-307.

[25] Tom Ochs DO, Dietrich Gross, Brian Patrick,Alex Gross, Cindy Dogan, Cathy Summers, William Simmons, Schoenfield M, Oxy-fuel combustion systems for pollution free coal fired power generation, 2004 clear water conference; 2004.

[26] White CM, Strazisar BR, Granite EJ, Hoffman JS, Pennline HW, Separation and capture of CO_2 from large stationary sources and sequestration in geological formations - Coalbeds and deep saline aquifers, Journal of the Air and Waste Management Association. 2003; 53 (6): 645-715.

[27] Krishnamoorthy G, Veranth JM, Computational modeling of CO/CO_2 ratio inside single char particles during pulverized coal combustion, Energy & Fuels. 2003; 17 (5): 1367-1371.

[28] Hu YQ, Kobayashi N, Hasatani M, Effects of coal properties on recycled-NO_x reduction in coal combustion with O_2/recycled flue gas, Energy Conversion and Management. 2003; 44 (14): 2331-2340.

[29] Zheng L, Clements B, Douglas MA, Simulation of an oxy-fuel retrofit to a typical 400 MWe utility boiler for CO_2 capture. 26th international technical conference on coal utilization and fuel systems, Clearwater, Florida 2001.

[30] Hu YQ, Kobayashi N, Hasatani M, The reduction of recycled-NO_x in coal combustion with O_2/recycled flue gas under low recycling ratio, Fuel. 2001; 80 (13): 1851-1855.

[31] Okazaki K, Ando T, NO_x reduction mechanism in coal combustion with recycled CO_2, Energy. 22 (2-3): 207-215.

[32] Zhang J, Kelly KE, Eddings EG, Wendt JOL, CO_2 effects on near field aerodynamic phenomena in 40 kW, co-axial, oxy-coal, turbulent diffusion flames, International Journal of Greenhouse Gas Control. 2011; 5, Supplement 1 (0): S47-S57.

[33] Zhang J, Kelly KE, Eddings EG, Wendt JOL, Ignition in 40 kW co-axial turbulent diffusion oxy-coal jet flames, Proceedings of the Combustion Institute. 2011; 33 (2): 3375-3382.

[34] Yu D, Morris WJ, Erickson R, Wendt JOL, Fry A, Senior CL, Ash and deposit formation from oxy-coal combustion in a 100 kW test furnace, International Journal of Greenhouse Gas Control. 2011; 5, Supplement 1 (0): S159-S167.

[35] Morris WJ, Yu D, Wendt JOL, Soot, unburned carbon and ultrafine particle emissions from air- and oxy-coal flames, Proceedings of the Combustion Institute. 2011; 33 (2): 3415-3421.

[36] Miller JA, Bowman CT, Mechanism and modeling of nitrogen chemistry in combustion, Progress in Energy and Combustion Science. 1989; 15 (4): 287-338.

[37] Jan E J, Formation and reduction of nitrogen oxides in fluidized-bed combustion, Fuel. 1994; 73 (9): 1398-1415.

[38] Glarborg P, Jensen AD, Johnsson JE, Fuel nitrogen conversion in solid fuel fired systems, Progress in Energy and Combustion Science. 2003; 29 (2): 89-113.

[39] Sánchez A, Eddings E, Mondragón F, Fourier transform infrared (FTIR) online monitoring of NO, N2O, and CO2 during oxygen-enriched combustion of carbonaceous materials, Energy & Fuels. 2010; 24 (9): 4849-4853.

[40] Croiset E, Thambimuthu K, Palmer A, Coal combustion in O_2/CO_2 mixtures compared with air, The Canadian Journal of Chemical Engineering. 2000; 78 (2): 402-407.

[41] Wall T, Liu Y, Spero C, Elliott L, Khare S, Rathnam R, Zeenathal F, Moghtaderi B, Buhre B, Sheng C, Gupta R, Yamada T, Makino K, Yu J, An overview on oxyfuel coal combustion--State of the art research and technology development, Chemical Engineering Research and Design. 2009; 87 (8): 1003-1016.

[42] Shimizu T, Hirama T, Hosoda H, Kitano K, Inagaki M, Tejima K, A twin fluid-bed reactor for removal of CO_2 from combustion Pprocesses, Chemical Engineering Research and Design. 1999; 77 (1): 62-68.

[43] Yu F-C, Fan L-S, Kinetic study of high-pressure carbonation reaction of calcium-based sorbents in the calcium looping process (CLP), Industrial & Engineering Chemistry Research. 2011; 50 (20): 11528-11536.

[44] Florin N, Fennell P, Synthetic CaO-based sorbent for CO_2 capture, Energy Procedia. 2011; 4 (0): 830-838.

[45] Florin NH, Blamey J, Fennell PS, Synthetic CaO-based sorbent for CO_2 capture from large-point sources, Energy & Fuels. 2010; 24 (8): 4598-4604.

[46] Blamey J, Lu DY, Fennell PS, Anthony EJ, Reactivation of CaO-based sorbents for CO_2 capture: mechanism for the carbonation of $Ca(OH)_2$, Industrial & Engineering Chemistry Research. 2011; 50 (17): 10329-10334.

[47] Abanades JC, Anthony EJ, Wang J, Oakey JE, Fluidized bed combustion systems integrating CO_2 capture with CaO, Environmental Science & Technology. 2005; 39 (8): 2861-2866.

[48] Lasheras A, Ströhle J, Galloy A, Epple B, Carbonate looping process simulation using a 1D fluidized bed model for the carbonator, International Journal of Greenhouse Gas Control. 2011; 5 (4): 686-693.

[49] Ströhle J, Galloy A, Epple B, Feasibility study on the carbonate looping process for post-combustion CO_2 capture from coal-fired power plants, Energy Procedia. 2009; 1 (1): 1313-1320.

[50] Hawthorne C, Trossmann M, Galindo Cifre P, Schuster A, Scheffknecht G, Simulation of the carbonate looping power cycle, Energy Procedia. 2009; 1 (1): 1387-1394.

[51] Koornneef J, Junginger M, Faaij A, Development of fluidized bed combustion--An overview of trends, performance and cost, Progress in Energy and Combustion Science. 2007; 33 (1): 19-55.

[52] Oka SN, Anthony EJ, fluidized bed combustion, in, Marcel Dekker, 2003.

[53] Danafar F, Fakhru'l-Razi A, Salleh MAM, Biak DRA, Fluidized bed catalytic chemical vapor deposition synthesis of carbon nanotubes—A review, Chemical Engineering Journal. 2009; 155 (1–2): 37-48.

[54] Leckner B, Szentannai P, Winter F, Scale-up of fluidized-bed combustion – A review, Fuel. 2011; 90 (10): 2951-2964.

[55] Rüdisüli M, Schildhauer TJ, Biollaz SMA, van Ommen JR, Scale-up of bubbling fluidized bed reactors — A review, Powder Technology. 2012; 217 (0): 21-38.

[56] Bartels M, Lin W, Nijenhuis J, Kapteijn F, van Ommen JR, Agglomeration in fluidized beds at high temperatures: mechanisms, detection and prevention, Progress in Energy and Combustion Science. 2008; 34 (5): 633-666.

[57] E.J A, Fluidized bed combustion of alternative solid fuels; status, successes and problems of the technology, Progress in Energy and Combustion Science. 1995; 21 (3): 239-268.

[58] Gomez-Barea A, Leckner B, Modeling of biomass gasification in fluidized bed, Progress in Energy and Combustion Science. 2010; 36 (4): 444-509.

[59] Ravelli S, Perdichizzi A, Barigozzi G, Description, applications and numerical modelling of bubbling fluidized bed combustion in waste-to-energy plants, Progress in Energy and Combustion Science. 2008; 34 (2): 224-253.

[60] Alauddin ZABZ, Lahijani P, Mohammadi M, Mohamed AR, Gasification of lignocellulosic biomass in fluidized beds for renewable energy development: A review, Renewable and Sustainable Energy Reviews. 2010; 14 (9): 2852-2862.

[61] Chen J, Lu X, Progress of petroleum coke combusting in circulating fluidized bed boilers—A review and future perspectives, Resources, Conservation and Recycling. 2007; 49 (3): 203-216.

[62] Bo L, Fluidized bed combustion: Achievements and problems, Symposium (International) on Combustion. 1996; 26 (2): 3231-3241.

[63] Grübler A, Nakićenović N, Victor DG, Dynamics of energy technologies and global change, Energy Policy. 1999; 27 (5): 247-280.

[64] Institute EPR, The current state of atmospheric fluidized-bed combustion technology, in, World Bank, 1989.

[65] Fluidized bed combustion and gasification: a guide for biomass waste generators, in, Chattanooga: Southeastern regional biomass energy program, 1994.

[66] Scala F, Salatino P, Limestone attrition under simulated oxyfiring fluidized-bed combustion conditions, Chemical Engineering and Technology. 2009; 32 (3): 380-385.

[67] Mukherjee S, Borthakur PC, Chemical demineralization/desulphurization of high sulphur coal using sodium hydroxide and acid solutions, Fuel. 2001; 80 (14): 2037-2040.

[68] Ali A, Srivastava SK, Haque R, Chemical desulphurization of high sulphur coals, Fuel. 1992; 71 (7): 835-839.

[69] Çulfaz M, Ahmed M, Gürkan S, Removal of mineral matter and sulfur from lignites by alkali treatment, Fuel Processing Technology. 1996; 47 (2): 99-109.

[70] Ochs TL, Oryshchyn DB, Gross D, Patrick B, Gross A, Dogan C, Summers CA, Simmons W, Schoenfeld M, Oxy-fuel combustion systems for pollution free coal fired power generation, 2004.

[71] Zheng L, Furimsky E, Assessment of coal combustion in O_2+CO_2 by equilibrium calculations, Fuel Processing Technology. 2003; 81 (1): 23-34.

[72] Boushaki T, Sautet JC, Salentey L, Labegorre B, The behaviour of lifted oxy-fuel flames in burners with separated jets, International Communications in Heat and Mass Transfer. 2007; 34 (1): 8-18.

[73] Lacas F, ccedil, ois, Leroux B, Darabiha N, Experimental study of air dilution in oxy-liquid fuel flames, Proceedings of the Combustion Institute. 2005; 30 (2): 2037-2045.

[74] Vervisch L, Labegorre B, eacute, veillon J, Hydrogen-sulphur oxy-flame analysis and single-step flame tabulated chemistry, Fuel. 2004; 83 (4-5): 605-614.

[75] Hu Y, Naito S, Kobayashi N, Hasatani M, CO_2, NO_x and SO_2 emissions from the combustion of coal with high oxygen concentration gases, Fuel. 2000; 79 (15): 1925-1932.

[76] Croiset E, Thambimuthu KV, NOx and SO_2 emissions from O_2/CO_2 recycle coal combustion, Fuel. 2001; 80 (14): 2117-2121.

[77] Liu H, Okazaki K, Simultaneous easy CO_2 recovery and drastic reduction of SO_x and NO_x in O_2/CO_2 coal combustion with heat recirculation[small star, filled], Fuel. 2003; 82 (11): 1427-1436.

[78] Liu H, Shiro K, Ken O, Drastic SO_x removal and influences of various factors in O_2/CO_2 pulverized coal combustion system, Energy & Fuels. 2001; 15 403-412.

[79] Liu H, Ramlan Z, Bernard MG, Comparisons of pulverized coal combustion in air and in mixtures of O_2/CO_2, Fuel. 2005; 84 833–840.

[80] Andersson K, Johnsson F, Process evaluation of an 865 MWe lignite fired O_2/CO_2 power plant, Energy Conversion and Management. 2006; 47 (18-19): 3487-3498.

[81] Chen J-C, Liu Z-S, Huang J-S, Emission characteristics of coal combustion in different O_2/N_2, O_2/CO_2 and O_2/RFG atmosphere, Journal of Hazardous Materials. 2007; 142 (1-2): 266-271.

[82] Kiga T, Takano S, Kimura N, Omata K, Okawa M, Mori T, Kato M, Characteristics of pulverized-coal combustion in the system of oxygen/recycled flue gas combustion, Energy Conversion and Management. 1997; 38 (Supplement 1): 129-134.

[83] Klostermann, Efficiency Increase of the oxyfuel process by waste heat recovery considering the effects of flue gas treatment., 3rd workshop of the IEA GHG international oxy-combustion network Yokohama, Japan. 2008.

[84] Andersson K, Fundamental oxy-fuel combustion research carried out within the ENCAP Project., International Oxy-combustion Network for CO_2 Capture. Report on inaugural (1st) workshop, Cottbus, Germany, 29-30 Nov 2005. Report 2006/4, Cheltenham, UK, IEA. 2006.

[85] Sarofim, Oxy-fuel combustion: progress and remaining issues, *2nd meeting of the oxy-fuel network*, Windsor, CT, USA. 2007.

[86] Ahn J, Okerlund R, Fry A, Eddings EG, Sulfur trioxide formation during oxy-coal combustion, International Journal of Greenhouse Gas Control. 2011; 5, Supplement 1 (0): S127-S135.

[87] Borgwardt RH, Rochelle GT, Sintering and sulfation of calcium silicate-calcium aluminate, Industrial & Engineering Chemistry Research. 1990; 29 (10): 2118-2123.

[88] Borgwardt RH, Calcium oxide sintering in atmospheres containing water and carbon dioxide [Erratum to document cited in CA110(18):157398y], Industrial & Engineering Chemistry Research. 1990; 29 (9): 1984-1984.

[89] Borgwardt RH, Calcium oxide sintering in atmospheres containing water and carbon dioxide, Industrial & Engineering Chemistry Research. 1989; 28 (4): 493-500.

[90] Borgwardt RH, Bruce KR, Blake J, An investigation of product-layer diffusivity for calcium oxide sulfation, Industrial & Engineering Chemistry Research. 1987; 26 (10): 1993-1998.

[91] Borgwardt RH, Roache NF, Bruce KR, Method for variation of grain size in studies of gas-solid reactions involving calcium oxide, Industrial & Engineering Chemistry Fundamentals. 1986; 25 (1): 165-169.

[92] Borgwardt RH, Roache NF, Reaction of hydrogen sulfide and sulfur with limestone particles, Industrial & Engineering Chemistry Process Design and Development. 1984; 23 (4): 742-748.

[93] Borgwardt RH, Harvey RD, Properties of carbonate rocks related to sulfur dioxide reactivity, Environmental Science & Technology. 1972; 6 (4): 350-360.

[94] Borgwardt RH, Kinetics of the reaction of sulfur dioxide with calcined limestone, Environmental Science & Technology. 1970; 4 (1): 59-63.

[95] Hu G, Dam-Johansen K, Wedel S, Kinetics of the direct sulfation of limestone at the initial stage of crystal growth of the solid product, AIChE Journal. 2011; 57 (Compendex): 1607-1616.

[96] Hu G, Shang L, Dam-Johansen K, Wedel S, Hansen JP, Initial kinetics of the direct sulfation of limestone, AIChE Journal. 2008; 54 (Compendex): 2663-2673.

[97] Hu G, Dam-Johansen K, Wedel S, Hansen JP, Direct sulfation of limestone, AIChE Journal. 2007; 53 (Compendex): 948-960.

[98] Hu G, Dam-Johansen K, Wedel S, Peter Hansen J, Review of the direct sulfation reaction of limestone, Progress in Energy and Combustion Science. 2006; 32 (Compendex): 386-407.

[99] Jensen A, Johnsson JE, Dam-Johansen K, Nitrogen chemistry in FBC with limestone addition, in: Proceedings of the 1996 26th International Symposium on

Combustion. Part 2 (of 2), July 28, 1996 - August 2, 1996, Combustion Inst, Napoli, Italy, 1996, pp. 3335-3342.

[100] Lin W, Johnsson JE, Dam-Johansen K, van den Bleek CM, Interaction between emissions of sulfur dioxide and nitrogen oxides in fluidized bed combustion, Fuel. 1994; 73 (Compendex): 1202-1208.

[101] Illerup JB, Dam-Johansen K, Lundén K, High-temperature reaction between sulfur dioxide and limestone--VI. The influence of high pressure, Chemical Engineering Science. 1993; 48 (11): 2151-2157.

[102] Silcox GD, Kramlich JC, Pershing DW, A mathematical model for the flash calcination of dispersed calcium carbonate and calcium hydroxide particles, Industrial & Engineering Chemistry Research. 1989; 28 (2): 155-160.

[103] Milne CR, Silcox GD, Pershing DW, Kirchgessner DA, Calcination and sintering models for application to high-temperature, short-time sulfation of calcium-based sorbents, Industrial & Engineering Chemistry Research. 1990; 29 (2): 139-149.

[104] Milne CR, Silcox GD, Pershing DW, Kirchgessner DA, High-temperature, short-time sulfation of calcium-based sorbents. 2. Experimental data and theoretical model predictions, Industrial & Engineering Chemistry Research. 1990; 29 (11): 2201-2214.

[105] Anthony EJ, Granatstein DL, Sulfation phenomena in fluidized bed combustion systems, Progress in Energy and Combustion Science. 2001; 27 (Compendex): 215-236.

[106] E.G. Eddings LW, bench- and pilot-scale fluidized bed research on oxycoal combustion, 1st Oxy-fuel CFBC Workshop, University of Ottawa -CanmetENERGY, Ottawa, Ontario, Canada, June 27-28, 201. 2011.

[107] Jia L, Tan Y, Anthony EJ, Emissions of SO_2 and NO_x during Oxy-Fuel CFB combustion tests in a mini-circulating fluidized bed combustion reactor, Energy and Fuels. 2010; 24 (Compendex): 910-915.

[108] Jia L, Hughes R, Lu D, Anthony EJ, Lau I, Attrition of calcining limestones in circulating fluidized-bed systems, Industrial and Engineering Chemistry Research. 2007; 46 (Compendex): 5199-5209.

[109] Anthony EJ, Jia L, Charland JP, Laursen K, Agglomeration behavior of dolomitic sorbents during long-term sulfation, Energy and Fuels. 2003; 17 (Compendex): 348-353.

[110] Werner Weisweiler GKR, Kinetics of lime-limestone sulfation: review of lime reactivity and sulfation kinetics in the dry limestone desulfurization processes, High Temperatures- High Pressures. 1981; 13 333-345.

[111] Baker EH, The calcium oxide-carbon dioxide system in the pressure range 1-300 atmospheres, Journal of the Chemical Society (Resumed). 1962; 464-470.

[112] Hill KJ, Winter ERS, Thermal dissociation pressure of calcium carbonate, The Journal of Physical Chemistry. 1956; 60 (10): 1361-1362.

[113] Anthony EJ, Granatstein DL, Sulfation phenomena in fluidized bed combustion systems, Progress in Energy and Combustion Science. 2001; 27 (2): 215-236.

[114] Dam-Johansen K, Stergaard K, High-temperature reaction between sulphur dioxide and limestone--II. An improved experimental basis for a mathematical model, Chemical Engineering Science. 1991; 46 (3): 839-845.

[115] Robert HB, Sintering of nascent calcium oxide, Chemical Engineering Science. 1989; 44 (1): 53-60.

[116] Krishnan SV, Sotirchos SV, Effective diffusivity changes during calcination, carbonation, recalcination, and sulfation of limestones, Chemical Engineering Science. 1994; 49 (8): 1195-1208.

[117] Adanez J, Gayan P, Garcia-Labiano F, Comparison of mechanistic models for the sulfation reaction in a broad range of particle sizes of sorbents, Industrial & Engineering Chemistry Research. 1996; 35 (7): 2190-2197.

[118] Garcia-Labiano F, Abad A, de Diego LF, Gayan P, Adanez J, Calcination of calcium-based sorbents at pressure in a broad range of CO_2 concentrations, Chemical Engineering Science. 2002; 57 (13): 2381-2393.

[119] Duo W, Laursen K, Lim J, Grace J, Crystallization and fracture: formation of product layers in sulfation of calcined limestone, Powder Technology. 2000; 111 (1-2): 154-167.

[120] Borgwardt RH, Roache NF, Bruce KR, Method for variation of grain size in studies of gas-solid reactions involving CaO, Industrial & Engineering Chemistry, Fundamentals. 1986; 25 (1): 165-169.

[121] Ye Z, Wang W, Zhong Q, Bjerle I, High temperature desulfurization using fine sorbent particles under boiler injection conditions, Fuel. 1995; 74 (5): 743-750.

[122] Cheng J, Zhou J, Liu J, Zhou Z, Huang Z, Cao X, Zhao X, Cen K, Sulfur removal at high temperature during coal combustion in furnaces: a review, Progress in Energy and Combustion Science. 2003; 29 (5): 381-405.

[123] Ghosh-Dastidar A, Mahuli SK, Agnihotri R, Fan L-S, Investigation of high-reactivity calcium carbonate sorbent for enhanced SO_2 capture, Industrial & Engineering Chemistry Research. 1996; 35 (2): 598-606.

[124] Zhong Q, Direct sulfation reaction of SO_2 with calcium carbonate, Thermochimica Acta. 1995; 260 125-136.

[125] Hajaligol MR, Longwell JP, Sarofim AF, Analysis and modeling of the direct sulfation of calcium carbonate, Industrial & Engineering Chemistry Research. 1988; 27 (12): 2203-2210.

[126] Snow M, Longwell JP, Sarofim AF, Direct sulfation of calcium carbonate, Ind. Eng. Chem. Res. 1988; 27 268-213.

[127] Liu H, Katagiri S, Kaneko U, Okazaki K, Sulfation behavior of limestone under high CO_2 concentration in O_2/CO_2 coal combustion, Fuel. 2000; 79 (8): 945-953.

[128] Hu G, Dam-Johansen K, Wedel S, Peter Hansen J, Review of the direct sulfation reaction of limestone, Progress in Energy and Combustion Science. 2006; 32 (4): 386-407.

[129] Tullin C, Nyman G, Ghardashkhani S, Direct sulfation of calcium carbonate: the influence of carbon dioxide partial pressure, Energy & Fuels. 1993; 7 (4): 512-519.

[130] Stanger R, Wall T, Sulphur impacts during pulverised coal combustion in oxy-fuel technology for carbon capture and storage, Progress in Energy and Combustion Science. 2011; 37 (1): 69-81.

[131] Wang C, Jia L, Tan Y, Anthony EJ, The effect of water on the sulphation of limestone, Fuel. 2010; 89 (Compendex): 2628-2632.

[132] Hecht ES, Shaddix CR, Molina A, Haynes BS, Effect of CO_2 gasification reaction on oxy-combustion of pulverized coal char, in, Elsevier Ltd, Langford Lane, Kidlington, Oxford, OX5 1GB, United Kingdom, 2011, pp. 1699-1706.

[133] Murphy JJ, Shaddix CR, Effect of reactivity loss on apparent reaction order of burning char particles, Combustion and Flame. 2010; 157 (3): 535-539.

[134] Biggs MJ, Agarwal PK, The CO/CO_2 product ratio for a porous char particle within an incipiently fluidized bed: a numerical study, Chemical Engineering Science. 1997; 52 (6): 941-952.

[135] Karsner GG, Perlmutter DD, Reaction regimes in coal oxidation, AIChE Journal. 1981; 27 (6): 920-927.

[136] Karsner GG, Perlmutter DD, Model for coal oxidation kinetics. 1. Reaction under chemical control, Fuel. 1982; 61 (1): 29-34.

[137] Polat S, Harris IJ, Low-temperature oxidation of Victorian brown coal, Fuel. 1984; 63 (5): 669-672.

[138] Mess D, Sarofim AF, Longwell JP, product layer diffusion during the reaction of calcium oxide with carbon dioxide, Energy & Fuels. 1999; 13 (5): 999-1005.

[139] Campbell FR, Hills AWD, Paulin A, Transport properties of porous lime and their influence on the decomposition of porous compacts of calcium carbonate, Chemical Engineering Science. 1970; 25 (6): 929-942.

[140] Xie JY, Zhong BJ, Fu WB, Shi Y, Measurement of equivalent diffusivity during the calcination of limestone, Combustion and Flame. 2002; 129 (4): 351-355.

[141] J. Szekely JWEaHYS, Gas-solid reaction, Academic Press. 1976.

[142] Levenspiel O, Chemical reaction engineering, Wiley, New York 1962.

[143] Iisa K HM, Yrjas P, Twenty-Fourth Symposium (International) on Combustion/The Combustion Institute, 1992; 1349–1356.

[144] Krishnan SV, Stratis, Sotirchos V, Sulfation of high purity limestones under simulated pfbc conditions, in, Wiley Subscription Services, Inc., A Wiley Company, 1993, pp. 244-255.

[145] Qiu K, Lindqvist O, Direct sulfation of limestone at elevated pressures, Chemical Engineering Science. 2000; 55 (16): 3091-3100.

[146] Fuertes AB, Velasco G, Fuente E, Alvarez T, Study of the direct sulfation of limestone particles at high CO_2 partial pressures, Fuel Processing Technology. 1994; 38 (3): 181-192.

[147] Zevenhoven R, Yrjas P, Hupa M, Sulfur dioxide capture under PFBC conditions: the influence of sorbent particle structure, Fuel. 1998; 77 (4): 285-292.

[148] Dam-Johansen K, Stergaard K, High-temperature reaction between sulphur dioxide and limestone--I. Comparison of limestones in two laboratory reactors and a pilot plant, Chemical Engineering Science. 1991; 46 (3): 827-837.

[149] Fuertes AB, Velasco G, Fuente E, Parra JB, Alvarez T, Sulphur retention by limestone particles under PFBC conditions, Fuel Processing Technology. 1993; 36 (1-3): 65-71.

[150] Alvarez E, Gonzaez JF, High pressure thermogravimetric analysis of the direct sulfation of Spanish calcium-based sorbents, Fuel. 1999; 78 (3): 341-348.

[151] Can G, Salatino P, Scala F, A single particle model of the fluidized bed combustion of a char particle with a coherent ash skeleton: Application to granulated sewage sludge, Fuel Processing Technology. 2007; 88 (6): 577-584.

[152] Zhou W, Zhao C, Duan L, Liu D, Chen X, CFD modeling of oxy-coal combustion in circulating fluidized bed, International Journal of Greenhouse Gas Control. 2011; 5 (6): 1489-1497.

[153] Wang C, Jia L, Tan Y, Anthony EJ, Influence of water vapor on the direct sulfation of limestone under simulated oxy-fuel fluidized-bed combustion (FBC) conditions, in, American Chemical Society, 2540 Olentangy River Road, P.O. Box 3337, Columbus, OH 43210-3337, United States, 2011, pp. 617-623.

[154] Wang C, Jia L, Tan Y, Simultaneous carbonation and sulfation of CaO in oxy-fuel CFB combustion, Chemical Engineering and Technology. 2011; 34 (10): 1685-1690.

[155] Walker ME, Abbasian J, Chmielewski DJ, Castaldi MJ, Dry gasification oxy-combustion power cycle, Energy and Fuels. 2011; 25 (5): 2258-2266.

[156] Tan Y, Jia L, Wu Y, Anthony EJ, Experiences and results on a 0.8MWth oxy-fuel operation pilot-scale circulating fluidized bed, Applied Energy. 2012; 92 343-347.

[157] Takkinen S, Hyppanen T, Saastamoinen J, Pikkarainen T, Experimental and modeling study of sulfur capture by limestone in selected conditions of air-fired and oxy-fuel circulating fluidized-bed boilers, in, American Chemical Society, 2540 Olentangy River Road, P.O. Box 3337, Columbus, OH 43210-3337, United States, 2011, pp. 2968-2979.

[158] Stewart MC, Symonds RT, Manovic V, MacChi A, Anthony EJ, Effects of steam on the sulfation of limestone and NOx formation in an air- and oxy-fired pilot-scale circulating fluidized bed combustor, Fuel. 2012; 92 (1): 107-115.

[159] Scheffknecht G, Al-Makhadmeh L, Schnell U, Maier J, Oxy-fuel coal combustion-A review of the current state-of-the-art, International Journal of Greenhouse Gas Control. 2011; 5 (SUPPL. 1): S16-S35.

[160] Jia L, Tan Y, Wang C, Anthony EJ, Experimental study of oxy-fuel combustion and sulfur capture in mini-CFBC, Energy and Fuels. 2007; 21 (6): 3160-3164.

[161] Jia L, Tan Y, McCalden D, Wu Y, He I, Symonds R, Anthony EJ, Commissioning of a 0.8 MWth CFBC for oxy-fuel combustion, 2011.

[162] Garcia-Labiano F, Rufas A, De Diego LF, Obras-Loscertales MDL, Gayan P, Abad A, Adanez J, Calcium-based sorbents behaviour during sulphation at oxy-fuel fluidised bed combustion conditions, Fuel. 2011; 90 (10): 3100-3108.

[163] Font O, Cordoba P, Leiva C, Romeo LM, Bolea I, Guedea I, Moreno N, Querol X, Fernandez C, Diez LI, Fate and abatement of mercury and other trace elements in a coal fluidised bed oxy combustion pilot plant, Fuel. 2012; 95 272-281.

[164] Duan L, Zhao C, Zhou W, Qu C, Chen X, O_2/CO_2 coal combustion characteristics in a 50kWth circulating fluidized bed, International Journal of Greenhouse Gas Control. 2011; 5 (4): 770-776.

[165] De Diego LF, de las Obras-Loscertales M, Garcia-Labiano F, Rufas A, Abad A, Gayan P, Adanez J, Characterization of a limestone in a batch fluidized bed reactor for sulfur retention under oxy-fuel operating conditions, International Journal of Greenhouse Gas Control. 2011; 5 (5): 1190-1198.

[166] Yamada T, Pilot scale experiments giving direct comparison between air and oxy firing of coals and implication for large scale plan design, 2nd Workshop of the IEA international oxy-combustion research network : Hilton Garden Inn, Windsor, USA. 2007.

[167] Woycenko DM, Kamp WLvd, Roberts PA, Combustion of pulverised coal in a mixture of oxygen and recycled flue gas Summary of the APG research program, International Flame Research Foundation (IFRF), Ijmuiden, The Netherlands. 1995.

[168] Scala F, Salatino P, Limestone fragmentation and attrition during fluidized bed oxyfiring, Fuel. 2010; 89 (4): 827-832.

[169] Wang Y, Lin S, Suzuki Y, Experimental study on CO_2 capture conditions of a fluidized bed limestone decomposition reactor, in, Elsevier, P.O. Box 211, Amsterdam, 1000 AE, Netherlands, 2010, pp. 958-963.

[170] Scala F, Salatino P, The influence of sorbent properties and reaction conditions on attrition of limestone by impact loading in fluidized beds, in: 20th International Conference on Fluidized Bed Combustion; 2009 May 18-21, Xian, China, 2009.

[171] Scala F, Montagnaro F, Salatino P, Assessment of limestone attrition in fluidized bed combustion, in: 2006 AIChE Spring National Meeting - 5th World Congress on Particle Technology; 2006 April 23 - 27, 2006, Orlando, FL, United states, 2006.

[172] Scala F, Montagnaro F, Salatino P, Sulphation of limestones in a fluidized bed combustor; The relationship between particle attrition and microstructure, Canadian Journal of Chemical Engineering. 2008; 86 (3): 347-355.

[173] Scala F, Salatino P, Flue gas desulfurization under simulated oxyfiring fluidized bed combustion conditions: The influence of limestone attrition and fragmentation, Chemical Engineering Science. 2010; 65 (1): 556-561.

[174] Shimizu T, Peglow M, Yamagiwa K, Tanaka M, Sakuno S, Misawa N, Suzuki N, Ueda H, Sasatsu H, Gotou H, A simplified model of SO_2 capture by limestone in 71 MWe pressurized fluidized bed combustor, Chemical Engineering Science. 2002; 57 (19): 4117-4128.

[175] Ryu H-J, Grace JR, Lim CJ, Simultaneous CO_2/SO_2 capture characteristics of three limestones in a fluidized-bed reactor, Energy and Fuels. 2006; 20 (4): 1621-1628.

[176] Shimizu T, Hasegawa M, Inagaki M, Effect of water vapor on reaction rates of limestone-catalyzed NH_3 oxidation and reduction of N_2O under fluidized bed combustion conditions, Energy and Fuels. 2000; 14 (1): 104-111.

[177] Montagnaro F, Salatino P, Scala F, The influence of temperature on limestone sulfation and attrition under fluidized bed combustion conditions, Experimental Thermal and Fluid Science. 2010; 34 (3): 352-358.

[178] Chen Z, Grace JR, Jim Lim C, Limestone particle attrition and size distribution in a small circulating fluidized bed, Fuel. 2008; 87 (7): 1360-1371.

[179] Wang C, Jia L, Tan Y, Anthony EJ, Carbonation of fly ash in oxy-fuel CFB combustion, Fuel. 2008; 87 (7): 1108-1114.

[180] Montagnaro F, Nobili M, Salatino P, Telesca A, Valenti GL, Hydration products of FBC wastes as SO_2 sorbents: comparison between ettringite and calcium hydroxide, Fuel Processing Technology. 2008; 89 (1): 47-54.

[181] Scala F, Salatino P, Attrition of limestones by impact loading in fluidized beds: The influence of reaction conditions, Fuel Processing Technology. 2010; 91 (9): 1022-1027.

[182] Yao X, Zhang H, Yang H, Liu Q, Wang J, Yue G, An experimental study on the primary fragmentation and attrition of limestones in a fluidized bed, Fuel Processing Technology. 2010; 91 (9): 1119-1124.

[183] Jia L, Hughes R, Lu D, Anthony EJ, Lau I, Attrition of calcining limestones in circulating fluidized-bed systems, Industrial and Engineering Chemistry Research. 2007; 46 (15): 5199-5209.

[184] Saastamoinen JJ, Shimizu T, Attrition-enhanced sulfur capture by limestone particles in fluidized beds, Industrial and Engineering Chemistry Research. 2007; 46 (4): 1079-1090.

[185] Scala F, Montagnaro F, Salatino P, Enhancement of sulfur uptake by hydration of spent limestone for fluidized-bed combustion application, Industrial and Engineering Chemistry Research. 2001; 40 (11): 2495-2501.

[186] Nakazato T, Yano F, Ohyama K, Uchibori T, Nakagawa N, Moisture absorption characteristics of porous calcium oxide powders produced by calcination of pulverized limestone with inorganic salts using a powder-particle fluidized bed, Journal of the Ceramic Society of Japan. 2007; 115 (7): 443-446.

[187] Anthony EJ, Bulewicz EM, Jia L, Reactivation of limestone sorbents in FBC for SO_2 capture, Progress in Energy and Combustion Science. 2007; 33 (2): 171-210.

[188] Zhang L, Yang X-M, Xie J-J, Ding T-L, Yao J-Z, Song W-L, Lin W-G, Effect of coal and limestone addition position on emission of NO_x and N_2O during coal combustion in a circulating fluidized bed combustor, Zhongguo Dianji Gongcheng Xuebao/Proceedings of the Chinese Society of Electrical Engineering. 2006; 26 (21): 92-98.

[189] Johnston J, The thermal dissociation of calcium carbonate, Journal of the American Chemical Society. 1910; 32 (8): 938-946.

[190] Smyth FH, Adams LH, The system, calcium oxide-carbon dioxide, Journal of the American Chemical Society. 1923; 45 (5): 1167-1184.

[191] Ulerich NH, Newby RA, Keairns DL, A thermogravimetric study of the sulfation of limestone and dolomite -- prediction of pressurized and atmospheric fluidized-bed desulfurization, Thermochimica Acta. 1980; 36 (1): 1-16.

[192] Bulewicz EM, Kandefer S, Jurys C, Desuphurization during the fluidized combustion of coal using calcium-based sorbents at pressures up to 600 kPa, Journal of the Institute of Energy. 1986; 59 (441): 188-195.

[193] Dennis JS, Hayhurst AN, the effect of CO_2 on the kinetics and extent of calcination of limestone and dolomite particles in fluidised beds, Chemical Engineering Science. 1987; 42 (10): 2361-2372.

[194] Hajaligol MR, Longwell JP, Sarofim AF, Analysis and modeling of the direct sulfation of $CaCO_3$, Industrial and Engineering Chemistry Research. 1988; 27 (12): 2203-2210.

[195] Lyngfelt A, Leckner B, SO2 capture fluidised-bed boilers: re-emission of SO_2 due to reduction of $CaSO_4$, Chemical Engineering Science. 1989; 44 (2): 207-213.

[196] Haji-Sulaiman MZ, Scaroni AW, Yavuzkurt S, Optimum sulfation temperature for sorbents used in fluidized bed coal combustion, Fuel Processing Technology. 1990; 25 (3): 227-240.

[197] Spartinos DN, Vayenas CG, Kinetics of sulphation of limestone and precalcined limestone, Chemical Engineering and Processing. 1991; 30 (2): 97-106.

[198] Iisa K, Hupa M, Yrjas P, Product layer diffusion in the sulphation of calcium carbonate, Symposium (International) on Combustion. 1992; 24 (1): 1349-1356.

[199] Nyman G, Ghardashkhani S, Direct sulfation of $CaCO_3$: the influence of CO_2 partial pressure, Energy and Fuels. 1993; 7 (4): 512-519.

[200] Yrjas P, Iisa K, Hupa M, Comparison of SO_2 capture capacities of limestones and dolomites under pressure, Fuel. 1995; 74 (3): 395-400.

[201] Munoz-Guillena MJ, Linares-Solano A, Salinas-Martinez de Lecea C, High temperature SO_2 retention by CaO, Applied Surface Science. 1996; 99 (2): 111-117.

[202] Adanez J, GarcIa-Labiano F, Fierro V, Modelling for the high-temperature sulphation of calcium-based sorbents with cylindrical and plate-like pore geometries, Chemical Engineering Science. 2000; 55 (18): 3665-3683.

[203] Chen C, Zhao C, Liu S, Wang C, Direct sulfation of limestone based on oxy-fuel combustion technology, Environmental Engineering Science. 2009; 26 (10): 1481-1488.

[204] Chen C-M, Zhao C-S, Zhao Y, Direct sulfation reaction kinetics of limestone, Ranshao Kexue Yu Jishu/Journal of Combustion Science and Technology. 2009; 15 (5): 388-392.

[205] Wang X, Bai P, Yan Z, Liu H, Qiu J, Zhang S, Feng Q, Simulation of direct sulfation of limestone in oxy-fuel combustion, Huagong Xuebao/CIESC Journal. 2010; 61 (12): 3243-3250.

[206] J. Szekely, J. W. Evans, Sohn HY, gas-solid reaction, 1977.

[207] Ross T, Krishna R, multicomponent mass transfer, in, JOHN WILEY & SONS, INC, 1993.

[208] Silcox GD, Analysis of the SO_2-lime reaction system: mathematical modeling and experimental studies with emphasis on stoker application, Ph.D dissertation, Dept. of Chemical Engineering, University of Utah. 1985.

[209] Bhatia SK, Perlmutter DD, A random pore model for fluid-solid reactions: II. Diffusion and transport effects, AIChE Journal. 1981; 27 (2): 247-254.

[210] Reyes S, Jensen KF, Estimation of effective transport coefficients in porous solids based on percolation concepts, Chemical Engineering Science. 1985; 40 (9): 1723-1734.